INVESTIGATION OF THE ION NETWORKS IN *PSEUDOMONAS AERUGINOSA*: ROLES IN PHYSIOLOGY AND PATHOGENESIS

Sara Foreman

Submitted in Partial Fulfillment of the Requirements
for the Degree of

DOCTOR OF PHILOSOPHY

Approved by:
Dr. Blanca Barquera, Chair
Dr. Wilfredo Colón
Dr. George Makhatadze
Dr. Mattheos Koffas

Department of Chemistry and Chemical Biology
Rensselaer Polytechnic Institute
Troy, New York

[December 2020]
Submitted November 2020

TABLE OF CONTENTS

LIST OF TABLES

LIST OF FIGURES

ACKNOWLEDGEMENT

I would like to thank all of my past and present lab mates for providing an encouraging and friendly atmosphere in our lab every day. It is wonderful to work with people that you look forward to seeing every day, and I am so thankful to have had that these past few years.

I would like to thank all of the mentors that I have had at RPI. Teaching with Dr. Liz Sprague was an incredibly enjoyable and informative experience, and I always left class with a smile on my face and a dinner recipe in mind. There was never a dull moment when working with Dr. Michael Aldersley, who was an excellent resource for thinking outside of the box. Dr. Yang Bai provided me invaluable support and guidance during my venture into next generation sequencing and I am forever grateful for all of the help provided me. It was an honor and a treat to get to learn from her and work alongside her. And last but not least, Dr. Joel Morgan, who has saved the day on countless occasions. Without Joel's expert help in lab and friendly hellos during my long days of fluorescence scanning, I would not be where I am now, and I am truly appreciative of every time that he has gone out of his was to help me solve whatever problems arise.

I would also like to thank my wonderful family, who have supported and encouraged me endlessly for every day leading up to this one. I am immensely lucky to have the mother, father, and sister that I do, and I dedicate this document to them.

And finally, the biggest thanks that I can give goes to my fantastic advisor Dr. Blanca Barquera. You gave me a chance when you accepted me into your lab, and I am so grateful that you did. I have learned so much during my time in this lab and had such a great time doing so. Your support, your guidance, your kindness and your passion have motivated and inspired me more than I can express. Thank you so much for everything that you have done to get me to where I am today.

ABSTRACT

Pseudomonas aeruginosa is a remarkably ubiquitous microorganism featuring an extensive environmental presence, broad infectious profile, and multi-drug resistance. This pervasiveness is a product of *P. aeruginosa's* ability to adapt in the face of environmental stress. At the cellular level, environmental stress comes in the form of variable H^+ and Na^+ concentrations. Thus, survival across microbial habitats necessitates response to and regulation of these ions. The primary proteins responsible for H^+ and Na^+ regulation are the NADH dehydrogenases NDH-2, NUO and NQR and Na^+/H^+ antiporters NhaP, NhaP2, NhaB and Mrp. Together, these enzymes are responsible for the generation of energy efficient electrochemical ion gradients and the maintenance of cellular pH and Na^+ homeostasis. In addition, these transporters have been previously implicated in the viability and infectious success of *P.aeruginosa*, indicating that they may play a greater role in cell physiology at large.

To define the cellular utility of possessing such complementary transporters and determine their contributions to the adaptive physiology of the cell, this work investigates the kinetic parameters and survival phenotypes in a series of gene deletion mutants. NADH dehydrogenase activity is measured spectrophotometrically via the monitoring of NADH consumption. Antiport activity is measured as a function of substrate-stimulated H^+ flux. Cell survival is assessed via growth under a variety of conditions of pH, salinity, and nutrient availability, and the impacts of transporter absence on cell physiology are probed through transcriptome analysis by RNA sequencing. Observed deviations from the activity and growth profiles of wild-type *P. aeruginosa* are attributed to the absent transporter, outlining the contributions made by each enzyme.

Growth defects range in intensity, and phenotypic changes vary by mutant, however the results of this characterization point to a greater role for these ion transporters in the regulation of

pathogenesis in *P. aeruginosa*. This study reveals NQR as the major NADH dehydrogenase employed by *P. aeruginosa* and an important player in infection-relevant virulence traits. Our findings suggest that regulation of cellular NADH may convey virulence ques in *P. aeruginosa.* We define the four Na^+/H^+ antiporters present in *P. aeruginosa* and characterize the physiological impacts of the deletion of all for antiporters from the *P. aeruginosa* genome. The profiles revealed in this study begin to outline the roles played by each of these enzymes in *P. aeruginosa* and inform our understanding of ion regulation in this microbe.

1. INTRODUCTION

1.1 *Pseudomonas aeruginosa*

Pseudomonas aeruginosa is a prevalent bacterium of the gammaproteobacteria class of bacteria with a rod-shaped morphology and a single, polar flagellum.[1,2] It is native to many traditional terrestrial and aquatic environments including soil, vegetation, freshwater and saltwater habitats, but has also been isolated from more extreme settings including uranium mines and deep sea thermal vents.[3-6] *P. aeruginosa* is a common member of the skin microbiota of most humans and can be found globally in nearly all man-made environments, including reputedly sterile hospital settings.[7]

In addition to its widespread environmental presence, *P. aeruginosa* is a harmful opportunistic pathogen with a broad infectious profile. Consistent with its environmental versatility, *P. aeruginosa* can inhabit a wide range of hosts and host infection sites in both plants and animals.[8] In humans, *P. aeruginosa* infection can result in life threatening colonization of the lungs, urinary tract, dermal burns and wounds, ears, eyes and joints and is the primary cause of mortality in cystic fibrosis patients.[9-13] These infections are frequently hospital-acquired; *P. aeruginosa* is the 4th most common nosocomial pathogen and is oftentimes encountered by immunocompromised or otherwise afflicted patients, in which *P. aeruginosa* infection becomes a fatal comorbidity.[12]

The environmental and medical prevalence of this bacterium demonstrates a key feature of the species: the ability to not only withstand, but effectively proliferate in a remarkably wide range of habitats. To do this, *P. aeruginosa* must adapt to maintain essential cell processes despite variable, and often inhospitable external conditions. In bacteria, this requires the maintenance of efficient energy processing and favorable internal conditions to support cell biochemistry, two

features which *P. aeruginosa* is uniquely equipped to uphold.

1.2 Metabolism and Metabolic Adaptations in *Pseudomonas aeruginosa*

P. aeruginosa has several attributes which provides the species its intrinsic resilience and durability. A large 6.3Mbp genome with more than 5000 open reading frames (ORFs) and a large repertoire of regulatory genes provides *P. aeruginosa* with an impressive adaptive and regulatory capacity, which is thought to provide much of its environmental tolerance.[14] Another notable attribute of *P. aeruginosa* is its highly adaptable metabolism.[15, 16] The respiratory chain of *P. aeruginosa* is one of the most diverse among bacteria.[2] It is composed of a variety of enzymes with varying substrates, substrate affinities, energetic efficiencies and membrane gradient contributions, the assortment of which is representative of the adaptability which is built into *P. aeruginosa*'s central metabolism. *P. aeruginosa* can utilize a range of reducing agents to initiate respiration via its 17 predicted dehydrogenases and can terminate respiration at one of five terminal oxidases or five terminal N-reductases, by way of the cytochrome bc_1 complex, providing *P. aeruginosa* the flexibility necessary to respond to and tolerate dynamic environmental conditions.[2]

Maintaining such a diverse collection of respiratory enzymes has been documented to be advantageous to *P. aeruginosa,* allowing the bacteria to fine tune its respiratory pathways to best suit its environmental conditions. Expression of central metabolic enzymes has been found to be altered in response to different conditions of oxygen availability,[17,18] nutrient and micronutrient availability,[19,20] temperature,[21] and pH.[22] When faced with varying oxygen concentrations, *P. aeruginosa* will alter the expression of its five terminal oxidases to optimize oxygen affinity and energy conservation efficiency relative to the environmental oxygen availability.[17,18] Similarly, when grown in the presence of different carbon sources, *P. aeruginosa* will modify its metabolic pathways, via changes in carbon flux and the expression of its respiratory enzymes, to maximize

the efficiency of nutrient catabolism and energy generation. It was recently shown that cells grown with acetate as the sole carbon source featured a substantial increase in terminal oxidase expression, as well as an increase in expression of enzymes of the denitrification pathways.[20] This is a notable result as the denitrification pathways have been previously believed to be reserved for growth under anaerobic conditions, however this instance of the aerobic utilization of these pathways demonstrates *P. aeruginosa*'s ability to deploy different respiratory enzymes as a means of responding to external conditions.

In addition to enabling its environmental ubiquity, such adaptations are particularly relevant to *P. aeruginosa* pathogenesis as colonization of infection sites, specifically of the cystic fibrosis (CF) lung, will present the cell with nutrient and oxygen challenges.[23] In fact, *P. aeruginosa*'s highly adaptable central metabolism has recently been directly implicated in its pathogenesis. Perinbam et. al. have identified a shift in the central metabolism which is associated with the onset of virulence in *P. aeruginosa*, specifically in relation to the cycling of NADH. It was found that cells transitioning into a virulent state would feature a greater proportion of enzyme-bound NADH and increased production of both NAD^+ and NADH, indicating that this redox pair plays a role in the onset and regulation of virulence in *P. aeruginosa.*[24]

1.2.1 NADH Dehydrogenases of *Pseudomonas aeruginosa*

In its respiratory chain, *P. aeruginosa* has three different NADH dehydrogenases which are responsible for the oxidation of cellular NADH: two type-I NADH dehydrogenases, NUO and NQR, and one type-II NADH dehydrogenase, NDH-2.[25] All three NADH dehydrogenases serve as a point of entry for electrons into the electron transport chain, accepting electrons from NADH and passing them to the quinone pool. However, these enzymes differ in their ion pumping and energy conservation properties, giving rise to a functional divergence at this primary step in *P.*

aeruginosa respiration.

NUO, encoded for by the *nuoABDEFGHIJKLMN* operon, uses the free energy of the NADH:quinone redox reaction to translocate protons across the cell membrane to the periplasmic space.[26] NUO is a multi-subunit protein complex homologous to the mitochondrial complex 1 and the stoichiometry is believed to be $2H^+/e^-$, contributing to the generation of a proton gradient.[27]

NQR, encoded for by the *nqrABCDEF* operon, similarly conserves energy by coupling the electron transfer to the translocation of ions across the membrane, however the identity of the substrate ion has been a point of contention in recent literature.[28,29] In all other instances in which NQR is present in a bacterial species it has been characterized as Na^+-translocating,[30] however the ion translocation of Pa-NQR has yet to be definitively characterized. Preliminary data indicate that the NQR in *P. aeruginosa* is Na^+-translocating, but a more complete characterization is required.[29] In either case, NQR will also contribute to the establishment of an electrochemical membrane potential which can be utilized by the cell.

NDH2 catalyzes the transfer of electrons from NADH to quinone without ion pumping or energy conservation. NDH2 is a common respiratory enzyme among bacteria and some higher order organisms. It is encoded for by a single gene and is anchored to the membrane by single transmembrane helix, with the bulk of the enzyme residing at the cytoplasmic surface of the membrane.[31] Although this dehydrogenase does not contribute to the electrochemical membrane potential its activity has been implicated in a rescue-redox system than can help to balance the NAD^+/NADH ratio.[31]

Given the demonstrated tunability of the respiratory pathways in *P. aeruginosa*, it is possible that the variety of NADH dehydrogenases, each with distinct functional properties, offers an adaptive advantage to *P. aeruginosa*. However, the unique ion-translocating properties of

these kindred enzymes indicates that any changes in their expression or utilization will also impact the dynamics of ion management in the cells. Therefore, if *P. aeruginosa* modulates the expression and utilization of the NADH dehydrogenases like it does its other respiratory enzymes, it may provide a means of regulating not only energetic efficiency, but also ion homeostasis, in response to environmental conditions. This relationship between bioenergetics and ionic homeostasis at a critical step in *P. aeruginosa* respiration represents a critical intersection between these two cellular processes and may indicate another facet of metabolic flexibility in this bacterium.

1.3 Ion Regulation and Utilization in *Pseudomonas aeruginosa*

One important adaptive advantage of this microbe is the ability to employ more than one chemiosmotic coupling ion.[2] In bacterial physiology, ions play two roles. They can both contribute to cell bioenergetics and threaten cell survival if not maintained at precise internal and external concentrations. In bacteria there are two main types of enzymes responsible for the translocation of ions across the membrane; primary ion transporters, such as the NADH dehydrogenases described above, and secondary ion transporters. Primary ion transporters couple the translocation of ions to exergonic reactions, enabling the transport of ions against their concentration gradient and subsequently transforming the kinetic chemical energy into potential energy in the form of electrochemical ion gradients.[32] The resulting electrochemical ion gradients can be used to fuel a variety of cellular processes, including ATP synthesis, cell mobility, nutrient uptake, and drug efflux.[32,33] In addition, secondary ion transporters, also known as antiporters, are fueled by the ion gradients as well, in many cases acting as an interface between parallel ion circuits as demonstrated in Figure 1.1.

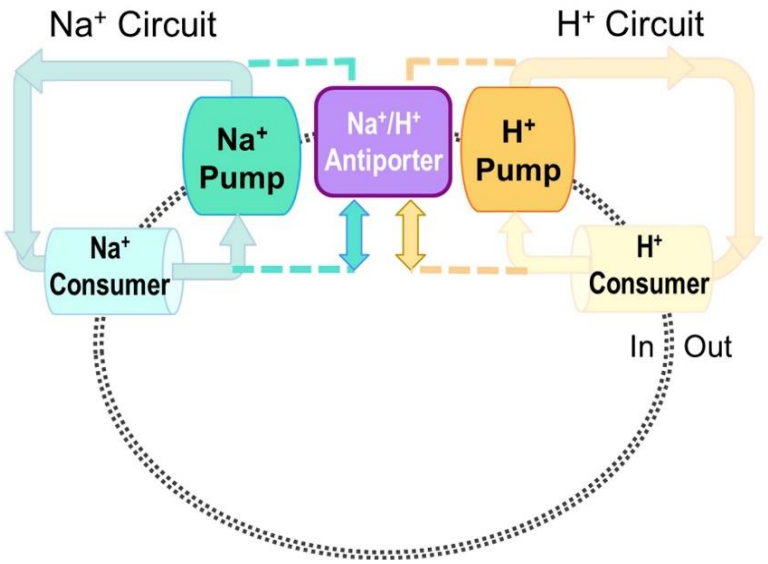

Figure 1.1: Representation of the Na^+ and H^+ ion cycles across cell membranes.

Secondary ion transporters are some of the most important and ubiquitous tools in cellular H^+ and Na^+ homeostasis.[34] Na^+/H^+ antiporters are transmembrane transport proteins found in prokaryotic and eukaryotic systems alike. They are responsible for the exchange of intracellular Na^+ (and other alkali metal ions) for extracellular H^+. In bacterial cells, these proteins provide (i) extrusion of toxic Na^+, (ii) intracellular pH regulation under alkaline conditions, and (iii) cell volume control.[35] Additionally, the Na^+ extrusion catalyzed by the antiporters will also contribute to the generation of a Na^+-motive force. Therefore, by virtue of their activity, antiporters not only play a role in homeostasis, but also in cellular energetics. There are four known Na^+/H^+ antiporters in *P. aeruginosa*: NhaB,[36] NhaP,[37] NhaP2[38] and Mrp.[39] Each of these transporters catalyze the exchange Na^+ and H^+ across the membrane, however they differ in their properties of ion affinity, stoichiometry, and enzyme kinetics. Together with the ion translocating NADH dehydrogenases NUO and NQR, these enzymes constitute the ion circuits present in *P. aeruginosa* (Figure 1.2). As a central feature of most bacterial energetics, these ion circuits simultaneously satisfy both bioenergetic and homeostatic requirements of the cell, however the mechanisms underlying their

coordinated management and interpolation remain unclear.

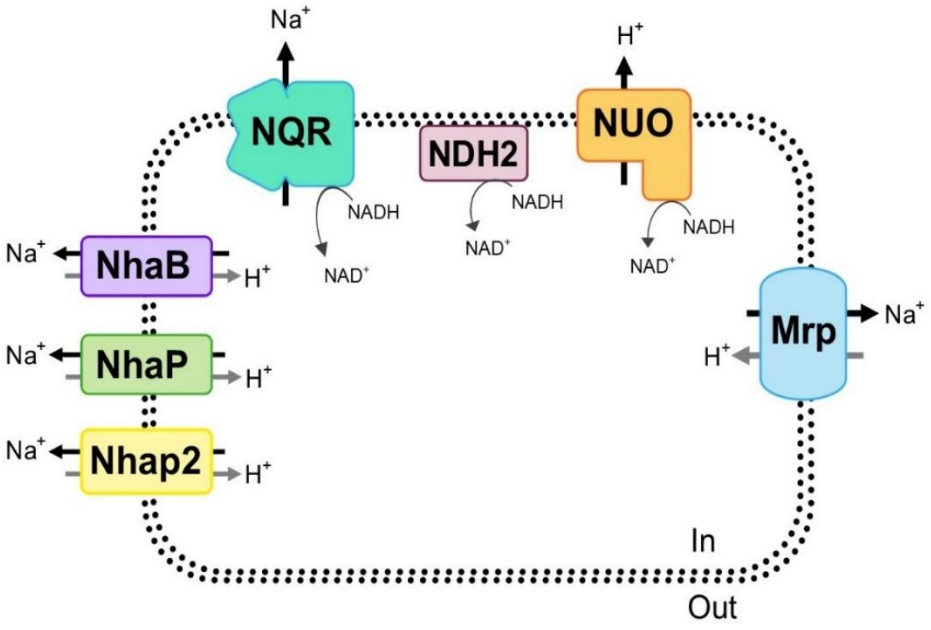

Figure 1.2: Representation of the NADH dehydrogenases and Na^+/H^+ antiporters in *P. aeruginosa*.

1.3.1 Single Gene Product Na^+/H^+ Antiporters

Of the four previously identified Na^+/H^+ antiporters in *P. aeruginosa*, three are encoded for by single genes. NhaP, encoded by PA3887, was the first Na^+/H^+ antiporter identified in *P. aeruginosa*.[37] Upon cloning and characterization in an antiporter devoid *Escherichia coli* strain, NhaP was proposed to feature optimal activity around pH 7.5 with strict selectivity for Na^+ transport, with very little affinity for Li^+.[37] Ion exchange by NhaP is thought to be electroneutral ($1Na^+/1H^+$), suggesting that this enzyme may primarily contribute to cytosolic pH homeostasis and cell volume regulation.[40] This antiporter remains unique to *P. aeruginosa*, with very little homology to any known antiporters, and is thought to be only a minor contributor to total Na^+/H^+ antiport in the bacteria.

Researchers went on to discover the NhaB antiporter, encoded by PA1820, sharing 62% identity with its *E. coli* counterpart. This antiporter, likewise cloned into *E. coli*, was found to

feature a broader pH profile compared with that of NhaP, with maximum activity recorded at higher pH values, and displayed greater activity with not only Li^+, but Na^+ as well.[36] The *E. coli* homolog of this transporter was reported to be essential under alkaline pH and was determined to exchange $3H^+/2Na^+$, suggesting potential electrogenic activity in *P.aeruginosa.*[41]

The final single gene encoded antiporter, NhaP2, encoded for by PA5021, is the most recently proposed in *P.aeruginosa.*[38] There is little characterization for this transporter in *P.aeruginosa*, however it shares 65% identity with the previously assessed NhaP2 of *Vibrio cholerae*. The VcNhaP2 homolog was defined as having optimal activity at lower pH values, a notable complement to the above transporters, and features specific activity for electroneutral exchange of K^+ rather than Na^+.[42] However, a *P. aeruginosa* mutant strain featuring the deletion of the NhaP2 antiporter suffered a growth defect in the presence of 400 mM NaCl compared with wildtype, indicating that this enzyme does contribute to Na^+ tolerance as well in *P. aeruginosa*.[38]

1.3.2 Multiple Resistance and pH Antiporter

Researchers went on to discover the Mrp antiporter, a member of the Multiple resistance and pH family, alternatively designated Sha or Mnh. This antiporter is unique from the previously mentioned enzymes as it is a multi-gene encoded protein complex composed of 6 subunits in *P. aeruginosa* (PA1054-PA1059).[39] This monovalent cation transporter is found in a wide range of microorganisms and has been shown to play an important role in the physiology of those bacteria which possess it.[43] Like NUO, the Mrp antiporter shares considerable homology with complex I, as shown in a recent structural determination completed with the Mrp homolog from *Anoxybacillus flavithermus* (~35% homology).[44] The sequence and structure, as well as several key residues, are highly conserved between the MrpA, MrpD and MrpC subunits and the NuoL, NuoN and NuoK subunits, respectively. Probable Na^+ and H^+ translocation pathways were identified and the

stoichiometry of exchange was proposed to be $2H^+/1Na^+$, suggesting that Mrp may play an important role in alkaline pH homeostasis.[44] The Mrp antiporter in *P.aeruginosa* was found to have a strict optimal pH for Na^+/H^+ antiport activity, functioning best from pH 8-8.5.[39] Deletion strains featuring insertional inactivation of the *mrpA* subunit (PA1054) showed greater sensitivity to Na^+ than those lacking NhaP, indicating a greater relative importance for Mrp rather than NhaP in Na^+ tolerance in *P. aeruginosa*.[39] A summary of the functional parameters of each of the four Na^+/H^+ antiporters present in *P. aeruginosa* is located in Table 1.1.

Table 1.1: Functional properties of the Na^+/H^+ antiporters present in *P. aeruginosa.*

Antiporter	Originally Discovered	Proposed Stoichiometry	Substrate Ion	Optimal pH
NhaB	*Escherichia coli*	$3H^+/2Na^+$ [a]	Na^+, Li^+	7.0-9.0[b]
NhaP	*P. aeruginosa*	$1H^+/1Na^+$	Na^+	7.5[b]
NhaP2	*P. aeruginosa*	Unknown	Na^+, K^+	6.0-7.5[c]
Mrp	*Bacillus halodurans*	$2H^+/1Na^+$ [d]	Na^+	8.0-8.5[b]

[a]As determined in *E. coli* homolog[41]
[b]As determined for *P. aeruginosa* protein expressed in *E. coli*[36,37,39]
[c]As determined in *V. cholerae*[42]
[d]As determined in *A. flavithermus*[44]

1.4 History of NADH Dehydrogenases and Na^+/H^+ Antiporters in Bacterial Pathogenesis

In addition to playing a central role in bioenergetics and ion homeostasis in many bacteria, these transporters have also been shown to play important roles in the infectious success of many prominent pathogens. In *Vibrio cholerae*, virulence traits and toxin production have been shown to be intricately linked to sodium bioenergetics.[45] Inhibition of NQR in *V. cholerae* resulted in

decreased toxin production by the bacteria, a trait which is central to the infectious success of the pathogen.[46] In *Mycobacterium tuberculosis* mutants with disruptions in NUO or NDH2 were found to have attenuated virulence in both intravenous and aerosol mouse models.[47] In addition, absence of the *nuoG* subunit specifically was shown to significantly reduce *M. tuberculosis* virulence in mice and was proposed to play a key role in the inhibition of cell apoptosis in infected cells, a critical step in *M. tuberculosis* virulence.[48,49] The loss of the energy-coupling NUO in *Pseudomonas fluorescens* has been cited as causing a competitive disadvantage in root-tip colonization.[50] In *Staphylococcus aureus*, a bacterium which does not possess any Type-I NADH dehydrogenases, its NDH2 and Mrp homologs were both found to be important during infection. Mutants having one or both of the Type-II NADH dehydrogenases deleted featured reduced virulence trait production including biofilm formation and toxin production, as well as a reduced colonization of mouse organs.[51] Deletion of one of the *S. aureus* Mrp homologs, *mnhA1*, led to a significant reduction in virulence towards mice, although deletion of a second Mrp homolog, Mnh2, had no impact on *S. aureus* virulence.[52] And in *Yersinia pestis*, its two Na^+/H^+ antiporters, NhaA and NhaB, were found to be essential for survival and infectious success *in vivo*,[53] underscoring the importance of ion management in pathogenesis.

There is evidence that these transporters are important in *P. aeruginosa* virulence as well. A mutant lacking a functional NUO was shown to have attenuated virulence in both an insect (*Galleria mellonella*) and plant (lettuce) model,[54] indicating a relationship between the activity of the NADH dehydrogenases and successful virulence. In antiporter mutant strains, the absence of NhaP2 was shown to reduce virulence towards barley in a seed germination infection model,[38] and a mutant lacking a functional Mrp had attenuated virulence in a mouse model of pulmonary infection, as well as reduced colonization of the lungs.[39] Evidence collected in our lab supports the

relationship between these transporters and infectious success in *P. aeruginosa*, however the mechanisms by which these two cell process are related remains unclear.

In *P. aeruginosa*, virulence is controlled by a complex chemical signal cascade called quorum sensing. This system is composed of a network of cell-to-cell communication enabling *P. aeruginosa* to detect changes in local cell density and coordinate single cell physiology to benefit and prolong the longevity of the population. As cell density increases, the concentration of quorum signaling molecules will increase until reaching a critical point, at which time the bacterial community will initial a coordinated physiological transition leading to virulence factor production and biofilm formation.[55] *P. aeruginosa* will then produce and excrete toxins including pyocyanin, elastases and rhamnolipids,[55] which will help to fend off host immune defenses and competing bacterial species. In addition, *P. aeruginosa* forms a complex extracellular polymeric matrix known as biofilm which encapsulate the cells, providing physical protection and fostering the 'sharing' of community resources by cells within the biofilm.[56] The existence of these complex community behaviors in *P. aeruginosa*, which dictate the physiology of not only single cells, but entire communities of cells, demonstrates that the resilience of this bacterium goes beyond the capacities of singles cells.

1.5 Project Overview

The versatility of this bacterium has made *P. aeruginosa* not only an interesting case study in bacterial adaption, but also a prominent threat in its capacity as an opportunistic pathogen. The adaptability of this microbe is believed to contribute to its infectious success and has made treating *P. aeruginosa* infection increasingly difficult. Although pathogenesis in *Pseudomonas aeruginosa* has been extensively investigated, less is known about the role of energic and homeostatic adaptations during infection. To probe the role of ion systems in *P. aeruginosa* physiology, we

here analyze the individual and collective roles of the three NADH dehydrogenases and four Na^+/H^+ antiporters employed by this microbe.

To define the cellular utility of maintaining such complementary transporters and determine their functional contributions to the adaptive physiology of the cell, this work will focus on the characterization of the kinetic parameters, expression profile, and survival phenotype in a series of NADH dehydrogenase and Na^+/H^+ antiporter deletion mutant strains of *P. aeruginosa*. In developing a comprehensive profile of the enzyme activities and physiological contributions of each, this work looks to define how *P. aeruginosa* utilizes adaptation of its ion transporting networks to respond to and withstand environmental stress, as well as regulate pathogenicity. It is critical to understand the relationships between ion management, biochemistry and pathogenicity in this bacterium as our findings demonstrate how interconnected these mechanisms are. To interrupt one aspect of *P. aeruginosa* physiology is to induce significant changes in the resulting phenotype, and to efficiently target this pathogen, it is necessary to understand the adaptive mechanisms which it employs. This knowledge will contribute to a more complete picture of both *P. aeruginosa* physiology and prokaryotic bioenergetics at large.

2. EXPERIMENTAL METHODS AND PROTOCOLS

2.1 Growth and Maintenance of *P. aeruginosa*

2.1.1 Growth Medium

All bacteria were grown in Luria-Bertani (Lennox) broth (LB) (10g tryptone, 5g yeast extract, 5g NaCl per liter) unless otherwise specified. For mutants suffering increased sodium sensitivity, the Na^+ concentration in the LB medium was adjusted appropriately, as indicated when necessary. Minimal medium adapted from synthetic CF sputum medium (SCFM)[57] containing 0.2 M $NaHPO_4$, 0.2 M Na_2HPO_4, 2.28 mM NH_4Cl, 14.9 mM KCl, 10 mM MOPS, 271 μM K_2SO_4, 2.5 g/L casamino acids, 1.754 mM $CaCl_2$, 0.606 mM $MgCl_2$, 36 μM $FeSO_4$, 3 mM glucose and the desired concentration of NaCl was used to assess growth in nutrient limited conditions.

2.1.2 Bacterial Growth Curves

The growth of bacterial strains was monitored following a method adapted from that reported previously.[52] Medium containing 10 g/L tryptone, 5 g/L yeast extract and 60 mM bis tris propane was prepared and adjusted to feature the desired pH and [Na^+] conditions to be tested. Overnight cultures were grown in 5mL LB for 16 hours at 37°C with shaking at 200rpm. Culture density was measured via absorbance at 500 nm and cell suspensions were diluted to an OD_{500} of 1.0 using fresh LB broth of the corresponding pH and minimum [Na^+] to be tested. 10 uL of the diluted culture was used to inoculate 190 uL of fresh medium in a 96-well plate (Costar transparent flat bottom) to a starting OD_{500} of 0.05. Plates were covered and incubated at 37°C with continuous orbital shaking at 217 rpm (Tecan Infinite Magellan M1000 Pro). OD_{500} was measured every 30 minutes over 20 hours of continuous growth. OD_{500} values were corrected for background absorbance and averaged across two biological replicates with three technical replicates each, with standard deviation for each timepoint calculated accordingly. Doubling times and the related

statistical analyses were calculated in R using the growth-rates package with the easy linear fitting method.[58,59]

2.2 Mutant Generation

To assess the individual and collective properties of the ion-transporting enzymes of *P. aeruginosa*, we obtained and/or generated a collection of mutant strains designed to interrupt the expression, and by extension the function, of select enzymes in the *P. aeruginosa* genome. The construction of these mutant strains allows for the functional isolation of the enzymes of interest, enabling the investigation of their individual properties.

2.2.1 Summary of Mutant Strains

The wild-type *P. aeruginosa* strain PAO1 was obtained from the University of Washington[60] and used as the background strain for all subsequent mutations unless otherwise indicated. Mutation of the genes of interest was achieved by two methods: (i) transposon insertion to disrupt gene expression or (ii) gene deletion from the chromosome. All transposon insertion mutants were purchased from the University of Washington transposon library.[60]

2.2.1.1 NADH Dehydrogenase Mutant Strains

Mutant strains which featured disruption and/or deletion of one or more of the NADH:quinone oxidoreductase enzymes are summarized below in Table 2.1.

Table 2.1: NADH dehydrogenase mutant strains.

Strain	***Description***	***Source of Reference***
Δ*nqrF*	PW6010, *nqr*F-G08:: ISlacZ/hah	60
Δ*nuoG*	PW5420, *nuo*G-C11:: ISphoA/hah	60
Δ*ndh*	PW8644, *ndh*-F12:: ISlacZ/hah	60
Δ*nqrF*Δ*nuoG*	Chromosomal deletion of *nqrF* in the Δ*nuoG* background	this study
Δ*nqrF*Δ*ndh*	Chromosomal deletion of *nqrF* in the Δ*ndh* background	this study
Δ*nuoG*Δ*ndh*	Chromosomal deletion of *ndh* in the Δ*nuoG* background	this study

The single deletion mutant strains were purchased from the Two-Allele Library.[60] The double deletion mutant strains were generated by the gene deletion protocol outlined below (Section 2.2.2), using the indicated single deletion mutant strains as backgrounds. Primers and vectors used in the creation and maintenance of the NADH dehydrogenase mutant strains are summarized in Table 2.2 and Table 2.3, respectively.

Table 2.2: Primers employed for the design and confirmation of NADH dehydrogenase mutants.

Primer	***Description***	***Sequence 5'-3'***
nqrF_cfrm_R1	For confirmation of the Δ*nqrF* strain.	cgtgatcggattcgagattt
lacZ_cfrm		gcgtagatacgacgcacca
ndh_cfrm_R1	Used with above lacZ_cfrm primer for confirmation of the Δ*ndh* mutant.	ctacccatcagattgcccat
nuoG_cfrm_F1	For confirmation of the Δ*nuoG* mutant.	tatccacgtagacggcaaga
hah138_cfrm		cgggtgcagtaatatcgccct
PaNqrKO_HR_Down_F	For amplification of Downstream Homologous Recombination (DHR) arm for deleting NQR operon from *P. aeruginosa* genome.	gggcccgaagactagaccagcgc gagaatatcctgctgga
PaNqrKO_HR_Down_R		gggcccgaagactatcgcgaaata gttgcggtaatcgcc
PaNqrKO_HR_UP_F	For amplification of Upstream Homologous Recombination (UHR) arm for deleting NQR operon from *P. aeruginosa* genome.	gggcccgaagactattgccgtagta ctcaccgcggcattg
PaNqrKO_HR_UP_R		gggcccgaagactaggtccaggcc acgttttatcttg
F_NqrKO_Scrn	For amplification of sequence -1049 bp to +1022 bp of NQR operon in the *P. aeruginosa* chromosome for confirmation of operon deletion.	tggcgatcatcatgttctcc
R_NqrKO_Scrn		gtcatggacgttctccttgg
Down-HR-F1	For amplification of DHR arm for deleting *ndh* from *P. aeruginosa* genome.	gggcccgaagactagacccgagc cacgcctcaagctgc
Down-HR-R1		gggcccgaagactagtcgtattgct ggccagcctcatgc
Up-HR-F1	For amplification of UHR arm-1 for deleting *ndh* from *P. aeruginosa* genome.	gggcccgaagactattgcatcaacc tgctcagcctgaagg
UP-HR-R1		gggcccgaagactacctcggggct cagtcggctggaca
Up-HR-F2	For amplification of UHR arm-2 for deleting *ndh* from *P. aeruginosa* genome.	gggcccgaagactagaggaccag cagaaggtcgagcag
Up-HR-R2		gggcccgaagactaggtccgacga tcacgatgcgatgg
UP_Ndh2_Seq_F	For amplification of sequence -395 bp to +198 bp of *ndh* location in the *P. aeruginosa* chromosome for confirmation of gene deletion.	cctggaaaagcacatcgaccac
Ndh2_upGene_R		cgcttcatcaatctcgtcgacg

Table 2.3: Vectors employed for the design of NADH dehydrogenase mutants.

Plasmid	*Description*	*Source of Reference*
pEX18Gm	*sacB* counter-selectable suicide vector Gm^R	this study
pEX18Gm-*nqrF*KO	pEX18Gm vector containing the *nqrF* gene deletion assembly	this study
pEX18Gm-*ndh*KO	pEX18Gm vector containing the *ndh* gene deletion assembly	this study

2.2.1.2 Na^+/H^+ Antiporter Mutant Strains

Mutant strains which featured disruption of one or more of the Na^+/H^+ antiporter enzymes are summarized below in Table 2.4. In the case of the three single-gene encoded antiporters: NhaB, NhaP, and NhaP2, single genes PA1820, PA3887, and PA5021, respectively, were deleted from the genome. For the multi-subunit antiporter Mrp, the gene encoding the MrpA subunit, PA1054, was removed from the genome, a mutation which has previously been shown to be sufficient for the inactivation of the complex.[39]

Table 2.4: Na^+/H^+ antiporter mutant strains.

Strain	*Description*	*Source of Reference*
Δ*nhab*	Chromosomal deletion of PA1820.	this study
Δ*nhap*	Chromosomal deletion of PA3887.	this study
Δ*nhap2*	Chromosomal deletion of PA5021.	this study
Δ*mrpA*	Chromosomal deletion of PAA1054.	this study
Δ*nhap*Δ*nhap2*Δ*mrpA*	Chromosomal deletion of the *nhap*, *nhap2*, and *mrpA* genes to isolate the NhaB antiporter.	this study
Δ*nhab*Δ*nhap2*Δ*mrpA*	Chromosomal deletion of the *nhab*, *nhap2*, and *mrpA* genes to isolate the NhaP antiporter.	this study
Δ*nhab*Δ*nhap*Δ*mrpA*	Chromosomal deletion of the *nhab*, *nhap*, and *mrpA* genes to isolate the NhaP2 antiporter.	this study
Δ*nhab*Δ*nhap*Δ*nhap2*	Chromosomal deletion of the *nhab*, *nhap*, and *nhap2* genes to isolate the Mrp antiporter.	this study
Δ*nhab*Δ*nhap*Δ*nhap2*Δ*mrpA*	Chromosomal deletion of the *nhab*, *nhap*, *nhap2*, and *mrpA* genes, generating a mutant strain having no Na^+/H^+ antiporters.	this study

Primers and vectors used in the creation and maintenance of the Na^+/H^+ antiporter mutant strains are summarized in Table 2.5 and Table 2.6, respectively.

Table 2.5: Primers employed for the design and confirmation of the Na^+/H^+ antiporter mutant strains.

Primer	***Description***	***Sequence 5'-3'***
nhab_Up_F	For amplification of UHR arm for deleting *nhab* from *P. aeruginosa* genome	taaaacgacggccagtgccaccgcgtaggtacgattgac
nhab_Up_R		aatgactgacgatggactccacggcaag
nhab_Down_F	For amplification of UHR arm for deleting *nhab* from *P. aeruginosa* genome	ggagtccatcgtcagtcattggctttgagcgtcgg
nhab_Down_R		agtcgacctgcaggcatgcagcggcgctgaccctgtgg
nhabKO_cfrm_F	For confirmation of the Δ*nhab* mutant.	ccgatgtcgatctccttgat
nhabKO_cfrm_R		tcaacgtgatcatcctgctc
nhapKO_cfrm_F	For confirmation of the Δ*nhap* mutant.	gaagcggtcgataatggtgc
nhapKO_cfrm_R		gagttcaacggagcactcgac
nhap2KO_cfrm_F	For confirmation of the Δ*nhap2* mutant.	ctacttcctgacctgggaag
nhap2KO_cfrm_R		gtgaatgcaggttagtggtg
mrpKO_cfrm_F	For confirmation of the Δ*mrpA* mutant.	caagatcgaaggcaccaag
mrpKO_cfrm_R		gatcgagcatgagcacgatg

Table 2.6: Vectors employed for the design of the Na^+/H^+ antiporter mutant strains.

Plasmid	***Description***	***Source of Reference***
pEX18Gm	*sacB* counter-selectable suicide vector Gm^R	this study
pEX18Gm-*nhab*KO	pEX18Gm vector containing the *nhab* gene deletion assembly, as constructed using the NEBuilder assembly protocol	this study
pEX18Gm-*nhap*KO	pEX18Gm vector containing the *nhap* gene deletion sequence	Genewiz
pEX18Gm-*nhap2*KO	pEX18Gm vector containing the *nhap2* gene deletion sequence	Genewiz
pEX18Gm-*mrpA*KO	pEX18Gm vector containing the *mrpA* gene deletion sequence	Genewiz

2.2.1.3 K^+/H^+ Antiporter Mutant Strains

Mutant strains which featured deletion of one of the probable K^+/H^+ antiporter genes from the *P. aeruginosa* genome are summarized below in Table 2.7. Each of the identified probable K^+/H^+ antiporters are single gene products, thus the single genes PA3660 and PA3739 were deleted from the *P. aeruginosa* genome.

Table 2.7: K^+/H^+ antiporter mutant strains.

Strain	*Description*	*Source of Reference*
Δ*Pa3660*	Chromosomal deletion of the PA3660.	this study
Δ*Pa3739*	Chromosomal deletion of PA3739.	this study

Primers and vectors used in the creation and maintenance of the K^+/H^+ antiporter mutant strains listed in Table 2.7 are summarized in Table 2.8 and Table 2.9, respectively.

Table 2.8: Primers employed for the design and confirmation of the K^+/H^+ antiporter mutant strains.

Primer	*Description*	*Sequence 5'-3'*
3660_Up_F	For amplification of UHR arm for deleting *3660* from *P. aeruginosa* genome	taaaacgacggccagtgccagatgaatcgtcgtggtgc
3660_Up_R		tcagccagcttaggcagctatccgacattc
3660_Down_F	For amplification of DHR arm for deleting *3660* from *P. aeruginosa* genome	tagctgcctaagctggctgaccaatcgc
3660_Down_R		agtcgacctgcaggcatgcatgctacagcgaactctacttc
3660KO_cfrm_F	For confirmation of the Δ*3660* mutant.	gtagcgatcaggtcattggtg
3660KO_cfrm_R		ctacagcgaactctacttcgac
3739_Up_F	For amplification of UHR arm for deleting *3739* from *P. aeruginosa* genome	taaaacgacggccagtgccaggcatacagcacttcgag
3739_Up_R		agtcggcgatgttctggtccatcgaggattc
3739_Down_F	For amplification of DHR arm for deleting *3739* from *P. aeruginosa* genome	ggaccagaacatcgccgactagacttcaac
3739_Down_R		agtcgacctgcaggcatgcacaggtcgatctgttgcag
3739KO_cfrm_F	For confirmation of the Δ*3739* mutant.	gcaatagcgatagaagccacg
3739KO_cfrm_R		ggcaatgcgaatattgtcgaagc

Table 2.9: Vectors employed for the design of the K^+/H^+ antiporter mutant strains.

Plasmid	*Description*	*Source of Reference*
pEX18Gm	*sacB* counter-selectable suicide vector Gm^R	This study
Δ3660_ pEX18Gm	pEX18Gm vector containing deletion mutant sequence for PA3660, constructed using the NEBuilder Assembly Protocol.	This study
Δ3739_ pEX18Gm	pEX18Gm vector containing deletion mutant sequence for PA3739, constructed using the NEBuilder Assembly Protocol.	This study

2.2.2 Overview of Gene Deletion Design and Construction

Gene knockout mutant strains generated for this study were constructed according to a 2-step allelic exchange protocol adapted from that previously outlined by Hmelo et. al.[61] To achieve gene deletion, sequences flanking the gene of interest in the *P. aeruginosa* chromosome were identified and cloned together to effectively 'splice' the gene of interest from the chromosome sequence. The regions of homology flanking the gene of interest were assembled as a continuous sequence in an allelic exchange suicide vector, as visualized in Figure 2.1A, in effect deleting the identified gene. The mutant vector was then transformed into a conjugative donor strain, in this case S17 *E. coli*, and subsequently introduced into the desired *P. aeruginosa* background strain via biparental conjugation. Following successful conjugation, homologous recombination will initiate a first crossover event, indicated in Figure 2.1B, resulting in the integration of the vector sequence into the *P. aeruginosa* chromosome. The resulting strain can be selected for by antibiotic resistance via the antibiotic resistance cassette located in the vector sequence. A second cross over event will follow, resulting in the removal of the vector sequence and the seamless integration of the gene deletion mutant sequence into the *P. aeruginosa* chromosome. Cells having undergone a second crossover event are isolated by sucrose selection, with those cells still harboring the vector sequence having sensitivity to sucrose due to the presence of a *sacB* promoter/gene pair. Second crossover strains are then screened for successful mutation via PCR, with positive mutants featuring the integration of the flanking homologous regions as a continuous sequence in the chromosome, effectively excising the gene of interest and producing a mutant lacking the gene product.

Homologous recombination regions were selected upstream and downstream of the gene to be deleted, indicated as the upstream homologous recombination (UHR) region and downstream

homologous recombination (DHR) regions (Fig. 2.1A). The optimal length for the homologous regions, ranging from 500-800 bps in length, was selected relative to the length of the gene to be deleted to ensure maximum crossover efficiency.[61] pEX18 mutant vectors were obtained by two methods: (i) construction by Genewiz or (ii) via the NEBuilder Assembly protocol. For those vectors constructed in this study, primers were designed with the help of the NEBuilder Assembly Tool (Version 2.3.0) to include sequence extensions which enabled the cloning of the UHR and DHR regions into the pEX18 vector. Vectors contained a gentamycin resistance cassette and SacB promoter/gene pair to enable antibiotic and sucrose selection.[61]

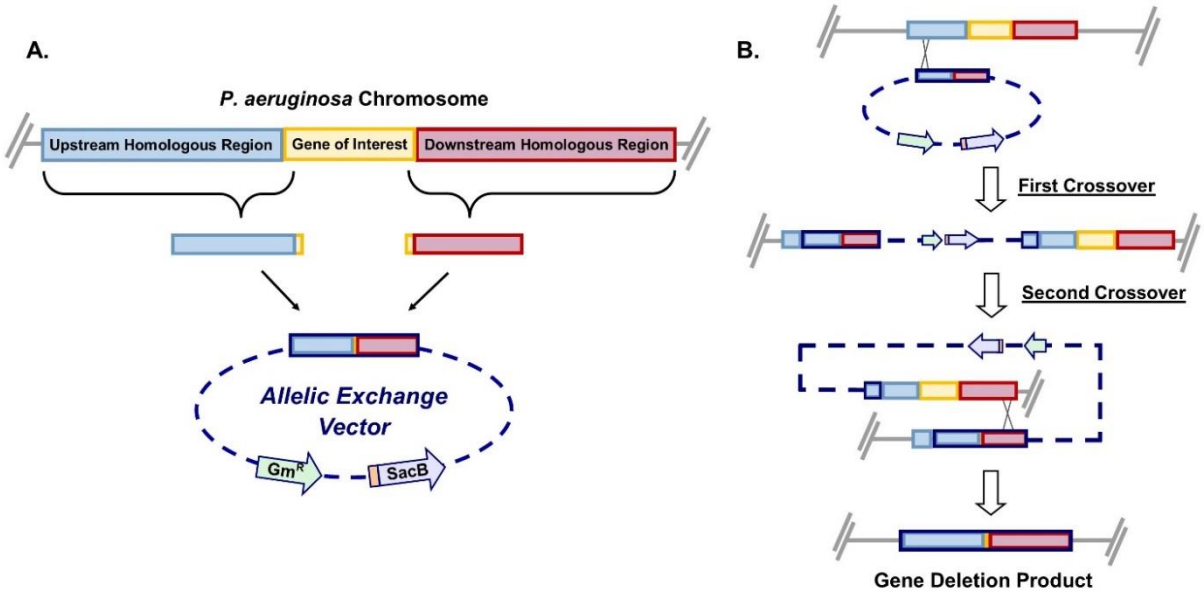

Figure 2.1: Overview of cloning procedure. (A) Design of the mutant allelic exchange vector. In the case of this study the vector is the pEX18 plasmid harboring a gentamycin resistance cassette (green) and a sacB promoter/gene pair (orange/purple) to enable antibiotic selection and sucrose sensitivity counter-selection. (B) Scheme demonstrating the process of two step allelic exchange.

2.2.3 Cloning Protocol and Mutant Confirmation

2.2.3.1 Transformation of S17 E coli

The conjugation capable *E. coli*, strain S17, was grown in 50mL LB inoculated with 1mL of an overnight culture. Cells were grown to mid-logarithmic phase (~3-4 hours) at 37°C with shaking at 200 rpm and subsequently harvested via centrifugation at 4200 rpm for 30 mins at 4°C.

Pelleted cells were rinsed with 20-25 mL of chilled 10% (v/v) glycerol to remove salts and centrifugation was repeated. A second wash of 1 mL of 10% (v/v) glycerol was performed and cells were pelleted at 10000xg for 30 mins at 4°C. Cells were then resuspended in 1 mL of 10% (v/v) glycerol and divided into 100-200 µL aliquots for electroporation. 2-5 µL of the mutant plasmid sample were added into a chilled aliquot of S17 *E. coli* cells and mixed briefly. Plasmids were transformed into electrocompetent S17 *E. coli* cells via electroporation by applying 2.5 V to the cell/plasmid mixture and immediately transferring to 1 mL of SOC media (20 g/L tryptone, 5 g/L yeast extract, 10 mM NaCl, 2.5 mM KCl, 10 mM $MgCl_2$, 10 mM $MgSO_4$, 20 mM glucose). Electroporated cells were then grown for 1 hour at 37°C with shaking at 200 rpm and 50-100 µL of the resulting culture were plated on LB agar plates containing 20 µg/mL gentamycin and incubated overnight at 37°C. The resulting colonies were screened for successful plasmid uptake by PCR and plasmid-harboring strains were cultured and stored as glycerol stocks at -80°C.

2.2.3.2 Biparental Conjugation

The *E. coli* S17 strain harboring the mutant plasmid of interest and the desired *P. aeruginosa* background strain are cultured to be crossed. Cultures of ~3 mL of no-salt LB (NSLB) are inoculated from an overnight culture. *E. coli* cultures are grown at 37°C with shaking at 200 rpm in the presence of 25-50 µg/mL gentamicin to maintain the mutant plasmid. *P. aeruginosa* cultures are grown at 42°C in order reduce the production of antibacterial effectors and generate cells with are more amendable to mating. Both cultures are grown to an OD_{600} ~0.5-0.6. Once cultures reach the desired density 1.5 mL of the *E. coli* culture and 0.5 mL of the *P. aeruginosa* culture are harvested via centrifugation at 10,000 x g for 5 minutes. The supernatant is discarded and the remaining pellets are resuspended in ~50 µL of fresh LB. The *E. coli* and *P. aeruginosa* cell suspensions are then mixed briefly by pipetting and deposited into a contained ‘puddle’ on a prewarmed LB agar plate. The plate is left open to allow the ‘puddle’ to dry next to a sterile flame,

after which the plate is incubated overnight at 30°C to enable the exchange of the mutant plasmid from the conjugative donor *E. coli* strain to the *P. aeruginosa* strain.

The resulting 'puddle' coculture is scrapped from the plate using a pipet tip and resuspended in 1 mL of sterile 1X phosphate buffered saline (PBS) containing 137 mM NaCl, 2.7 mM KCl, 8 mM Na_2HPO_4, 2 mM KH_2PO_4, pH 7.4. The resuspension mixture is then plated in varying amounts (50 μL, 100 μL, 200 μL) onto Vogel-Bonner minimal medium (VBMM) agar plates supplemented with 50 μg/mL gentamicin. VBMM agar is supplemented with 10 mM citrate as a carbon source and can be used to select against *E. coli* due to its inability to utilized citrate as a carbon source during aerobic growth.[62] Gentamicin is used to select for the cells which have successfully undergone the first cross over event. Plates are left to incubate aerobically overnight at 37°C. The resulting colonies are screened for successful plasmid integration and positive colonies are cultured in ~500 μL NSLB supplemented with 25-50 μg/mL gentamicin. The cultures are grown for 8-10 hours at 37°C with shaking at 200 rpm. Following growth, the cultures are serially diluted relative to the apparent density and the diluted cell samples are plated onto NSLB agar plates supplemented with 15% sucrose. The plates are left to incubate overnight at 37°C and the resulting colonies are screened for mutant sequence integration and successful gene deletion via PCR using the designated confirmation primers listed in Tables 2.5 and 2.8. Successful mutants were cultured were cultured and stored as glycerol stocks at -80°C. Single gene deletion strains were verified via sequencing of the confirmation product by Eurofins (Louisville, KY, USA). The triple and quadruple deletion strains summarized in Table 2.4 were verified via whole genome sequencing performed in the CBIS genomics core by Dr. Yang Bai.

2.3 Membrane Preparation

2.3.1 Membrane Fragment Preparation

Cultures were inoculated from overnight cultures to a starting OD_{600} of 0.05 in 1 L LB and

grown aerobically until mid-exponential (6.5 hours) and stationary (22 hours) phases. Cells were harvested by centrifugation in a Sorvall SLC-6000 rotor at 3860 x g for 30 min at 4ºC and washed with TCDG buffer. Cells were lysed via three passes through a microfluidizer cell disrupter at ~80 psi in the presence of PMSF and DNaseI. Cell debris was removed from solution by centrifugation at 5856.4 X g for 30 min at 4ºC and the remaining supernatant was centrifuged for at least 5 h in a Beckman Type Ti45 rotor at 185511.4 x g to collect the cell membranes. Membranes were resuspended in a small volume of TCDG buffer and frozen at -80°C until needed. Membrane protein concentration was determined using the Pierce Rapid Gold BCA Protein Assay Kit (Thermo). Measurements were done in triplicate and averaged.

2.3.2 Everted Vesicle Preparation

Cultures were inoculated from overnight LB cultures to a starting OD_{600} of 0.05 in 1 L LB and grown until stationary phase (~16 hours). Cells were harvested via centrifugation at 4200 rcf for 30 minutes at 4°C and washed with ~50 mL chilled TCDG buffer (10mM Tris-HCl, 140mM choline chloride, 10% glycerol and 0.5mM dithiothreitol, pH 7.5). Centrifugation was then repeated to re-pellet the cells and the subsequent pellet was resuspended in 35m mL TCDG buffer supplemented with PMSF to inhibit proteases released upon cell lysis and DNaseI to digest DNA released from the cell. Cells were simultaneously lysed and everted via a single pass through a french pressure cell at 10,000psi. Cell debris was pelleted via centrifugation at 11952 x g for 30 min at 4°C, followed by the harvesting of membranes by centrifugation at 185511.4g. Membranes were resuspended and homogenized in a small volume of TCDG buffer and frozen at -80°C until analysis. Protein concentration was determined using the Pierce Rapid Gold BCA Protein Assay Kit (Thermo). Measurements were done in triplicate at 1:20 dilutions and averaged.

2.4 Enzyme Activity Assays

2.4.1 NADH:Quinone Oxidoreductase Activity Assay

NADH:Ubiquinone oxidoreductase activity was measured spectrophotometrically following the changes in absorbance at 340 nm (ε_{NADH}= 6.22 mM^{-1} cm^{-1}) as reported previously.[63] Assays were conducted in 1mL reaction volumes containing 100 mM NaCl, 50 μM ubiquinone-1 (UQ1), and 25 μg/mL membrane protein prepared as outlined above (2.3.1). Reactions were initiated by the addition of 100 μM NADH, or 100 μM deaminoNADH (dNADH) where specified, and substrate absorbance was measured for 50 seconds following NADH addition.

2.4.2 Na^+/H^+ Antiporter Activity Assay

Antiporter activity was measured via the monitoring of acridine orange fluorescence in the presence of membrane vesicles as previously reported by Rosen.[64] 50ug aliquots of everted vesicles were suspended in BTP Buffer (50mM BisTris Propane, 140mM Choline Chloride, 5mM $MgCl_2$, pH 7.0-8.5 with HCl) containing 1μM acridine orange. The cuvette was placed into a Spex Fluorolog Tau-3 fluorescence spectrophotometer (Horiba) and allowed a 3-minute incubation with stirring at 25°C. Following incubation, time-based fluorescence monitoring was performed with excitation at 490nm, emission at 525nm and 2.25nm slits respectively. The signal was monitored for 100 seconds, after which 20 μL of 250 mM Tris-Succinate was added to solution to stimulate respiration and acridine orange resultingly became sequestered within membrane vesicles, causing the quenching of measurable fluorescence (Q). A period of 250 seconds is allowed for the system to reach steady-state fluorescence, after which the desired concentration of Na^+ is added to stimulate ion exchange across the membrane. As protons are translocated out of the membrane vesicles, acridine orange molecule will follow and regain their previously quenched fluorescence upon exiting the vesicle. The degree of fluorescence recovery resulting from Na^+ addition represents Na^+/H^+ antiporter activity (ΔQ). Fluorescence dequenching is monitored for 100 seconds following the addition of the substrate ion, at which point 2mM NH_4Cl is added to solution to reach a reference of maximum fluorescence (Q_{max}). Cation/H^+ antiport activity is calculated as

follows: $\Delta Q/(Q_{max} - Q) \times 100$. Michaelis Menten fitting and kinetic parameter calculation were carried out with GraphPad Prism 6 software (www.graphpad.com/ guides/prism/6).

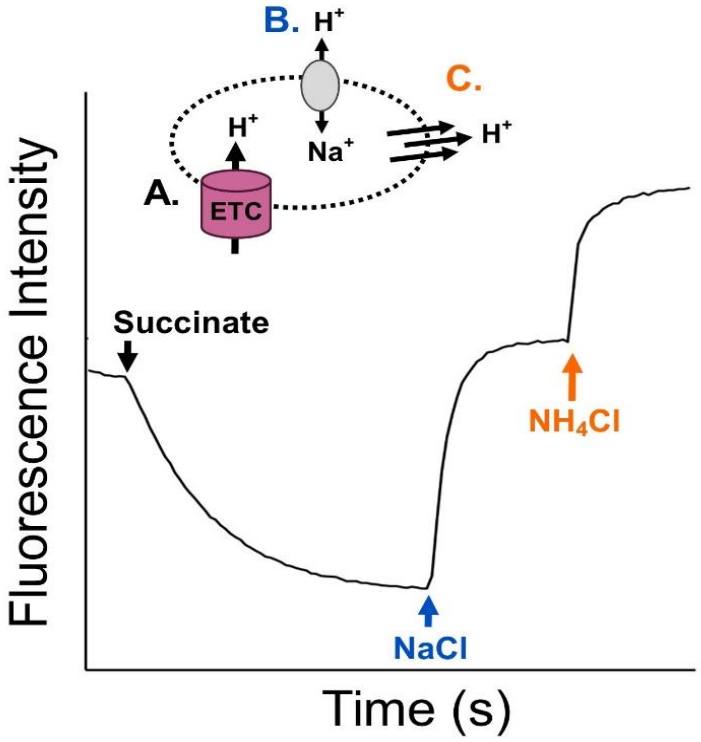

Figure 2.2: Overview of antiporter activity assay. Respiration is initiated by the addition of 2.5 mM tris-succinate (A), resulting in the accumulation of acridine orange inside the membrane vesicles and subsequent fluorescence quenching. Once a steady state is reached, the desired concentration of cation substrate (here represented as NaCl) is added to initiate antiporter activity (B), represented as the fluorescence 'de-quenching'. Addition of 1mM NH_4Cl dissipates the H^+ gradient and establishes the 100% fluorescence dequenching reference (C).

2.5 Transcription Profiling

2.5.1 Samples Preparation and Processing

Wild type and Δ*nqrF* strains were inoculated from overnight cultures (15 h) to a starting OD_{600} of 0.02 in 50 mL LB medium containing 50 mM NaCl. Three cultures of each strain were grown aerobically at 37°C with shaking at 200rpm until mid-exponential (4 h) and stationary (15 h) phases. 1.5 x 10^8 cells were harvested by centrifugation at 16,000 x g for 1 min at 4°C and rinsed with 1mL of ice-cold phosphate buffered saline (PBS). The three pellets for each strain and growth

phase were frozen with "RNA-later" (ThermoFisher). RNA extraction and processing, library preparation, and Illumina sequencing were performed by GENEWIZ (South Plainfield, NJ, USA). GENEWIZ processed the resulting data as follows: reads were evaluated for sequence quality and trimmed using Trimmomatic.[65] Trimmed reads were mapped to the *P. aeruginosa* reference genome (https://bacteria.ensembl.org/Pseudomonas_aeruginosa_pao1/Info/Index/) using the Bowtie2 aligner and unique gene hit counts were calculated using featureCounts from the Subread package.[66,67] Differential gene expression analysis was carried out using DESeq2.[68] The Wald test was used to generate log2-fold changes and P-values.

3. THE THREE NADH DEHYDROGENASES OF PSEUDOMONAS AERUGINOSA: THEIR ROLES IN ENERGY METABOLISM AND LINKS TO VIRULENCE

3.1 Introduction

Pseudomonas aeruginosa is an opportunistic pathogen characterized by an almost ubiquitous environmental presence and a broad infectious profile.[3,8] This microbe can inhabit a wide range of distinct niches and give rise to a variety of chronic infections in human hosts, many of which are life-threatening.[11] *P. aeruginosa* is the 4th most common nosocomial pathogen and the primary cause of mortality in cystic fibrosis (CF) patients.[12,23] The ability of this microbe to proliferate in so many different, and frequently hostile, environments has been attributed to its robust adaptability, arising from the flexibility of its metabolic processes.[14-16]

A key point where this metabolic flexibility is apparent is in the organization of the respiratory chain, which is one of the most highly branched among bacteria. The respiratory chain of *P. aeruginosa* includes several dehydrogenases, the cytochrome bc_1 complex, and five terminal oxidases that operate at different concentrations of oxygen.[2] It has been shown that this bacterium selectively expresses different respiratory enzymes/pathways depending on the availability of nutrients, oxygen, and other electron acceptors.[17-20,69] Such adaptations are important for colonization of infection sites, particularly in the lungs of patients suffering CF, where the bacteria are challenged with low nutrient and oxygen availability.[23] Therefore, this respiratory flexibility is likely to be a key factor in the success of *P. aeruginosa* as an opportunistic pathogen.

Perinbam et. al. recently identified a distinct shift in NADH metabolism which is associated with virulence in *P. aeruginosa*.[24] At the beginning of its respiratory chain, *P. aeruginosa* has three

---

This chapter has been submitted to: Hreha, T. N.; Foreman, S.; Duran-Pinedo, A.; Allen, J. P.; Diaz-Rodriguez, P.; Jones, J. A.; Ferrara, K.; Bourges, A.; Rodriguez, L.; Koffas, M. A. G.; Hahn, M.; Hauser, A. R.; Barquera, B. The Three NADH Dehydrogenases of *Pseudomonas aeruginosa*: Their Roles in Energy Metabolism and Links to Virulence. *PLOS One.* **2020.**

different NADH dehydrogenases which are responsible for the oxidation of cellular NADH: NUO, NQR, and NDH2.[2,25] All three of these enzymes carry out the same redox reaction, accepting electrons from NADH and passing them to the quinone pool, but they differ in their ion pumping and energy conservation properties. NQR and NUO conserve energy by coupling the electron transfer to the translocation of ions across the cell membrane, contributing to an electrochemical membrane gradient.[26-29,70] NDH2 catalyzes the same redox reaction without ion pumping or energy conservation, but its activity has been implicated in a rescue-redox system than can balance the $NADH/NAD^+$ ratio to avoid toxic effects of excess NADH.[26,31] Given the highly branched character of respiratory pathways in *P. aeruginosa*, it is likely that the three NADH dehydrogenases make the organism more adaptable. However, little is known about their actual physiological roles.

Two previous publications have addressed these questions. Torres et. al. characterized a series of deletion mutants and concluded that NUO and NDH2 together are the primary NADH dehydrogenases during aerobic growth in rich medium (LB), while NUO is required for anaerobic growth and virulence in plant (lettuce) and insect (*Galleria mellonella*) models.[54] They also concluded that NQR has minimal activity and plays only a minor role in *P. aeruginosa* physiology. In contrast, Liang et. al. reported that NQR is the most active NADH dehydrogenase in wild type *P. aeruginosa* (PAO1) during aerobic growth in rich medium.[71] These inconsistencies underline the importance of further study of the roles of these enzymes.

Here, we have characterized the roles of the three NADH dehydrogenases using a series of single-deletion mutants, each of which lacks one of the enzymes, and a series of double-deletion mutants, each of which has only one of the three. All of the mutant strains were able to grow well in both rich and minimal medium, although the strain lacking NUO consistently showed an

extended lag phase prior to entering exponential growth. In each of the mutants, the enzymes that remain all contributed to NADH dehydrogenase activity, in both exponential and stationary phases. From this we concluded that *P. aeruginosa* does not switch between different NADH dehydrogenases in different growth conditions. Instead, the presence of three parallel enzymes confers resilience on its energy production systems. Surprisingly, we also discovered that, in some of the deletion mutants, the virulence factor pyocyanin, which is normally characteristic of stationary phase, began to be produced earlier, and in much larger quantities than in the wild type. We tested one such strain, the one lacking NQR, in two model host systems, macrophages and mice, and found that in both cases the mutant bacteria had become much more effective in killing the mammalian host cells. These findings suggest that in *P. aeruginosa*, NADH metabolism is closely involved in the control of virulence.

3.2 Methods and Materials

3.2.1 Bacterial Strains and Growth Conditions

The wild-type PAO1 and single mutant strains were purchased from the Two-Allele Library.[60] All *P. aeruginosa* strains used for this study are shown in Table 2.1. Additional bacterial strains and plasmids used in this study are listed below in Table 3.1. Strains were grown in Luria Bertani (LB) broth (Miller) unless otherwise specified. When used, antibiotic concentrations were as follows: *Escherichia coli* strains were grown in 30 μg/mL kanamycin, 10 μg/mL tetracycline, 25 ug/mL gentamicin, and 12 μg/mL chloramphenicol. *P. aeruginosa* strains were grown in 50 μg/mL tetracycline, 100 μg/mL chloramphenicol, 100 μg/mL gentamicin. The NQR complementation strain pHERD28T-Cm-His-NQR-Cm was grown in the presence of 12 μg/mL chloramphenicol and 0.2 % (w/v) arabinose as an inducer of expression of the *nqr* operon.

3.2.2 NQR Complementation

The *nqr* operon was cloned into the pHERD28T-Cm-His-NQR-Cm using standard molecular biology protocols (Tables 3.1 and 3.2). The chloramphenicol resistance marker was amplified from pKD320 and inserted into the pHERD28T-HIS-NQR. pHERD28T-HIS-NQR backbone was amplified using Herculase Fusion polymerase. Insert and backbone were purified using EZNA Cycle Pure Kit (Omega BioTek) and assembled using the Gibson Assembly kit (NEB). The resulting mixture was transformed into Chemically Competent DH5alpha cells and screened via restriction digest. pHERD28C-His-NQR-Cm from DH5alpha was transformed into

Table 3.1: Strains and plasmids used in this study.

Strain	Description	Source
Escherichia coli		
S17 lpir	*thi pro hsdR hsdM recA* RP4 2-Tc::Mu-KnR::Tn7 (Tp^R, Sp^R, Sm^R)	This study
NEB 5-a	*fhuA2* Δ(*argF-lacZ*)U169 *phoA glnV44* Φ80 Δ(*lacZ*)M15 *gyrA96 recA1 relA1 endA1 thi-1 hsdR17*	NEB
Plasmids		
pEX18Gm	*sacB* counter-selectable suicide vector Gm^R	This study
pEX18Gm_BbsI	*sacB* counter-selectable suicide vector Gm^R	This study
pEX18Gm-*nqrF*KO	pEX18Gm vector containing the *nqrF* gene deletion assembly	This study
pEX18Gm-*ndh*KO	pEX18Gm vector containing the *ndh* gene deletion assembly	This study
pHERD28T-His	6X-histidine- araC-pBAD, Tp^R	73
pHERD28T-His-NQR	*nqr* operon cloned into the pHERD28T-His	This study
pHERD28C-His-NQR	pHERD28T-his-NQR Cm^R replacing Tm^R	This study
pKD3	Source of the chloramphenicol resistant cassette (Cm^R)	74

Table 3.2: Primers used in this study.

Primer	Sequence 5' to3'	Description/used for
Cm_FWDw/Homology	cttttctgtgactggtgagtttctcatcgcagtactgttgtattc	Amplification of the chloramphenicol resistance cassette from the pKD3 plasmid
Cm_REVw/Homology	gattcacaagaaggattcgacatggagaaaaaaatcactggatatacc	
pHERD28His_FWDNoTm	catgtcgaatccttcttgtgaatc	Amplification of the pHERD28T-HIS-NQR backbone
pHERD28His_REVNoTm	gaaactcaccagtcacagaaaag	

wild type (PAO1) by electroporation, according to Choi et al.[72] 6 mL of an overnight culture was centrifuged, washed twice with 1mL aliquots of 300 mM sucrose, and resuspended in 300 µL300 mM sucrose. 300 ng of vector were mixed with 100 µL of competent cells, and electroporated (20 µF, 200 Ohms, and 2.5 kV). Immediately after the voltage was applied, 1 mL of LB broth was added to the cells, and they were allowed to recover for 1 hour at 37°C, before plating on LB plus appropriate antibiotics. The pHERD28T-HIS-NQR strains was grown in LB in the presence of 0.2 % (w/v) arabinose to induce the expression of the nqr operon. The expression of NQR was first tested using a Western blotting using anti-Histidine tag antibodies. The NQR complex was partially purfied using a Ni-NTA using a similar protocol as reported before.[75]

3.2.3 Pyocyanin Assay

Pyocyanin was extracted using a modified version of the protocol described by Koley et al.[76] 5 mL cell cultures were inoculated with 1 x 10^8 cells from an overnight culture and allowed to grow at 37°C in an orbital shaker operating at 200 rpm for the desired length of time. Following growth, cells were removed by centrifugation and the cell supernatant was subjected to an organic extraction using 1-3 mL of chloroform. The organic lower layer was transferred to a new tube and centrifuged for 1 min at maximum speed. The organic supernatant was transferred to a new tube and dried under a N_2 stream until no solvent remained. The resulting pellet was resuspended in 1

mL 50 mM Tris-HCl pH 8.0, and absorbance was measured at 690 nm. The concentration of pyocyanin was determined using an extinction coefficient of 4,130 M^{-1} cm^{-1}.[76] For pyocyanin production in the complementation strain, concentration was normalized by the OD_{600} of the culture at the time of harvesting.

3.2.4 Biofilm Quantification

Biofilm formation was assessed according to the method outlined by Tram et. al.[77] Overnight cultures were diluted to an OD_{600} of 0.5 and transferred in 100 uL aliquots to a 96-well plate (Nunc). The plates were incubated at 37°C, without shaking, for 6 hours (mid attachment) or 24 hours (mature biofilm).[77,78] Following incubation, the supernatant was removed from each well, and the attached biofilm was washed three times with water, then incubated in 20μL 1% (w/v) crystal violet (Fisher) for 15 minutes. Wells were then washed three times with water, and the remaining crystal violet was extracted from the biofilm with 100 μL of MBDS (modified biofilm dissolving solution) consisting of 10 % (w/v) SDS and 80 % EtOH. The resulting MBDS solution was transferred to a new 96-well plate and absorbance at 600 nm was read in a plate reader (Tecan Infinite Magellan M1000 Pro).

For image analysis, overnight cultures were diluted to an OD_{600} of 0.5 and transferred in 200μL aliquots to an 8-well coverslip. Samples were incubated at 37°C for 6 or 24 hours. Biofilms were washed twice with phosphate-buffered saline (PBS) and fixed with 4% (v/v) paraformaldehyde in PBS. Fixed biofilms were permeabilized with 1 % (v/v) TritonX-100 in PBS, and then stained with 30 μM propidium iodide. The stained biofilms were washed 5 times with PBS before imaging. Images were captured by a Nikon eclipse Ti-U inverted microscope, equipped with a scan module, using a Nikon Plan Flour 60×, 1.30 oil DIC objective lens, and an infrared pulsed laser at 970 nm with a 530/43 nm emission filter. Z-stacked images were collected

over 10μm, and the image size was 20 μm × 20 μm (256 pixels × 256 pixels). Images were analyzed using VistaVision software (ISS, Colorado Springs, CO). Biofilm analysis was done through COMSTAT2 (www.comstat.uk).[79,80]

3.2.5 Antibiotic Resistance Determination

Antibiotic resistance was determined by inoculating 4 μL of an exponential phase culture (OD_{600} = ~0.5) into 1 mL of LB with appropriate antibiotic in a 24-well plate. Plates were grown with shaking at 37°C. The MIC was determined to be the concentration at which no detectable growth could be seen 24 hours after inoculation.

3.2.6 Macrophage Toxicity Model

Overnight cultures of *P. aeruginosa* WT and mutants were grown from a single colony in Dulbecco's modified Eagle's medium (DMEM) (Gibco), 10% (w/v) fetal bovine serum (FBS) (Hyclone) and 36 μM $FeSO_4$. Overnight cultures were diluted 1:100 in 10 mL DMEM + 10% FBS and grown for approximately three hours before 250,000 cells in a total of 200 μL were added to the macrophages. RAW 264.7 cells from a murine macrophage cell line (ATCC, Manassas, Virginia) were maintained in DMEM (Gibco) supplemented with 10 % (w/v) FBS. Macrophages were plated at a density of 12,500 cells/cm^2 on 24-well tissue culture polystyrene plates. After that, cell monolayers were incubated for 6 hours at 37ºC and 5% CO_2 with bacterial suspensions using a multiplicity of infection (MOI) of 1. Additionally, the initial number of cells was assessed by DNA measurement via PicoGreen assay (Invitrogen) per manufacturer's instructions. Calf thymus DNA (Sigma) was used as standard.

After the 6-hour incubation, the supernatant was collected, and macrophages were washed with DPBS (Lonza) and fixed with formalin 10% (Fisher) overnight at 4ºC. The next day wells were washed twice with DPBS and were imaged using a Zeiss Axiovert microscope. Cell toxicity

was evaluated using the Cytotoxicity Detection KitPLUS (lactate dehydrogenase, LDH; Roche). Supernatants were centrifuged at 2,500 rpm for 5 min at 4ºC and assayed in duplicate following manufacturer instructions. Absorbance was measured after 10, 20 and 25 minutes of reaction at 490 nm using a plate reader (Biotek).

3.2.7 Mouse Infection Model of Acute Pneumonia

P. aeruginosa cultures were grown overnight in 5 mL of MINS medium at 37°C with shaking (250 rpm), and then sub-cultured 1:100 into fresh MINS and regrown to exponential phase. The bacteria were collected by centrifugation and resuspended in PBS. Six- to eight-week-old female BALB/c were anesthetized by intraperitoneal injection of a mixture of ketamine (100 mg/mL) and xylazine (20 mg/mL). Mice were infected intranasally with the indicated colony-forming units (CFU) of bacteria in 50 mL of PBS. Bacterial inocula were confirmed by plating of serial dilutions onto Vogel-Bonner minimal (VBM) medium agar. All experiments were approved by the Northwestern University Institutional Animal Care and Use Committee.

For determination of the bacterial numbers in the lungs, mice were infected intranasally with c. 5-6 x 10^5 CFU of bacteria. Mice were euthanized at 24 hpi and the lungs were aseptically removed and homogenized in 5 mL of PBS. The bacterial load was determined following plating of serial dilutions onto VBM agar and incubation at 37°C for 24 hours. The results are expressed as the ratio of CFU recovered per lung (output) to the CFU present in the initial inoculum (input). The data shown are grouped from three independent experiments (n = 15 mice per strain). The black line indicates the geometric mean for each group.

For survival experiments, mice were infected intranasally with c. 4 x 10^6 CFU of the indicated bacterial strain. In all experiments, the mice were sacrificed when severe illness developed and were scored as dead. Survival was monitored for 96 hours after infection. This

experiment was repeated twice, and the results shown are from a single experiment (n = 10 mice per group). An exponential-rank test was used to analyze differences in mouse survival. A p-value < 0.05 was considered significant.

3.3 Results

3.3.1 NADH Dehydrogenase Mutants

To investigate the roles of the three NADH dehydrogenases of *P. aeruginosa*, we used mutant strains, each lacking one or more of these enzymes. We obtained three single-deletion strains (Δ*nqrF*, Δ*nuoG*, Δ*ndh*) from the University of Washington transposon library[60] and constructed three double-deletion strains, each of which retains only one of the three NADH dehydrogenases: NQR (Δ*nuoG*Δ*ndh*), NUO (Δ*nqrF*Δ*ndh)*, and NDH2 (Δ*nqrF*Δ*nuoG)*.

3.3.2 Growth of NADH Dehydrogenase Deletion Mutants

We examined the effect of the missing enzyme(s) by comparing the growth of each mutant with wild type in liquid cultures. We tested growth in a rich medium (Luria Bertani, LB) and "Synthetic Cystic Fibrosis Sputum Medium" (SCFM) a minimal medium designed to mimic the chemical conditions in the cystic fibrosis lung,[57] which can provide insights into the growth of these strains in infection-relevant settings. Since some of the NADH dehydrogenases conserve energy by pumping cations across the cell membrane, we also assayed growth at two different pH values (7.0 and 8.0) and in two different NaCl concentrations (170mM and 300mM).

Growth of the wild type was similar across all of the pH and $[Na^+]$ concentrations tested. Growth curves are shown in S1 Figure. Doubling times, calculated from early exponential growth, are in Tables A.1 and A.2. There are clear differences in growth between LB and SCFM. In the minimal medium the doubling times generally are longer and the final cell density lower in SCFM. In comparison, changes in pH and $[Na^+]$ had little systematic effect. However, at pH 8.0 and 300

mM NaCl, the doubling times in SCFM and LB are not statistically significantly different, and in these conditions, in both LB and SCFM, the growth curves show more than one phase.

Growth curves for the single-deletion mutants (Δ*nqrF*, Δ*nuoG*, Δ*ndh*) together with wild type are shown in Figure 3.1 and doubling times are shown in Tables A.1 and A.2. All of the single deletion mutants were able to grow well in both LB and SCFM and in all pH and [Na^+] conditions. The doubling times were generally longer than for the wild type, but never twice as long.

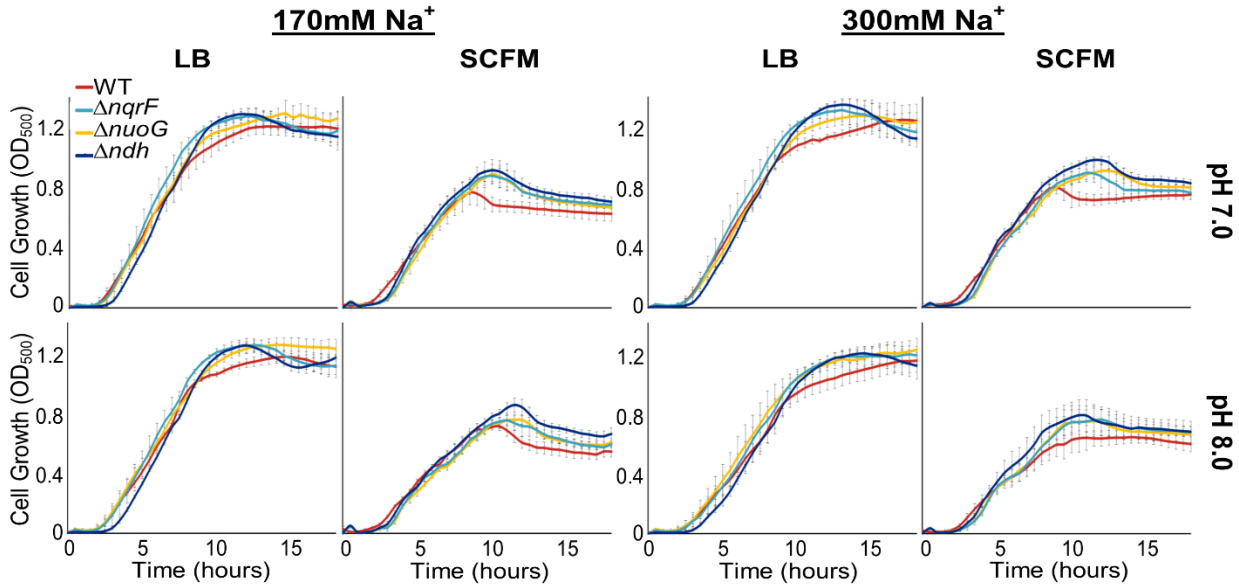

Figure 3.1: Comparison of growth of wild type and single deletion mutant strains. Growth curves of wild type PAO1 (red) and single deletion mutants Δ*nqrF* (cyan), Δ*nuoG* (yellow), and Δ*ndh* (dark blue) in LB and SCFM media at 170mM and 300mM NaCl concentrations, at pH 7.0 and 8.0. Changes in OD_{500} were measured using a Tecan Infinite M1000 Pro plate reader during 20 hours of growth at 37°C with continuous orbital shaking at 217 rpm. Each curve was constructed using two biological replicates with three technical replicates each, with standard deviation calculated accordingly and represented as error bars.

For the double-deletion mutants (Δ*nuoG*Δ*ndh*), (Δ*nqrF*Δ*ndh)*, and (Δ*nqrF*Δ*nuoG)*, growth curves are shown in Figure 3.2, and doubling times calculated from early exponential growth are compiled in Tables A.1 and A.2. As in the case of the single-deletion mutants, all of the double-deletion mutants were able to grow well. This indicates that after deletion of one or two of the three NADH dehydrogenases, the energetic pathways available to the cells are still capable of supporting robust growth.

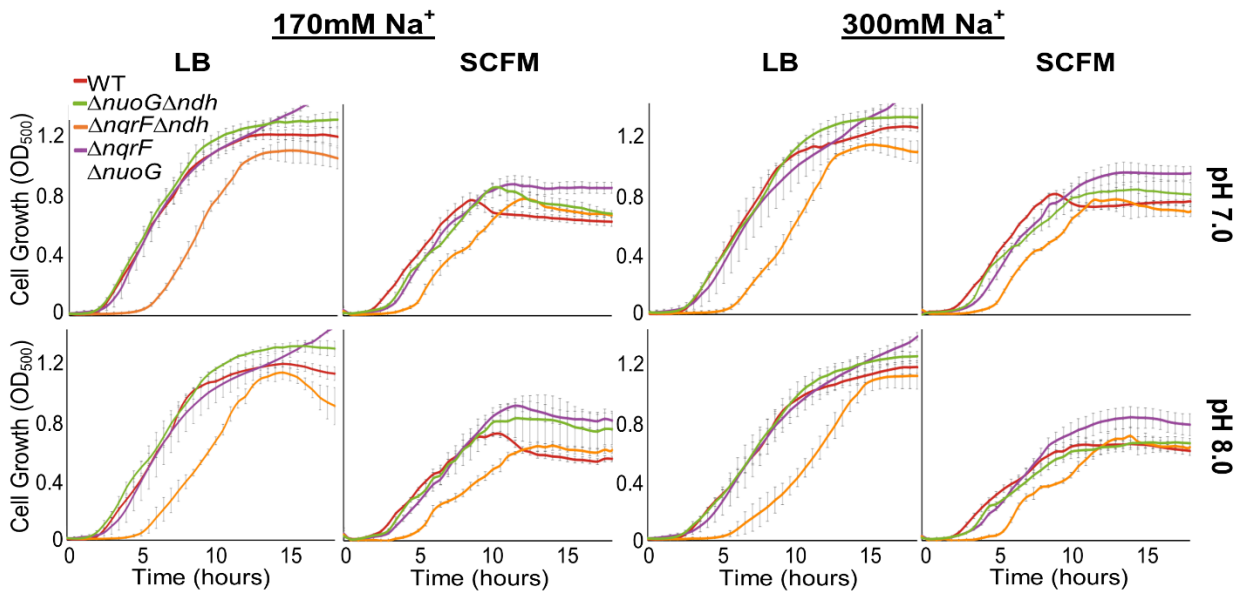

Figure 3.2: Comparison of growth of wild type and double deletion mutant strains. Growth curves of wild type PAO1 (red) and double deletion mutants Δ*nuoG*Δ*ndh* (green), Δ*nqrF*Δ*ndh* (orange), and Δ*nqrF*Δ*nuoG* (purple) in LB and SCFM media at 170mM and 300mM NaCl concentrations, at pH 7.0 and 8.0. Changes in OD_{500} were measured using a Tecan Infinite M1000 Pro plate reader during 20 hours of growth at 37°C with continuous orbital shaking at 217 rpm. Each curve was constructed using two biological replicates with three technical replicates each, with standard deviation calculated accordingly and represented as error bars.

For both single- and double-deletion mutants, rates and extents of growth were sufficient that cell membranes could be obtained for subsequent biochemical analysis (see below). The responses of the wild type to changes in type of medium (rich vs. minimal), pH and [Na^+] are still generally observed in the mutants. There are several small differences between results for wild type and the mutants. We note the following that could warrant future research: In all conditions of medium, pH and [Na^+] the mutant with only NUO (Δ*nqrF*Δ*ndh*), underwent an extended lag phase after which it was able to grow strongly. In SCFM this mutant appears to undergo diauxic growth, similar to what is observed in the wild type at pH 8 and 300 mM NaCl. In the mutant, this pattern is most marked at pH 8 where two distinct phases can be discerned, with a clear lag phase between. The doubling time of the mutant with only NQR (Δ*nuoG*Δ*ndh*) shows a strong pH dependence in SCFM, but not in rich medium. The mutant with only NDH2 (Δ*nqrF*Δ*nuoG)* shows a dependence on [Na^+] in rich medium; if there is a similar trend in SCFM it is far weaker.

3.3.3 NADH:quinone Oxidoreductase Activities in the Double Deletion Mutants

Growth measurements show that any one of the three NADH dehydrogenases is capable of supporting growth. The activity measurements confirm that all of the double-deletion strains have significant NADH dehydrogenase activity in both exponential and stationary phases. For example, in the extreme case the mutant with only NUO has only 15% of wild type activity. To quantify the NADH:quinone oxidoreductase activity for each of the three NADH dehydrogenases we measured the enzyme activity in membranes from the double deletion strains, each of which has only one NADH dehydrogenase. For each mutant strain, membranes were prepared from cells harvested in both exponential and stationary phases. NADH:quinone oxidoreductase activity was measured by following the oxidation of NADH spectrophotometrically and the activities were normalized according to total membrane protein concentration. Saturating concentrations of NADH and ubiquinone-1 were used in order to obtain initial turnover rates close to Vmax (see Materials and Methods). Use of double-deletion strains is the clearest available approach to understanding the contributions of each of the NADH dehydrogenases; many of the inhibitors typically used in respiratory chain studies are not sufficiently effective in *P. aeruginosa* (data not shown). The only selective alternative substrate, deamino-NADH, was used to analyze activity in membranes from the single-deletion strains (below).

Figure 3.3A shows initial activities for exponential and stationary phase membranes. In all cases the membranes retained significant NADH dehydrogenase activity indicating that the one remaining enzyme was expressed and active. Double deletion mutants showed significantly lower rates of NADH consumption than the wild type. In exponential phase, the mutant with only NUO had 15% of wild-type activity, while the mutants with only NDH2 and only NQR had 37% and

48%, respectively (Table A.3). In the case of stationary phase, the mutants with NQR, NUO, or NDH2 only had 48%, 46%, and 49% of wild-type activity, respectively (Table A.3). NADH dehydrogenase activity was consistently greater in membranes from stationary phase cells than in exponential phase membranes, but these data suggest that each enzyme is actively contributing to the total NADH dehydrogenase activity in wild type in both growth phases.

3.3.4 NADH:quinone Oxidoreductase Activities in the Single Deletion Mutants

We then carried out NADH dehydrogenase activity measurements on the three single deletion mutants, each of which retains two of the three enzymes. The results are summarized in Figure 3.3B. For all of the mutants, activity was lower than in the wild type, for membranes from both exponential and stationary phases. In the mutant that lacks an active NQR (Δ*nqrF*) the NADH dehydrogenase activity was 59% lower in exponential phase and 46% lower in stationary phase, compared to wild type (Table A.3). Of the three single deletion mutants, Δ*nqrF* had the greatest loss of activity in exponential phase, indicating that NQR is the major contributor to NADH dehydrogenase activity during exponential growth.

In the mutant lacking NDH2, activity in both exponential phase and stationary phase was approximately 62% relative to wild type, a decrease of 38% (Table A.3). This is consistent with the results from the double deletion mutant expressing only NDH2 (Δ*nqrF*Δ*nuoG*) which retained approximately 37% of NADH activity during exponential phase (Fig 3A). The contribution of NDH2 can also be assessed directly in membranes from wild-type cells by using deamino-NADH (dNADH) instead of NADH as a substrate. dNADH can be oxidized by NUO and NQR but not by NDH2.[81-83] Membranes from wild type cells harvested in stationary phase had 38% lower activity with dNADH compared to NADH (Figure A.2). In membranes from wild type cells harvested in exponential phase, dNADH activity was 30% lower than NADH dehydrogenase activity. Although

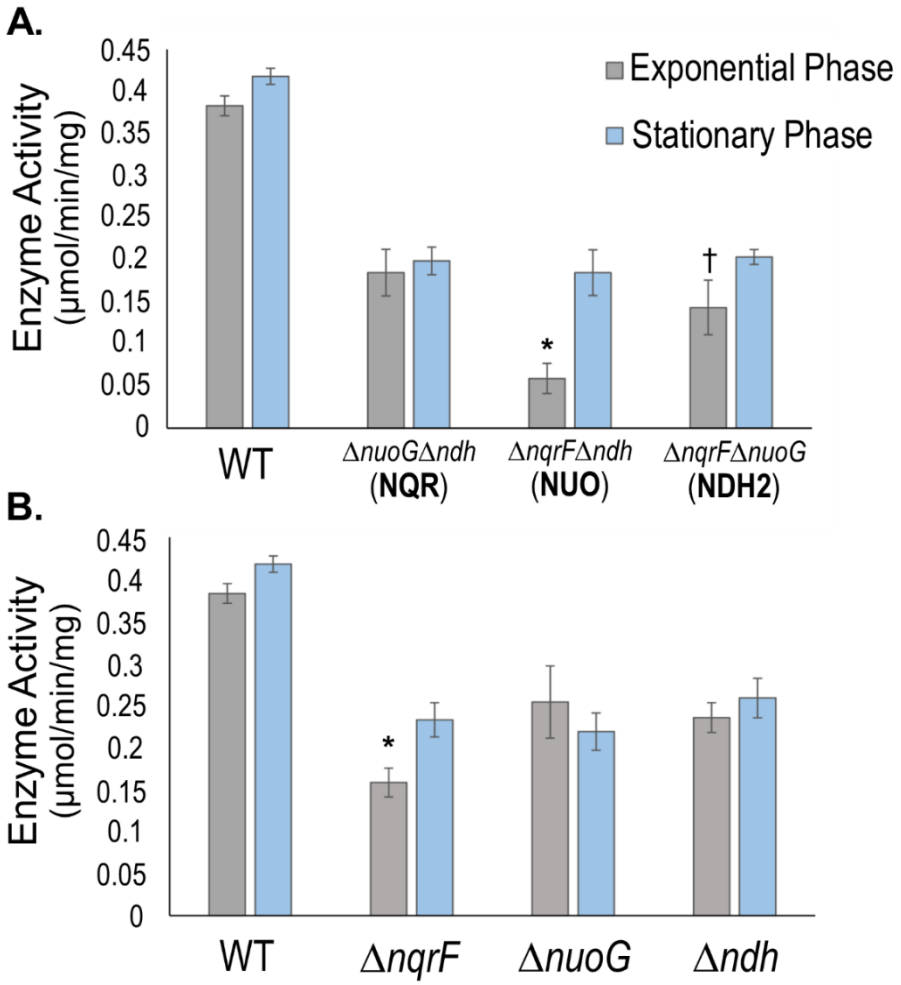

Figure 3.3: NADH:quinone oxidoreductase activities of membranes from single and double deletion mutants compared to wild type. (A) Activity in membranes from wild type (WT) and double deletion mutants Δ*nuoG*Δ*ndh* (NQR only), Δ*nqrF*Δ*ndh* (NUO only), and Δ*nqrF*Δ*nuoG* (NDH-2 only). (B) Activity in membranes from WT and single deletion mutants Δ*nqrF*, Δ*nuoG*, Δ*ndh*. Membranes were prepared from cells harvested in the exponential phase (grey) and stationary phase (blue). Enzyme activity is defined as the µmoles of NADH consumed per minute per mg of membrane protein. The reaction contained: 100 µM NADH, 50 µM ubiquinone-1 and 100 mM NaCl. Changes in absorbance were followed at 340nm (ε_{NADH}= 6.22 mM^{-1} cm^{-1}). Activities for all mutant strains were significantly lower ($p \leq 0.01$) than WT in all conditions tested, according to a one-way ANOVA analysis. The Δ*nqrF*Δ*ndh* double mutant activity was significantly lower ($p \leq 0.01$, *) than the activities of the other two double mutants. The Δ*nqrF*Δ*nuoG* double mutant activity was significantly lower ($p \leq 0.05$, †) than the Δ*nuoG*Δ*ndh* mutant. The Δ*nqrF* single mutant activity was significantly lower ($p \leq 0.01$, *) than the activities of the other two single mutants.

the almost exact correspondence of the numerical values for exponential phase membranes is probably fortuitous, these results are consistent in showing that NDH2 is responsible for a significant fraction of the total NADH dehydrogenase activity in both exponential and stationary phases.

3.3.5 Consequences of Deletion of NADH Dehydrogenases for the Physiology of *P. aeruginosa*

Two notable virulence traits of *P. aeruginosa* are (i) the production of biofilm and (ii) the secretion of pyocyanin. Both traits are controlled by quorum sensing and typically manifest themselves during stationary phase.[78] We noticed that some of the strains constructed for this study began to form biofilm earlier, and produced larger amounts of pyocyanin, than wild type. Based on these observations, we carried out a systematic study of biofilm formation and pyocyanin in these mutants.

3.3.5.1 Biofilm Formation

Production of biofilm was measured by tracking three different parameters: (i) crystal violet retention (a measure of total biofilm produced), (ii) biofilm thickness, and (iii) biofilm surface area (see 3.2.4). Samples were analyzed at mid-attachment phase (6 hours) and maturity (24 hours).[77,78] At mid-attachment, the crystal violet retention values for Δ*nqrF* and Δ*nuoG* were 1.55 AU and 1.43 AU, respectively, compared to 1.12 AU for the wild type (Figure 3.4). For both mutants, the difference from the wild type is statistically significant. However, at the 24-hour time point, there was no significant difference between the wild-type and mutant values. In contrast, in the Δ*ndh* mutant, the crystal violet assay showed less biofilm than the wild type at both 6-hour (0.94 AU) and 24-hour (1.68 AU) time points.

To assess biofilm thickness and area, two-photon fluorescence microscopy images of propidium iodide-stained biofilm were collected at 6- and 24-hour time points and analyzed using COMSTAT2 software.[79,80] At 6 hours, the biofilm formed by the Δ*nuoG* strain, was significantly thicker and covered a greater area than in the wild type. In the Δ*nqrF* and Δ*ndh* strains, biofilm thickness and surface area were both similar to wild type (Figure 3.4B, 3.4C and Figure A.3). At

24 hours, none of the mutants was different from the wild type in biofilm thickness or surface area. In the Δ*ndh* strain, at 6- and 24-hours, biofilm thickness and surface area were very similar to wild type, but at both time points, the crystal violet assay showed significantly less retention. This suggests that the biofilms formed by this mutant, although extensive and thick, may be less dense.

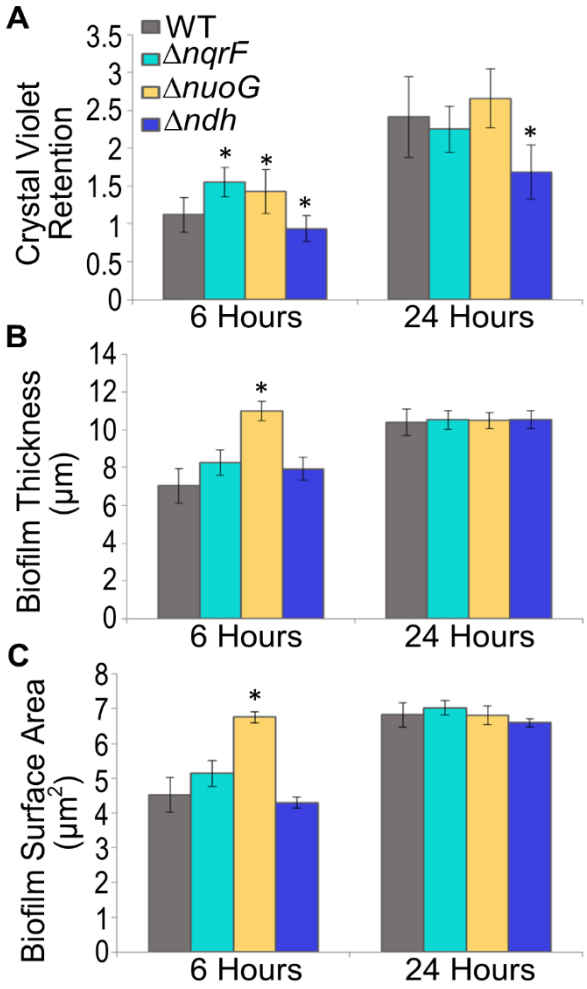

Figure 3.4: Biofilm formation by wild type (PAO1) and single deletion mutants. (A) Crystal violet retention was measured as the total amount of biofilm produced. WT (grey), Δ*nqrF* (cyan), Δ*nuoG* (yellow) and Δ*ndh2* (dark blue) were diluted to OD_{600} = 0.5 from an overnight culture, and grown in a 96-well plate, without shaking for 6 h (mid-attachment) or 24 hours (mature biofilm). Crystal violet retention of the biofilm was examined at each time point through optical density at 600 nm. (B) Surface area of the biomass from COMSTAT2 analysis of images taken with two-photon microscope. For all panels, error bars indicate standard error of the mean from three biological replicates, and stars indicate p-values ≤ 0.05 compared to wild type through a student's *t*-test. (C) Average thickness of the biofilm was measured using propodium iodide (30 μM) stained biofilms grown on 8-well coverslips for 6 or 24 hours. The fluorescence of the retained propodium iodide in the biofilm was measured with a two-photon microscope. COMSTAT2 analysis was used for image analysis.

3.3.5.2 Pyocyanin Secretion

Pyocyanin is a toxin produced by *P. aeruginosa* that can readily diffuse to target cells, where it will cause oxidative stress. Pyocyanin is a vivid blue color and can be identified by its visible spectrum and measured on the basis of absorbance at 690 nm.[84] Pyocyanin production is controlled by quorum sensing and is thus associated with stationary phase. In wild-type *P. aeruginosa*, in rich medium, production of pyocyanin could be observed after 16 hours of growth and the concentration reached a maximum of 3.6 μM at 18 hours (Figure 3.5). In each of the single deletion mutants, pyocyanin production began earlier and reached much higher concentrations (Fig 3.5). The Δ*nqrF* strain produced the highest levels of pyocyanin (43.5 μM at 20 hours post inoculation), 12 times more than wild type.

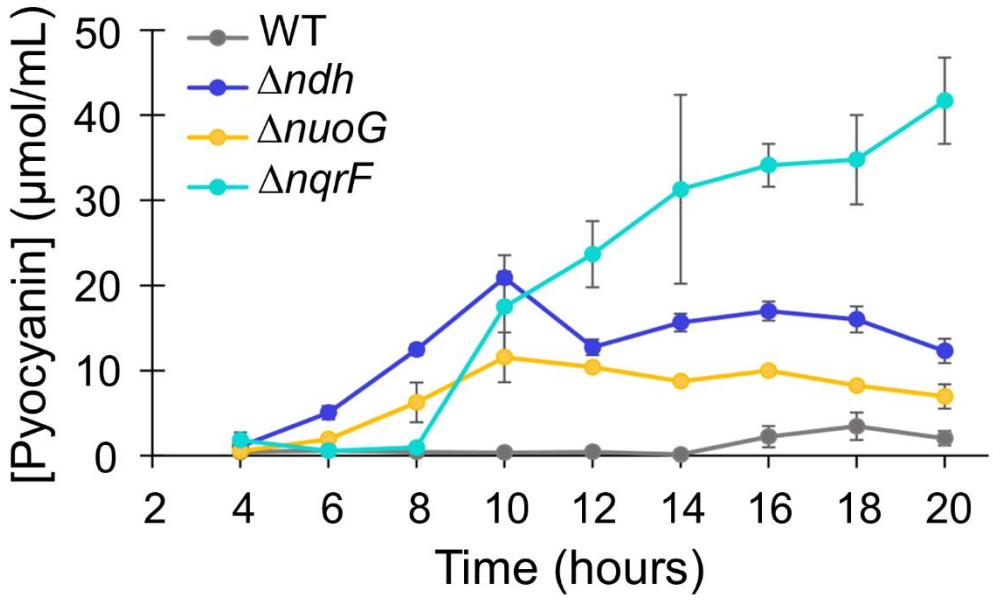

Figure 3.5: Pyocyanin production. Pyocyanin production in wild type PAO1 (grey), Δ*ndh* (dark blue), Δ*nuoG* (yellow) and Δ*nqrF* (cyan). The concentration (μM) was determined using the extinction coefficient for pyocyanin at 690 nm (4130 $M^{-1}cm^{-1}$). OD_{600} of the wild type and mutant cultures were similar at each time point, so data represent an accurate comparison of pyocyanin production in the different strains. Stars indicate p-values from a student's *t*-test ≤ 0.05, compared to wild type at each time point.

3.3.6 RNASeq Transcriptome Analysis of the Strain Lacking NQR (Δ*nqrF*)

To understand the physiological changes taking place in the mutant lacking NQR (Δ*nqrF*), we used RNA sequencing to compare their transcriptomes in both mid-exponential and stationary phases. Comparison of the mapped reads in Δ*nqrF* compared with wild type, revealed significant changes in the transcription of the genes coding for enzymes that make up the pyocyanin synthesis pathway. In exponential phase, the expression of each of the pyocyanin synthesis genes were ~6-8.5-fold greater in Δ*nqrF* (Figure 3.6, 3.7), a result which is consistent with the observed increase in pyocyanin production by this strain. Expression of the remaining NADH dehydrogenases NUO and NDH2 was shown not to change in Δ*nqrF* relative to wild type at either time point, indicating that the absence of a functional NQR does not affect the transcription of the other two enzymes.

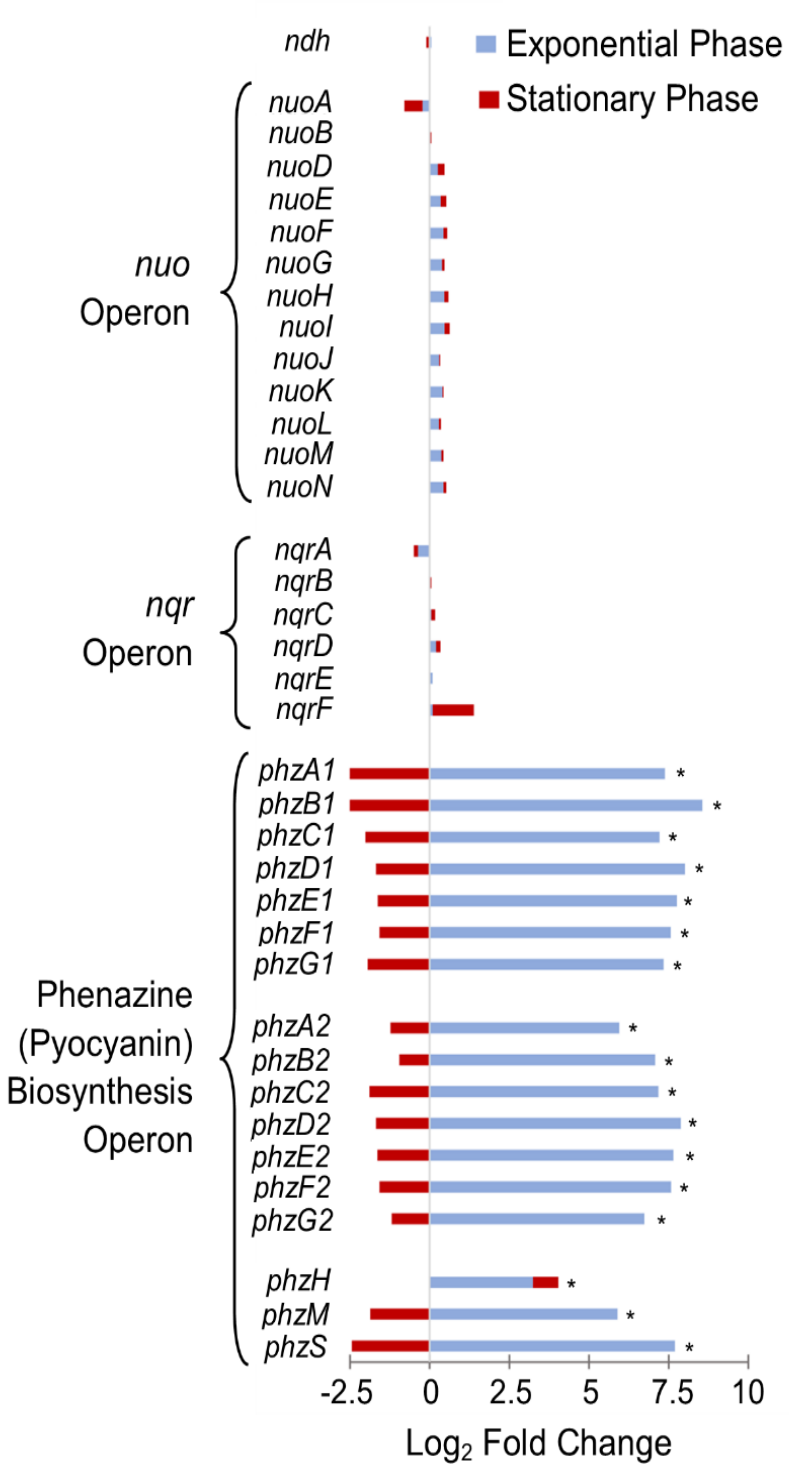

Figure 3.6: Transcriptome analysis of the Δ*nqrF* mutant strain compared to wild type. Differential expression of genes encoding NDH2, NUO, and the pyocyanin biosynthesis operons in the Δ*nqrF* mutant strain compared with wild type PAO1 during exponential and stationary phases. A positive value indicates an increased expression in Δ*nqrF* compared to wild-type. Stars indicate significant changes in expression with a P-value <0.05 as determined via the calculations outlined in Materials and Methods.

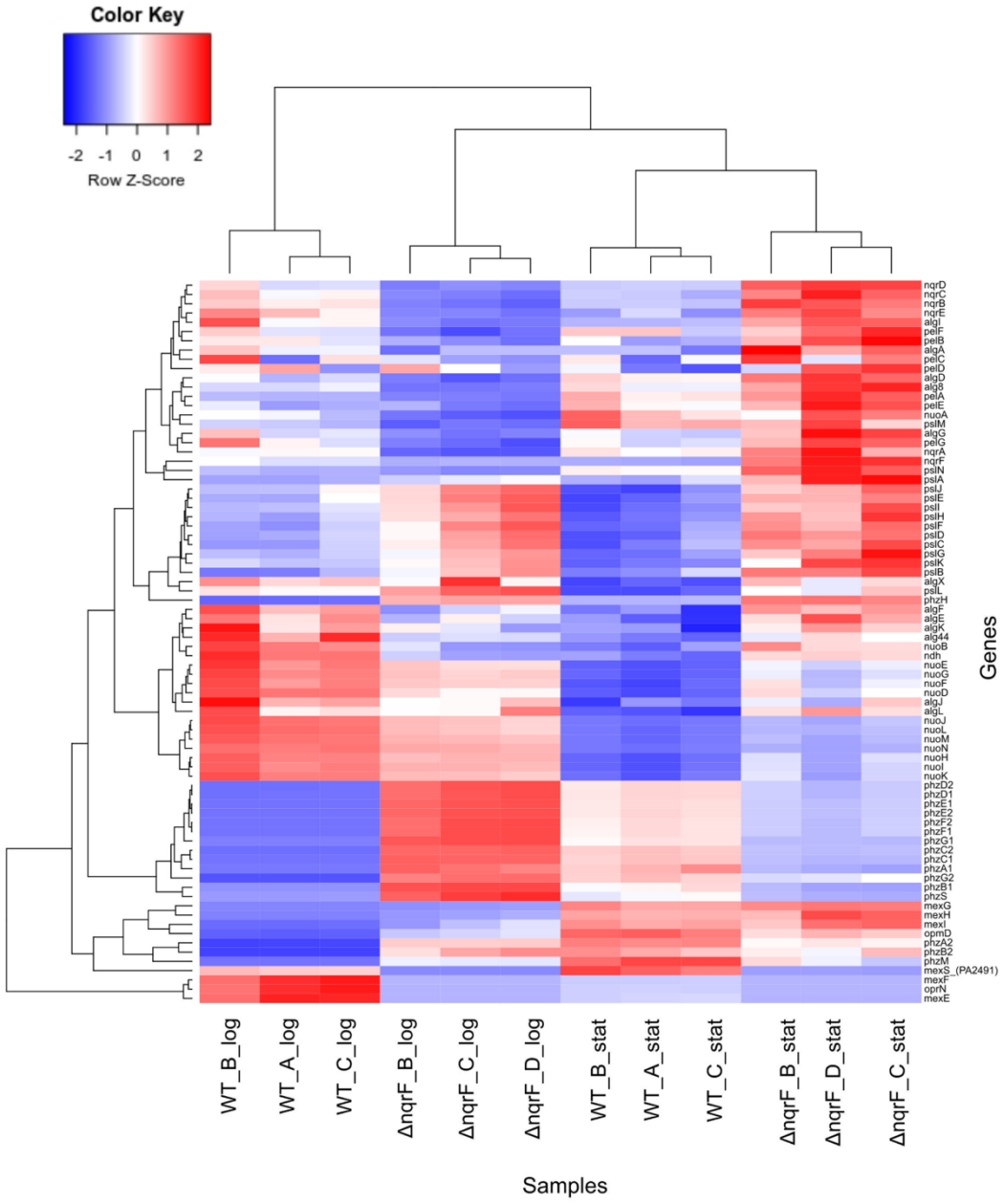

Figure 3.7: Heatmap of gene expression profiles in the transcriptome profiles of three biological replicates of the Δ*nqrF* and wild type strains in exponential and stationary phase. Select genes include those encoding *ndh*, *nuo operon*, pyocyanin biosynthesis operon, extracellular polysaccharides *alg*, *psl*, and *pel* operons, the genes coding for the MexEF-OrpN efflux pump and related genes and the MexGHI-OpmD efflux pump. All genes were normalized by gene length and χ^2 transformed before analysis. Most highly expressed genes were selected according to the sum of normalized counts across samples. Genes were selected from the NOISeq results and counts were χ^2 transformed before analysis. According to the Z-score, color bars in red correspond to higher expression.

3.3.7 Changes in Antibiotic Resistance in Single Deletion Mutants

P. aeruginosa is a multi-drug resistant pathogen with a wide range of intrinsic antibiotic resistance. Previous studies have shown that disruptions of NUO and NQR in *P. aeruginosa* result in increased resistance to the aminoglycosides gentamicin and tobramycin.[54,85] We examined the resistance of the three NADH dehydrogenase single deletion mutants to the antibiotics available in our laboratory, and our results reveal that Δ*nqrF*, Δ*nuoG* and Δ*ndh* all have different resistance profiles. Table 3.3 shows the minimum inhibitory concentrations (MIC) for the antibiotics tested in each of the single mutant strains and wild type. Relative to wild type, all the mutants showed higher sensitivity to chloramphenicol and trimethoprim, but lower sensitivity to kanamycin and gentamicin, each to a different degree. In the case of streptomycin, Δ*nqrF* and Δ*ndh* show lower sensitivity, while Δ*nuoG* is unchanged.

Table 3.3: Minimal inhibitory concentrations (MIC)[a] for wild type (PAO1), Δ*nqrF*, Δ*nuoG*, and Δ*ndh*.

Antibiotic	**WT**	**Δ*nqrF***	**Δ*nuoG***	**Δ*ndh***
		MIC (mg/mL)		
Streptomycin	35	90	35	240
Chloramphenicol	300	60	<50	35
Kanamycin	90	175	140	>1000
Trimethoprim	900	160	90	300
Gentamicin	3	175	5	<1000

[a]MICs were determined by inoculating 4 µL of an overnight culture into 1 mL LB + appropriate antibiotic in a 48-well plate. Plates were incubated at 37°C, in aerobic conditions for 24 hrs before determining MIC.

3.3.8 Infection in Animal and Cellular Models

The enhanced pyocyanin production we observed, suggested that these strains might also have altered virulence. We therefore tested virulence in two well established model systems: macrophages and mice.

3.3.8.1 Macrophage Model

In macrophages, compared to a bacteria-free control, infection by the wild type, or any of the three mutant strains, produced at least 3-times as much cell death (Figure 3.8). The cellular death rate caused by Δ*nuoG* was approximately the same as wild-type, while Δ*nqrF* and Δ*ndh* were able to kill macrophages 5- and 7-times more efficiently respectively.

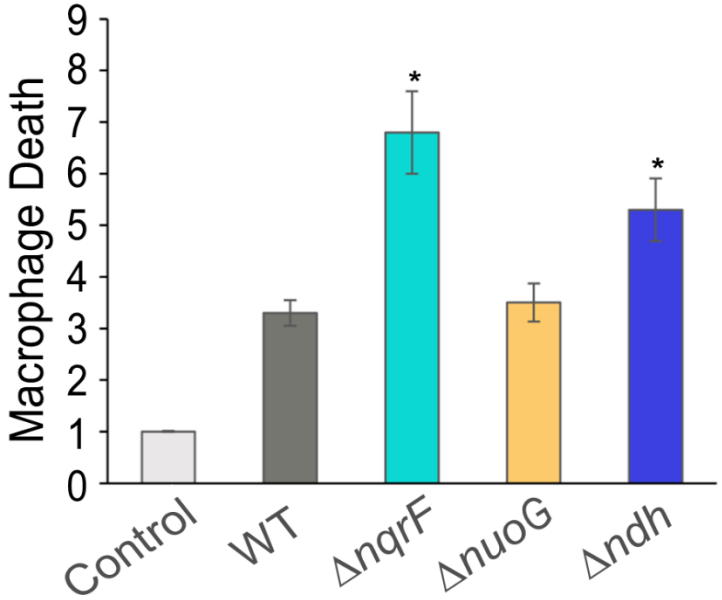

Figure 3.8: Macrophage toxicity assay. Wild type PAO1, Δ*nqrF*, Δ*nuoF* and Δ*ndh* mutants were cocultured in a 1:1 ratio with RAW 264.7 macrophages for 6 hours before a LDH assay was performed to determine macrophage cell death. A bacteria-free control group was included for reference. Data from three independent experiments are represented as the average macrophage death, with error bars indicating the standard error of the mean. Stars indicate p-values ≤ 0.05 compared to wild type, through a student's t-test.

3.3.8.2 Mouse Model

Given that the Δ*nqrF* strain exhibits the greatest killing capacity in the macrophage assay, we assessed whether this mutant was also defective in virulence in mice. The Δ*nqrF* strain was compared to wild type PAO1 in an intranasal aspiration mouse model of acute pneumonia. Mice infected with ~4 x 10^6 CFU of the Δ*nqrF* mutant progressed to prelethal illness more rapidly than those infected with wild-type PAO1 ($p < 0.05$) (Figure 3.9A). A second experiment was performed to assess the bacterial load in the lungs of infected mice. To avoid rapid death of the mice, a lower bacterial inoculum (~5-6 x 10^5 CFU) was given to the mice, which were then euthanized 24 hours

after infection. The lungs were sterilely removed, homogenized, and plated to measure bacterial loads. We found that the bacterial load was approximately the same in mice infected with wild type PAO1 and Δ*nqrF* **(**Figure 3.9B). Thus, the higher lethality of Δ*nqrF* is due to inherent virulence and not simply a better ability to colonize and proliferate in the lungs.

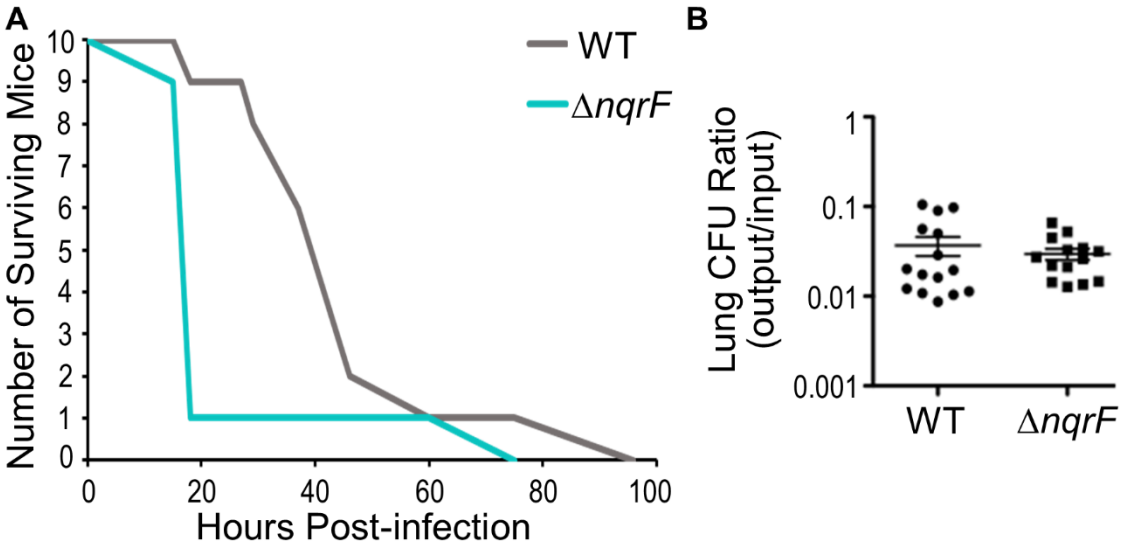

Figure 3.9: Survival of mice infected with wild type PAO1 and Δ*nqrF*. (A) Survival of BALB/c mice after intranasal aspiration of ~4 x10^6 CFU wild type or Δ*nqrF*. The survival curves were statistically different ($p < 0.05$; log rank test). (B) Bacterial burden in the lungs. Lungs were harvested from mice infected with ~5-6 x 10^5 CFU at 24 h post-infection, and the ratio of CFUs before inoculation and after death were counted. There is no significant difference between the bacterial burden from wild type PAO1 and Δ*nqrF*.

3.3.9 *In trans* Complementation of NQR

To confirm that the observed phenotype of the Δ*nqrF* strain is a direct effect of NQR inactivation, we created a complementation strain (pHERD28C-NQR), using the complete *nqr* operon, with a C-terminal histidine tag, in the pHERD plasmid, under control of the arabinose (*ara*) promotor. Membranes isolated from this strain showed essentially the same NADH oxidation activity as wild type (Figure 3.10A). After partial purification on a Ni-NTA column, the preparation was run on an SDS gel, where it showed the two fluorescent bands characteristic of the FMN cofactors of the NqrB and NqrC subunits (Figure 3.10B,C,D).[75] The strain also showed a reversion towards wild-type characteristics of biofilm formation and pyocyanin production. As

described above, the deletion strain lacking NQR, shows enhancement of some properties associated with virulence: biofilm formation begins earlier than in the wild type and the cells produce much more pyocyanin. Crystal violet retention analysis of mid-attachment phase samples revealed a significant decrease in measured biofilm production by the pHERD28C-NQR strain relative to that of Δ*nqrF*, representing a complete return to wild type characteristics (Figure 3.10E).

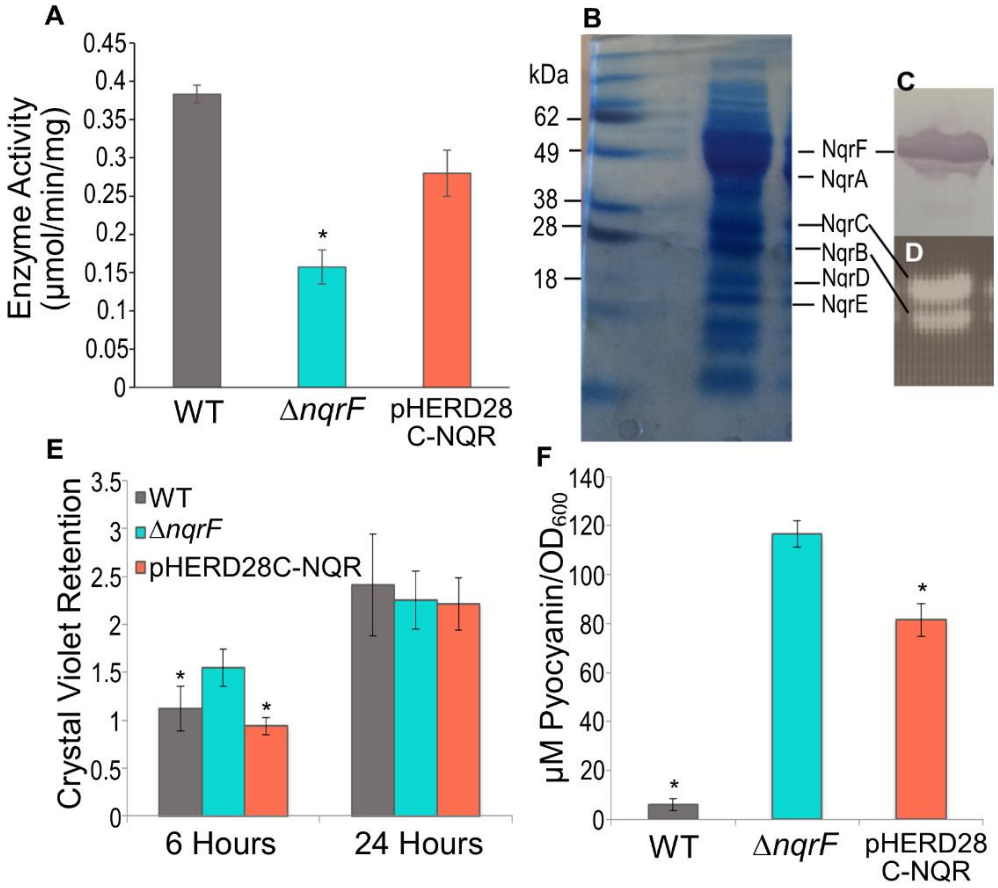

Figure 3.10: Complementation of NQR. (A) NADH:quinone oxidoreductase activities of wild type (PAO1), ΔnqrF, and nqr-complementation strain (pHERD28C-NQR). Enzyme activity is defined as the µmoles of NADH consumed per minute per mg of membrane protein. The reaction contains: 100 µM NADH, 50 µM ubiquinone-1 and 100 mM NaCl. Changes in absorbance were followed at 340nm (εNADH= 6.22 mM−1 cm−1). and NADH dehydrogenase deletion mutants. (B) SDS-gel (4-12%) of partially purified NQR complex expressed in the pHERD 28C-NQR (20 mg) run in Tris-glycine gel system stained with Coomassie Blue. (C) Western blotting using anti-His5X antibodies showing the NqrF subunit, where the histidine tag is attached. (D) Same gel as in (B) exposed to UV light before staining showing the fluorescent bands corresponding to the NqrB and NqrC subunits of the semi-purified NQR. E. Biofilm formation quantified as crystal violet retention at mid-attachment (6 hours) and mature (24 hours) biofilm. (F) Pyocyanin concentration (µM) following 24 hours of growth, measured at 690 nm (4130 $M^{-1}cm^{-1}$) and normalized to culture OD_{600}. OD_{600} of the wild type and mutant cultures were similar at each time point, ensuring that the data represent an accurate comparison of pyocyanin production between strains. Stars indicate p-values from a student's *t*-test ≤ 0.05.

In the case of pyocyanin production, at 24 hours post inoculation, pHERD28C-NQR produced an average of 85 μM pyocyanin/OD_{600} (Figure 3.10F). This is a significant decrease from the 117 μM of pyocyanin/OD_{600} produced by Δ*nqrF* at the same time point, but still much more than produced by wild type. Even so, the reversion toward wild type characteristics upon reintroduction of NQR confirms that it is the deletion of NQR which leads to the mutant phenotype.

3.4 Discussion

In this study we have characterized the roles of the three NADH:quinone oxidoreductases of *Pseudomonas aeruginosa*: NQR, NUO, and NDH2. We used single- and double-deletion mutants to assess the importance of each enzyme in the growth of *P. aeruginosa* and the contribution of each to the net NADH dehydrogenase activity. Our results suggest connections between the deletion of these enzymes and changes usually associated with the transition from exponential to stationary phase, including biofilm formation and pyocyanin production. Since these traits are known to be associated with virulence, this led to the discovery that some of the deletion mutants have enhanced lethality in infection models with both isolated macrophages and mice.

3.4.1 Effects of Single and Double NADH Dehydrogenase Deletions on Growth

None of the single NADH dehydrogenase deletion mutants caused an insurmountable defect in growth in any of the conditions we tested, including rich medium (LB) and minimal medium with glucose (SCFM), and at low and high pH and low and high [Na^+].

The double deletion mutants were constructed with the aim of having strains in which only one of the three NADH dehydrogenases would be present so that the contribution of each enzyme could be evaluated separately. All three double-deletion mutants were able to grow in all conditions tested. The only notable difference was in the mutant that has only NUO (Δ*nqrF*Δ*ndh*),

which had an extended lag phase lasting several hours, after which growth proceeded normally. Torres et al. reported a similar lag in the growth of their double deletion mutant which expressed NQR only (Δ*nuoIJ*Δ*ndh*).[54] In our hands the corresponding mutant (Δ*nuoG*Δ*ndh*) did not show this lag and grew normally. We do not have an explanation for this difference but taken together the results point to the conclusion that *P. aeruginosa* is able to grow fairly normally even when it has only one of the three NADH dehydrogenases. This reveals a remarkable robustness in the energy production systems of this bacterium.

3.4.2 Assessing the Contributions of NQR, NUO and NDH2 in Exponential Phase: NADH Dehydrogenase Activity in Isolated Membranes

In contrast to the growth curve analysis, where none of the mutants caused a pronounced growth defect, when NADH consumption was measured in isolated membranes, all of the mutants, single- and double-deletion, showed lower levels of activity (normalized to total protein) compared to the wild type. In the single mutants that lack: NQR (Δ*nqrF*), NUO (Δ*nuoG*) and NDH2 (Δ*ndh*), initial rates of NADH oxidation were 41%, 67%, and 62%, respectively, compared to wild type (Table A.3). In the double deletion mutants that have only: NQR (Δ*nuoG*Δ*ndh*), NUO (Δ*nqrF*Δ*ndh*) and NDH2 (Δ*nqrF*Δ*nuoG*), initial rates were 48%, 15%, and 37% respectively (Table A.3). When activity was measured in the wild type, using deamino-NADH, which does not react with NDH2, the initial rate was 70% compared to the reaction of wild type with NADH (Figure A.2). In the reaction with deamino-NADH, only NQR and NUO should be active, so this is comparable to the activity of Δ*ndh* mutant with NADH: 62% compared to wild type. The activity of wild type with deamino-NADH is 8% greater than the activity of the mutant lacking NDH2 (Δ*ndh*). One possible explanation is that, although deamino-NADH is described as not reactive with NDH2, there may actually be a small amount of residual activity with this substrate.[86]

One significant conclusion from these results is that, during exponential phase, out of the three NADH dehydrogenases, NQR appears to make the largest contribution to activity. Among the single-deletion mutants, the strain without NQR (Δ*nqrF*) shows the largest relative decrease in activity (59% decrease) (Table A.3). Similarly, among the double-deletion mutants, the two strains that have lost NQR (Δ*nqrF*Δ*ndh* and Δ*nqrF*Δ*nuoG*) show the largest loss of activity (85% and 63% decrease respectively). Taken together, these results show that, during exponential growth in *P. aeruginosa*, NQR likely accounts for the majority of NADH dehydrogenase activity. This finding is in agreement with the conclusions of Liang et al. on the basis of in-gel activity measurements.[71] Torres et al. also studied a series of NADH dehydrogenase deletion mutants in *P. aeruginosa* but concluded that NQR has only a minor role.[54] This difference is likely due to the fact that their measurements were made in essentially sodium-free conditions, where we would expect the activity of NQR to be very low, since this enzyme is Na^+-dependent.

3.4.3 Assessing the Contributions of NQR, NUO and NDH2 in Stationary Phase: NADH Dehydrogenase Activity in Isolated Membranes

The same set of measurements was also carried out in membranes from cells harvested during stationary phase. Initial rates of NADH oxidation, for single deletion strains lacking: NQR (Δ*nqrF*), NUO (Δ*nuoG*) and NDH2 (Δ*ndh*), were 54%, 53%, and 62% respectively compared to wild type (Table A.3). Initial rates in the double deletion mutants, that have only NQR (Δ*nuoG*Δ*ndh*), NUO (Δ*nqrF*Δ*ndh*) and NDH2 (Δ*nqrF*Δ*nuoG*), were 49%, 46%, and 48% respectively (Table A.3). These results do not point to any one of the enzymes as having a predominant role in NADH dehydrogenase activity during stationary phase. In the wild type, when deamino-NADH was used, activity was 62% compared to the reaction with NADH, consistent with a 38% contribution by NDH2. This compares to a loss of 51% of NADH activity in the strain

where only NDH2 is present. This discrepancy is likely due to the fact that deamino-NADH is a less efficient substrate.[86] This again suggests that the effects of the mutants on the physiology of the bacteria go beyond simply subtracting one or more enzymes.

3.4.4 Consequences of Deletion of NADH Dehydrogenases for the Physiology of *P. aeruginosa*

3.4.4.1 Pyocyanin Production and Biofilm Formation

When we first began to grow the NADH dehydrogenase mutants we noticed a striking blue color in the liquid cultures. In stationary phase, *P. aeruginosa* cultures typically take on a light blue hue, but the color we observed appeared earlier and was much more intense. The blue chromophore was easily identified as pyocyanin on the basis of its visible spectrum. Pyocyanin is a toxin, produced only by *P. aeruginosa*, that acts by causing oxidative stress in neighboring cells.[87] Its production is controlled by quorum sensing and usually starts in stationary phase, but all of the NADH dehydrogenase mutants began making pyocyanin earlier, during exponential growth phase, and in much larger concentrations than wild type cells. Pyocyanin production begins first in the strain without NDH2 (Δ*ndh*), about 6 hours after inoculation, but reaches the highest levels—about 12 times as much as wild type—in the strain without NQR (Δ*nqrF*). The final step in the pyocyanin synthesis pathway is catalyzed by the enzyme PhzS in a reaction that requires NADH as a reductant.[88] Our RNASeq analysis showed that, in the mutant without NQR (Δ*nqrF*), expression of genes coding for the pyocyanin synthesis pathway, including *phzS*, were elevated as much as 8.5-fold compared to wild type. The elevated pyocyanin production in the deletion mutants could be due to their diminished NADH dehydrogenase capacity or to the higher levels of PhzS, or both. Complementation of the strain lacking NQR (Δ*nqrF*) with the *nqr* operon on a plasmid, resulted in a decrease in pyocyanin production, but it did not fully restore the levels in

the wild type. This suggests that gene dosage effects are playing a role, since the plasmid is likely present in multiple copies. Also, expression is under the control of an arabinose promoter. Either of these could cause higher than normal levels of production.

3.4.4.2 Changes in Antibiotic Resistance in Single Mutants

Each of the single deletion mutants showed increased sensitivity to chloramphenicol and trimethoprim. This is likely due to changes in expression of an antibiotic efflux pump. Our RNASeq analysis of the Δ*nqrF* mutant showed that expression of MexEF-OprN, an efflux pump related to resistance against these antibiotics, is down-regulated 9-fold in exponential phase and 5-fold in stationary phase (Table A.4).[89,90] The mechanism of this connection between deletion of the gene coding for NQR and changes in expression of MexEF-OprN is not known.

All of the single deletion mutants also showed increased resistance towards kanamycin and gentamicin, and Δ *nqrF* and Δ *ndh* showed increased resistance towards streptomycin. The RNASeq data on Δ*nqrF* do not suggest a clear mechanism for these changes. However, alterations in antibiotic resistance related to NADH metabolism in *P. aeruginosa* have been reported elsewhere. Aminoglycosides, such as kanamycin, gentamycin and streptomycin depend on the proton motive force to enter the cell.[91-94] Some of the NADH dehydrogenase deletion mutants may affect ion transport providing a possible explanation for our results.

3.4.4.3 Infection Models

Since pyocyanin is a virulence factor, we decided to evaluate whether the NADH dehydrogenase mutations caused changes in the ability of *P. aeruginosa* to infect cells and the outcomes of the infections. For this, we chose two well-characterized models of *P. aeruginosa* infection: macrophages in cell culture and whole mice.

In the case of macrophages, single deletion strains without NQR (Δ*nqrF*) and NDH2

(Δ*ndh*) were both significantly more effective in killing macrophages, while the strain without NUO (Δ*nuoG*) was approximately the same as wild type. Although the current work does not establish a direct causal connection between pyocyanin and the death of macrophages, it is worth noting that effectiveness in killing correlates with the total amount of pyocyanin produced rather than the time when pyocyanin production begins. Although pyocyanin production begins earlier in the strains that lack NUO (Δ*nuoG*) and NDH2 (Δ*ndh*), the strain that lacks NQR (Δ*nqrF*) produces the highest concentrations of pyocyanin and is also the most effective in killing.

For tests with mice, we chose to use the single deletion mutants that was most effective in killing macrophages: the strain that lacks NQR (Δ*nqrF*). Tests were carried out using an acute pneumonia infection model which tracked progression to prelethal illness over time. The strain lacking NQR (Δ*nqrF*) killed the mice at a significantly faster rate than wild type. However, at 24 hours after infection, the bacterial loads in the lungs of mice infected with either mutant or wild type were approximately the same. This suggests that the increased lethality of the strain lacking NQR (Δ*nqrF*) is not due to faster, or more efficient, proliferation in the mouse lungs, but rather to enhanced virulence of the individual cells. It is possible that this is due to the higher pyocyanin production in the strain. Pyocyanin has been shown to induce neutrophil apoptosis and play a critical role in the establishment and success of airway infections in mice.[95,96] Strains deficient in pyocyanin have been found to be cleared more rapidly from the lung and result in higher levels of recovery relative to wild type. [95,96]

This putative role of pyocyanin does not appear to apply to all *P. aeruginosa* model-host systems. For example, inactivation of pyocyanin production had no effect on the virulence of *P. aeruginosa* on the silkworm *Bombyx mori*.[97] Similarly, Torres et al. tested the virulence of their *P. aeruginosa* NADH dehydrogenase deletion mutants in two model systems: a plant (lettuce) and an

insect (*Galleria mellonella*) and found no significant changes.[54]

The overall picture that emerges from this study is consistent with the conclusions from a series of studies on unusually-virulent strains of *P. aeruginosa* found in CF patient samples. They found that many high virulent strains produced pyocyanin and other virulence factors (including LasA protease; see Table A.4) earlier and in larger quantities than the less virulent strains. However, the cause of this variation was attributed to changes in the quorum sensing control mechanisms.[98-100] The current work suggests that there may also be a connection to energy metabolism and NADH utilization. We plan to further test this hypothesis by constructing a series of double mutants in which the genes involved in pyocyanin synthesis have been deleted from strain that lack one or more NADH dehydrogenases. These double mutants will be tested for virulence, in comparison with wild type and a pyocyanin single deletion mutant. We expect that, if pyocyanin is the direct cause of enhanced virulence in the NADH dehydrogenase mutants, these double mutants would be no more virulent than wild-type *P. aeruginosa.*

3.5 Conclusion

P. aeruginosa has three different enzymes: NUO, NQR and NDH2, all of which carry out the same redox function but have different energy conservation and ion transport properties. In order to better define the roles of these enzymes, we constructed two series of mutants: (i) three single deletion mutants, each of which lacks one NADH dehydrogenase and (ii) three double deletion mutants, each of which retains only one of the three enzymes. All of the mutants grew approximately as well as wild type, when tested in rich and minimal medium and in a range of pH and [Na^+] conditions, except that the strain with only NUO (Δ*nqrF*Δ*ndh*) has an extended lag phase. During exponential phase, the NADH dehydrogenases contribute to total wild-type activity in the following order: NQR > NDH2 > NUO. Some mutants, including the strain without NQR

(Δ*nqrF*) had increased biofilm formation, pyocyanin production, and killed more efficiently than wildtype in both macrophage and mouse infection models. Consistent with this, Δ*nqrF* showed increased transcription of genes involved in pyocyanin production. The relationship between NQR and pyocyanin production is proposed to be one of redox balancing in the cell. Upon deletion of the major NADH dehydrogenase, an excess of NADH may accumulate due to the absence of NQR activity. We propose here that this excess of NADH experienced by the cell is redirected to the pyocyanin biosynthetic pathway, the final step of which is NADH-dependent. In this way the cell can reestablish a suitable NAD^+/NADH ratio, however the consequence of this physiological adjustment is the generation of a hypervirulent strain. Further work needs to be done to characterize the relationship between NQR and pyocyanin production, as well as the role for NADH is virulence regulation in *P. aeruginosa*, however the evidence provided here suggests that NQR, by virtue of its oxidation of NADH, plays a central role in *P. aeruginosa* pathogenesis.

4. Na^+ Management in *Pseudomonas aeruginosa*: Characterization of the Na^+/H^+ Antiporters

4.1 Introduction

The fundamentals of cellular survival rely on the maintenance of efficient energy processing and favorable internal conditions supporting essential cell biochemistry. Meeting these basic requirements entails continuous remodeling of cellular metabolism and homeostatic processes to best suit changing external conditions. Two of the most important factors influencing cell physiology, and those which feature the most environmental variability, are H^+ and Na^+ concentrations.[35] Although essential for cellular life and proper functionality, fluctuations of these ions to concentrations which are too high or too low threaten cell viability.[40] Consequently, cells have evolved robust mechanisms for the precise regulation and processing of these prevalent ions.

One of the most ubiquitous tools in the regulation of H^+ and Na^+ ion systems is the Na^+/H^+ antiporter. These secondary ion transporters use the ion gradients generated via cellular respiration to fuel the translocation of Na^+ (and other ions) across the cell membrane. In bacteria, these transporters provide (i) cytoplasmic pH regulation, (ii) tolerance to fluctuations in alkalinity and osmotic pressure, (iii) efflux of toxic levels of substrate ions, and (iv) cell volume regulation.[34,35] In addition, Na^+/H^+ antiporters act as an interface between the H^+ and Na^+ electrochemical ion gradients, both of which can be used to fuel key cell process in bacteria including ATP synthesis, cell motility, uptake of amino acids and essential nutrients, and efflux of toxins and antibiotics.

As a central feature of most bacterial energetics, Na^+ and H^+ ion circuits need to be maintained to satisfy both bioenergetic and homeostatic requirements of the cell.[101] Therefore the activity of the Na^+/H^+ antiporters is important to the maintenance of both ionic homeostasis as well as efficient cellular energetics. However, the ways in which these systems are coordinated and coregulated, a feature which is likely critical to bacterial growth in dynamic environments, remains

poorly understood. To better characterize the physiology of Na^+ and H^+ ion circuits in bacteria, we have investigated their function in the prevalent pathogen *Pseudomonas aeruginosa*.

Pseudomonas aeruginosa is a remarkably ubiquitous gram-negative proteobacteria known for its extensive environmental presence and robust metabolic adaptability.[2] The systems that transport Na^+ and H^+ across the cell membrane in *P. aeruginosa* are of central importance for enabling this bacterium to survive and proliferate in a wide range of habitats, and have even been shown to contribute to the virulence of this pathogen. Previously implicated in *P. aeruginosa*'s survival and infectious success, its four antiporters, NhaP, NhaB, Mrp, and NhaP2, are thought to feature distinct characteristics of ion specificity, substrate stoichiometry, and condition-dependent activity and expression.[36-39]

NhaP was the first Na^+/H^+ antiporter identified in *P. aeruginosa*. It is thought to catalyze a $1Na^+/1H^+$ exchange and have little affinity for any other ions.[37] NhaB was the second antiporter characterized from *P. aeruginosa*. Sharing 62% identity with its *E. coli* counterpart, this antiporter has been shown to feature maximum activity at high pH and is capable of transporting both Na^+ and Li^+ across the membrane.[36] The stoichiometry of exchange in the NhaB from *E. coli* is $3H^+/2Na^+$ and is thought to be the same in the *P. aeruginosa* transporter.[41] NhaP2 of *P. aeruginosa*, sharing 65% homology with the *Vibrio cholerae* NhaP2,[42] is believed to transport both Na^+ and K^+ and has been shown to contribute to *P. aeruginosa* virulence towards barley.[38] In addition, as a notable complement to NhaB, NhaP2 is thought to feature maximum activity at lower pH.[42]

The fourth and final Na^+/H^+ antiporter in *P. aeruginosa*, Mrp, is unique form the previous three transporters. NhaP, NhaB and NhaP2 are encoded for by singles genes PA3887, PA1820 and PA5021, respectively. Mrp however, a member of the Multiple resistance and pH family, is a multi-subunit protein complex encoded for by 6 genes (PA1054-PA1059) in *P. aeruginosa*. This

antiporter is believed to be the major Na^+ extruder in *P. aeruginosa* and mutants lacking the Mrp antiporter were found to have attenuated virulence in mouse models,[39] suggesting that this transporter plays a critical role in *P. aeruginosa* physiology during infection.

The utilization of these functionally divergent enzymes is thought to produce a spectrum of adaptive techniques enabling finely tuned ion management across the many variable habitats in which *P.aeruginosa* is found. Although some of the characteristics of these antiporters have been described previously, there is a lacking in understanding of how these transporters work in coordination with each other and contribute to *P. aeruginosa* physiology. This work seeks to construct a comprehensive characterization of the physiological roles and kinetic parameters of each of the individual Na^+/H^+ antiporters of *P.aeruginosa.*

4.2 Results

4.2.1 Generation of Na^+/H^+ Antiporter Deletion Mutants

To investigate the physiological roles and kinetic parameters of each of the four Na^+/H^+ antiporters present in *P. aeruginosa* we constructed mutant strains featuring the chromosomal deletion of one or more of the antiporter-encoding genes. In the case of the three single-gene encoded antiporters: NhaB, NhaP, and NhaP2, single genes PA1820, PA3887, and PA5021, respectively, were deleted from the genome. For the multi-subunit antiporter Mrp, the gene encoding the MrpA subunit, PA1054, was removed from the genome, a mutation which has previously been shown to be sufficient for the inactivation of the complex.[39] Single antiporter deletion mutants have just one of the four Na^+/H^+ antiporters deleted from the chromosome. Triple antiporter deletion mutants have three of the four Na^+/H^+ antiporters deleted from the chromosome, allowing for the functional isolation of each individual Na^+/H^+ antiporter. A quadruple Na^+/H^+ antiporter mutant (Δ*nhab*Δ*nhap*Δ*nhap2*Δ*mrpA*) was constructed which has all four of the Na^+/H^+

antiporters deleted from the *P. aeruginosa* chromosome. Single deletion mutants were confirmed for gene deletion and sequence homology via sequencing of the confirmation PCR product by Eurofins Genomics (Louisville, KY, USA). The triple and quadruple mutants designed in this study were confirmed for successful gene deletion and sequence homology by NGS genomic sequencing (data not shown).

4.2.2 Deletion of Individual Na^+/H^+ Antiporters Results in Range of Growth and Activity Impacts. Growth of Na+/H+ Antiporter Deletion Mutants

To assess the impact of antiporter deletion in the series of mutants designed for this study we screened the pH and [Na^+] tolerance of these strains by measuring their growth in a range of pH and [Na^+] conditions. Rich medium (LB) containing the specified conditions of [Na^+] and pH was inoculated with the strain of interest and subsequent growth was monitored for 20 hours. The resulting growth profiles of the series of single antiporter deletion mutants Δ*nhaB,* Δ*nhaP,* Δ*nhaP2 and* Δ*mrpA* compared with wild-type PAO1 are shown below in Figure 4.1.

The most dramatic growth defect is observed in the strain lacking the Mrp antiporter. In conditions of relatively low salt (50mM) and neutral pH (7.5) this strain can grow as well as wild-type and all of the other single deletion mutants. But when the [Na^+] or pH are increased outside of that range, severe growth defects are immediately observed, in some cases appearing to be fatal to the cells. The lag phase is significantly prolonged as pH and [Na^+] are increased, with this mutant seemingly unable to grow in conditions of pH 8.5 300mM Na^+ and up. However, following a significant lag phase, the Δ*mrpA* mutant does eventually begin to grow and approach a final density comparable to wildtype. In the Δ*nhaP2* mutant, the predominant effect on growth is seen during late stationary phase. Under conditions of pH 8.5 and NaCl concentrations of 300 mM and above, the Δ*nhaP2* has a sustained growth defect. However, in all other conditions the growth of

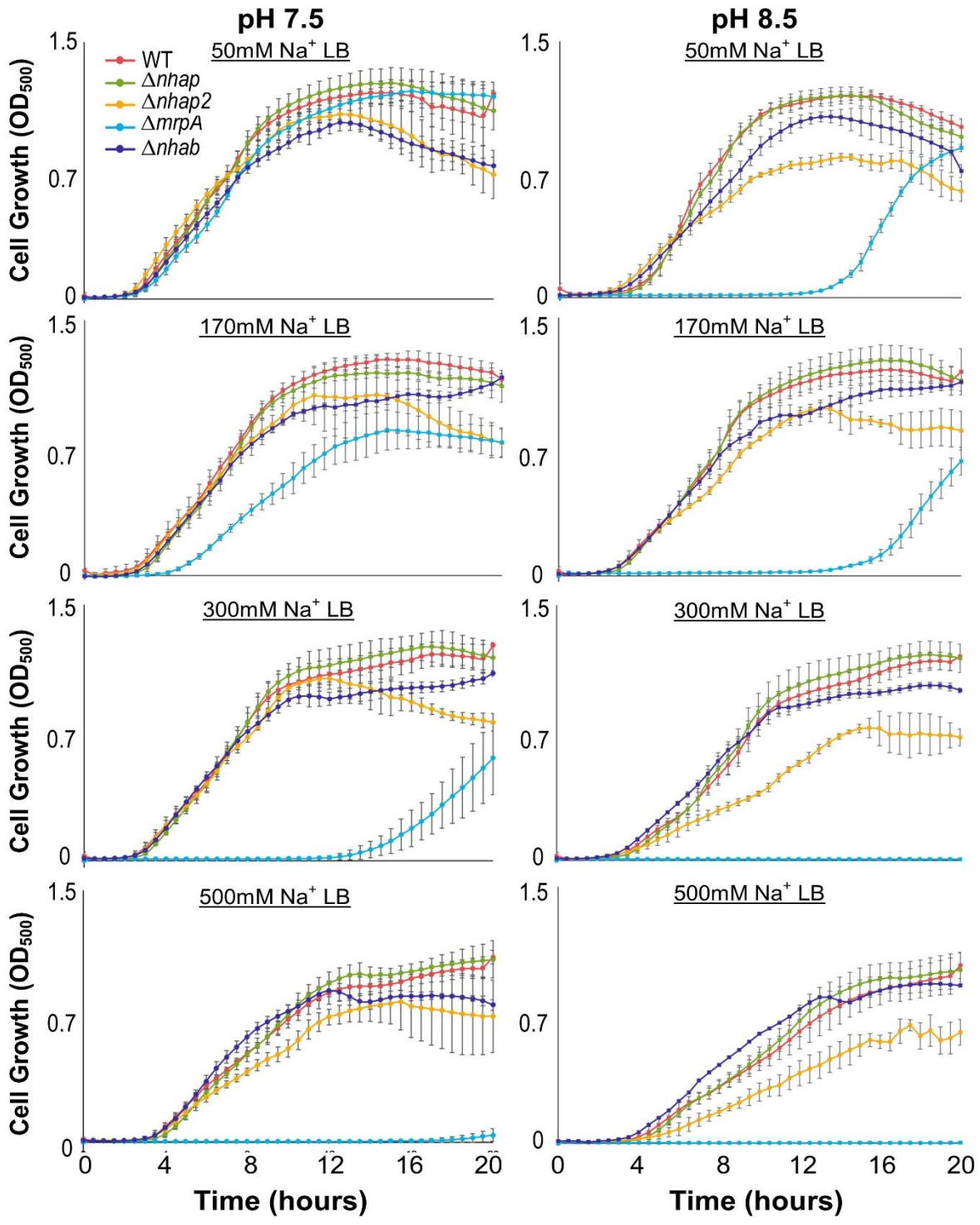

Figure 4.1: Comparison of growth of wildtype *P. aeruginosa* and single antiporter deletion mutants. Growth curves of wildtype (red) and antiporter deletions mutants Δ*nhab* (purple), Δ*nhap* (green), Δ*nhap2* (yellow) and Δ*mrpA* (cyan) in LB at 170mM and 300mM NaCl concentrations, at pH 7.0 and 8.0. Changes in OD_{500} were measured using a Tecan Infinite M1000 Pro plate reader during 20 hours of growth at 37°C with continuous orbital shaking at 217 rpm. Each curve was constructed using two biological replicates with three technical replicates each, with standard deviation calculated accordingly and represented as error bars.

this mutant does not significantly diverge from wildtype until the cells reach stationary phase, at which point the density of the Δ*nhaP2* culture is consistently lower that wildtype. In the remaining two single mutants, Δ*nhaP* and Δ*nhaB*, the effect of the antiporter deletion is less pronounced. The growth of the Δ*nhaP* mutant does not deviate from that of wildtype in any of the conditions tested, indicating that the absence of this transporter has no negative impact on growth in the conditions presented. In the Δ*nhaB* mutant strain a slight growth defect can be seen in several of the medium conditions during stationary phase growth, however the severity and onset of this defect appears to vary across different conditions of pH and [Na^+].

To investigate the pH and Na^+ tolerance provided by each individual transporter, we measured growth of the triple antiporter deletion mutants, each retaining only one of the four Na^+/H^+ antiporters, in a range of pH and [Na^+] conditions. The growth of the triple antiporter deletion mutants Δ*nhap*Δ*nhap2*Δ*mrpA* (NhaB only), Δ*nhab*Δ*nhab2*Δ*mrpA* (NhaP only), Δ*nhab*Δ*nhap*Δ*mrpA* (NhaP2 only), and Δ*nhab*Δ*nhap*Δ*nhap2* (Mrp only) compared with wildtype PAO1 are shown in Figure 4.2.

From the resulting growth curves, we can see that the presence of just one of the four Na^+/H^+ antiporters can support growth at pH 7.5 in Na^+ concentrations up to at least 0.5 M. The only notable growth defect appears in the form of a prolonged lag phase and reduced exponential phase growth rate in the Δ*nhab*Δ*nhap*Δ*mrpA* (NhaP2 only) mutant in conditions of 500 mM NaCl at pH 7.5, although this mutant does eventually reach stationary phase culture density comparable with the wildtype strain. At pH 8.5, however, the mutant strains show more unique growth defects. The Δ*nhap*Δ*nhap2*Δ*mrpA* (NhaB only) and Δ*nhab*Δ*nhap*Δ*nhap2* (Mrp only) mutants can support normal growth at pH 8.5. The Δ*nhab*Δ*nhap*Δ*mrpA* (NhaP2 only) and Δ*nhab*Δ*nhap2*Δ*mrpA* (NhaP only) mutant strains on the other hand both show significant growth defects. In the mutant retaining

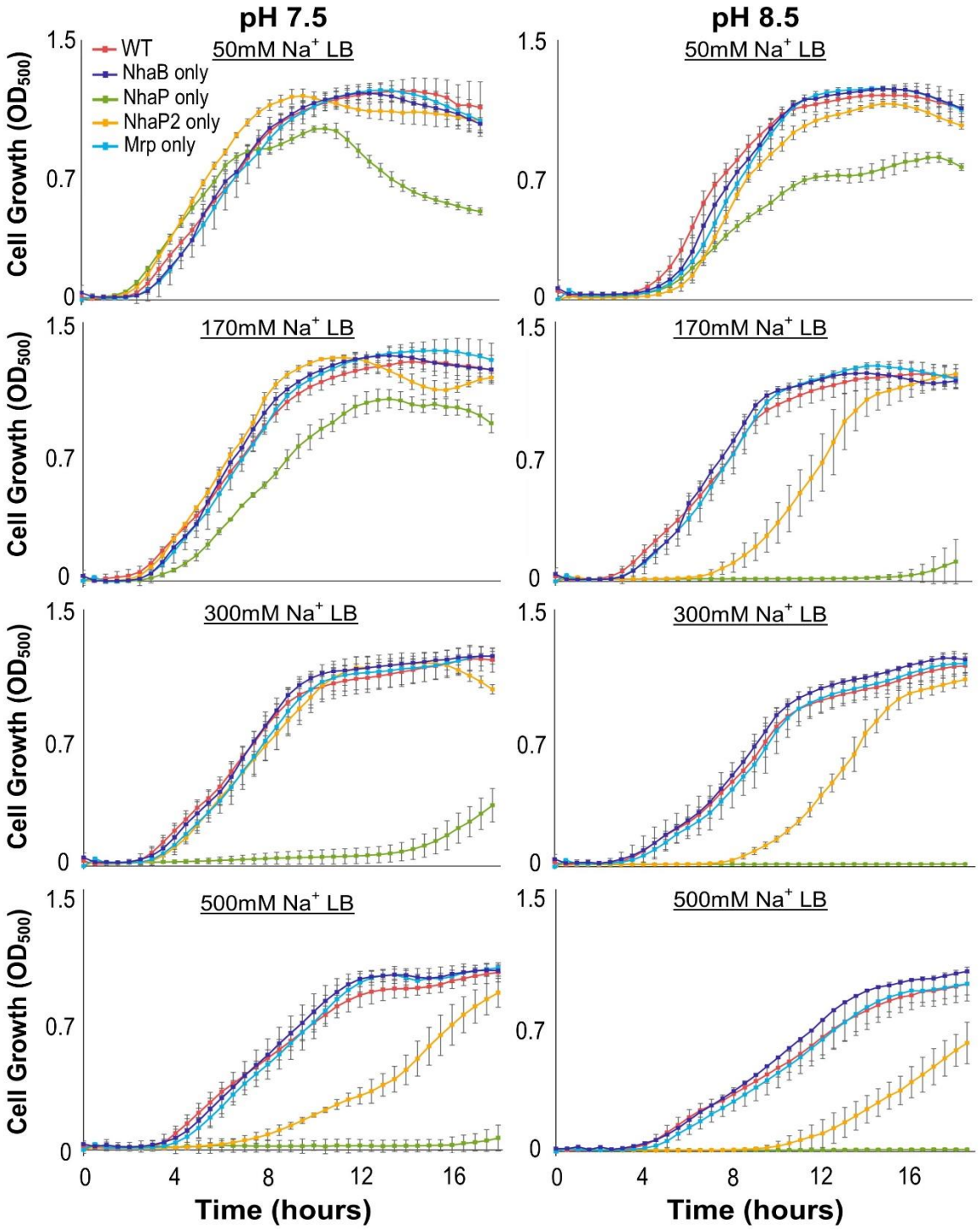

Figure 4.2: Comparison of growth of wildtype *P. aeruginosa* and triple antiporter deletion mutants. Growth curves of wildtype (red) and antiporter deletions mutants Δ*nhap*Δ*nhap2*Δ*mrpA* (purple), Δ*nhab*Δ*nhap2*Δ*mrpA* (green), Δ*nhab*Δ*nhap*Δ*mrpA* (yellow) and Δ*nhab*Δ*nhap*Δ*nhap2* (cyan) in LB at 170mM and 300mM NaCl concentrations, at pH 7.0 and 8.0. Changes in OD_{500} were measured using a Tecan Infinite M1000 Pro plate reader during 20 hours of growth at 37°C with continuous orbital shaking at 217 rpm. Each curve was constructed using two biological replicates with three technical replicates each, with standard deviation calculated accordingly and represented as error bars.

only the NhaP antiporter, the presence of NhaP alone cannot support growth in concentrations of 300 mM NaCl and above at pH 8.5. In conditions of 170 mM NaCl and pH 8.5, the NhaP2 only mutant strain again has a prolonged lag phase, a phenotype which is sustained as the Na^+ concentration of the growth medium is increased to 300 and 500 mM NaCl. The results indicate that each transporter features a unique capacity to support growth, suggesting the unique properties of each enzyme.

The quadruple antiporter deletion mutant strain (Δ*nhab*Δ*nhap*Δ*nhap2*Δ*mrpA*) featuring the deletion of genes encoding/essential for the functional expression of all four of the known Na^+/H^+ antiporters in *P. aeruginosa* was assayed for growth and found to demonstrate severe pH and Na^+ sensitivity. The quadruple mutant has a significant defect throughout growth in even the mildest condition of 50 mM NaCl at pH 7.5, as shown in Figure 4.3A compared with the growth of the wildtype strain. Decreasing the $[Na^+]$ to approximately 0 mM does not improve the growth of the mutant, as is shown in Figure 4.3B, indicating that the defect experienced in this strain is not limited to conditions of Na^+ stress. At pH 7.5, the quadruple mutant cannot maintain growth at NaCl concentrations above 50 mM. At pH 8.5 the quadruple mutant is 10X more Na^+ sensitive, with the strain being unable to grow beyond 5 mM NaCl. The growth of this mutant demonstrates the lethal effect of even moderate to low $[Na^+]$ when the cell lacks Na^+-effluxing antiporters. However, the ability to grow in up to 50 mM NaCl at pH 7.5 indicates that the cell is maintaining Na^+ homeostasis by some other means in these conditions. To understand the Na^+-efflux properties of each of the mutant strains and determine whether the quadruple deletion mutant has any $Na+/H^+$ antiport activity remaining, we proceeded to characterize the Na^+/H^+ antiport activity.

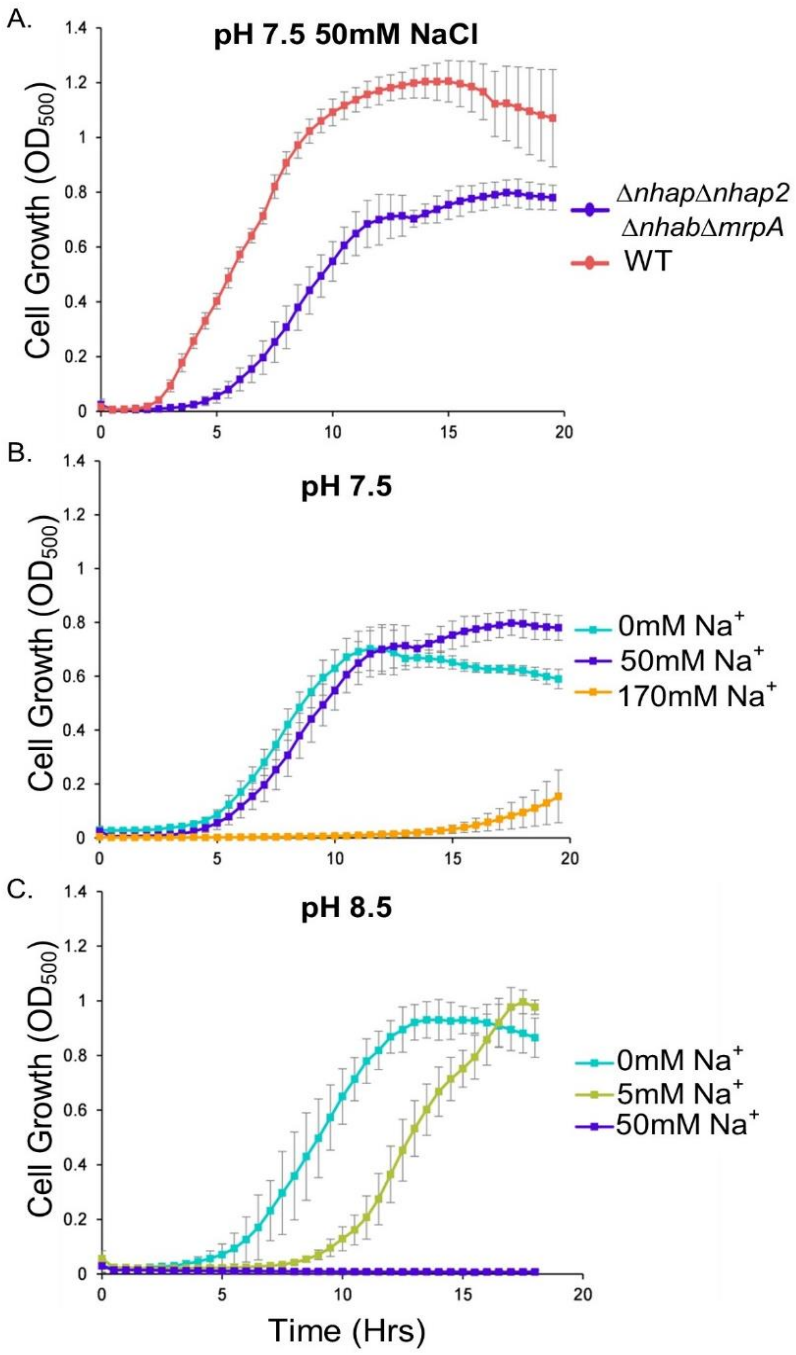

Figure 4.3: Growth of the quadruple deletion mutant Δ*nhab*Δ*nhap*Δ*nhap2*Δ*mrpA*. (A) Growth of wildtype PAO1 (red) compared with the growth of the quadruple antiporter deletion mutant (purple) in conditions of 50 mM NaCl at pH 7.5. (B) Growth of the quadruple antiporter mutant in varying external NaCl concentrations at pH 7.5. (C) Growth of the quadruple mutant in varying external NaCl concentrations at pH 8.5. Each curve was constructed using two biological replicates with three technical replicates each, with standard deviation calculated accordingly and represented as error bars.

4.2.3 Na^+/H^+ Antiport Activity and Enzyme Kinetics

Previous efforts have been made to characterize the kinetic parameters of the Na^+/H^+ antiporters of *P. aeruginosa*, however such approaches relied on the expression of the *P. aeruginosa* enzymes in a Na^+/H^+-void strain of *E. coli*, thus removing the enzymes from their native organism. In this work we have undertaken the challenge of characterizing these transporters in their native organism, providing what we consider to be an analysis with greater fidelity to the kinetics of these enzymes in *P. aeruginosa*.

To assess the kinetic parameters of each of the individual Na^+/H^+ antiporter we measured antiporter activity in everted membrane vesicles prepared from each of the triple antiporter deletion mutants which retain only one Na^+/H^+ antiporter. Everted membrane vesicles were prepared from cells grown to stationary phase and lysed via a single pass through a French pressure cell. Na^+/H^+ antiport activity was measured by the acridine orange fluorescence quenching method described previously[64] and the activities were normalized according to total membrane protein concentration. By varying the concentration of substrate NaCl added to stimulate Na^+/H^+ antiport, we constructed enzyme saturation curves for each of the Na^+/H^+ antiporters and performed Michealis Menten model fitting using GraphPad Prism 6 software. The corresponding plots and kinetic parameters are summarized in Figure 4.4 and Table 4.1, respectively.

From this analysis we can see that each of the transporters have unique properties of ion affinity and maximum velocity of ion transport. At pH 7.5, according to the maximum turnover rate, the transporters individual capacities to transport Na^+ are ordered as follows: NhaP > NhaB > NhaP2 > Mrp. As it exists in the Δ*nhab*Δ*nhap2*Δ*mrpA* triple deletion mutant, NhaP was found to have the greatest Vmax of 62% fluorescence dequenching at pH 7.5. However, the NhaP antiporter was also found to have the highest Km value at pH 7.5, indicating that, of the four Na^+-

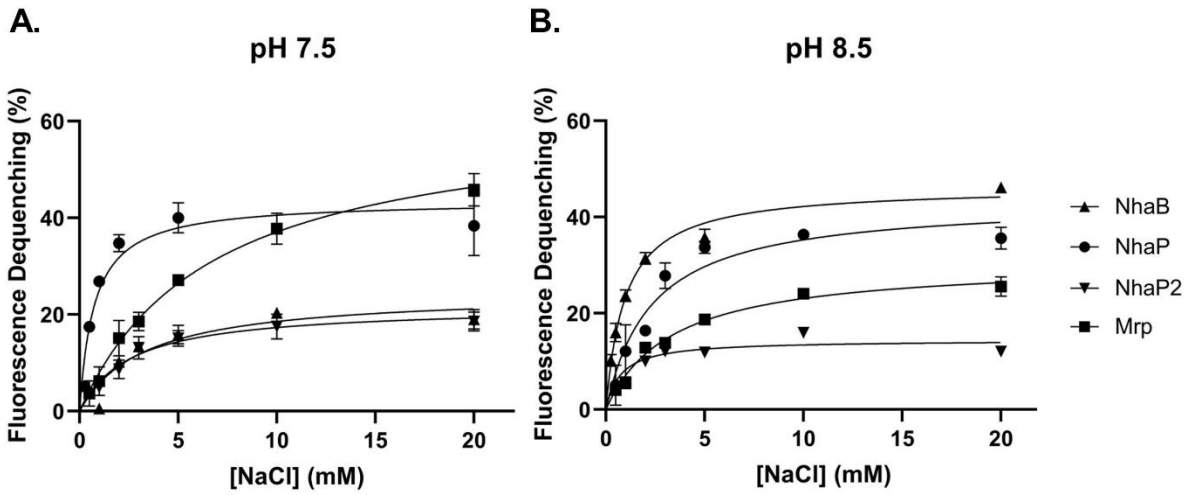

Figure 4.4: Michaelis menten enzyme saturation plot for the Na^+/H^+ antiporters of *P. aeruginosa*. Enzyme saturation plots with Michaelis Menten fitting for NhaB (triangle), NhaP (circle), NhaP2 (inverted triangle) and Mrp (square) at pH 7.5 (A) and pH 8.5 (B). Antiporter activity was measured in the presence of varying substrate (NaCl) concentrations and the resulting enzyme saturation plot was subjected to Michaelis Menten model fitting using GraphPad Prism 6 software. Error bars represent the standard error of replicate assays.

Table 4.2: Kinetic parameters of Na^+/H^+ antiport in *P. aeruginosa*.

Antiporter	pH 7.5		pH 8.5	
	Km (mM)	Vmax[a]	Km (mM)	Vmax[a]
NhaB	0.7 ± 0.2	44	1.0 ± 0.1	46
NhaP	6.7 ± 0.6	62	2.3 ± 0.7	43
NhaP2	3.3 ± 1.7	25	--	12
Mrp	2.6 ± 0.5	22	3.3 ± 0.5	31

[a]Vmax; % fluorescence dequenching

transporters, NhaP has the highest maximum rate of substrate turnover, but the lowest affinity for Na^+ at pH 7.5. When ordered according to greatest affinity for Na^+ at pH 7.5, the transporters are ranked as follows: NhaB > Mrp > NhaP2 > Nhap. Interestingly, the trends observed in triple deletion mutant growth at pH 7.5 were found to follow a similar progression, suggesting that Na^+ affinity is of greater importance than maximum turnover rate *in vivo* during growth at pH 7.5.

At pH 8.5 the Vmax of NhaP is down to 43% fluorescence dequenching, supporting the previous observation that NhaP has optimal activity at pH 7.5. However, the Km value for NhaP at pH 8.5 is less than half that of pH 7.5, indicating that NhaP has much greater Na^+ affinity at pH 8.5 compared with pH 7.5. The Km and Vmax values for NhaB and Mrp do not vary significantly between pH conditions, although both values are greater at pH 8.5 compared with pH 7.5. The most notable pH-dependence was experienced by the NhaP2 antiporter, with a maximum turnover rate significantly lower than pH 7.5 and a Km value which was determined to be too low for reliable measurement. This result again appears to support previous observations that the NhaP2 antiporter is of greater importance at low pH.[42]

Given the differences in substrate ions between the four transporters, we also assessed the K^+ and Li^+ antiport activity in the triple deletion mutants. Maximum antiport activities under saturating conditions of substrate ion are summarized in Figure 4.5. All of the triple deletion mutants had lower K^+ and Li^+ antiport activity compared to wildtype. In the Δ*nhap*Δ*nhap2*Δ*mrpA*

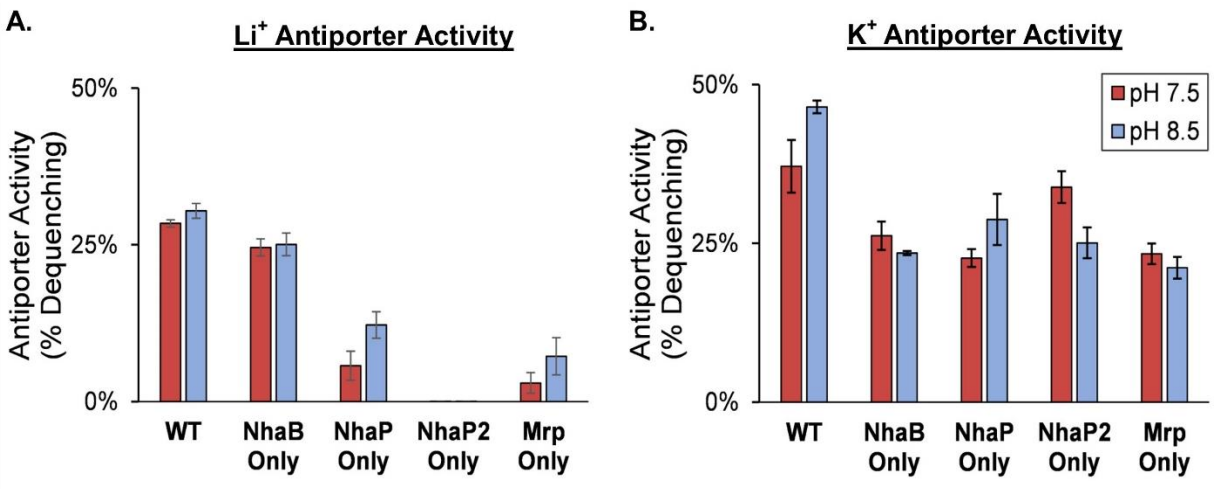

Figure 4.5: K^+ and Li^+ antiport activity in triple antiporter deletion mutants compared with wildtype. Li^+/H^+ antiport activity (A) and K^+/H^+ antiport activity (B) was measured according to the fluorescence quenching method described previously (2.4.1.1) in membranes from stationary phase cultures of wildtype PAO1 and each of the triple antiporter deletion mutants. Antiporter activity was stimulated by the addition of saturating concentrations of substrate ion (20mM) at pH 7.5 (red) and pH 8.5 (blue). Antiporter activity is averaged from two biological replicates with 2 technical replicates each. Error bars represent the standard deviation between replicates.

mutant the majority of Li^+/H^+ antiport activity is still present at both pH 7.5 and pH 8.5, confirming that NhaB is the primary Li^+-extruder in *P. aeruginosa.* Both NhaP and Mrp also had measurable Li^+/H^+ antiport activity, although to a lesser extent. The Δ*nhab*Δ*nhap*Δ*mrpA* mutant had no measurable Li^+/H^+ antiport, indicating that NhaP2 is unable to transport Li^+. Each of the triple deletion mutants had appreciable K^+/H^+ antiport activity, with NhaP2 notably having the greatest K^+/H^+ antiport activity at pH 7.5. However, we have identified additional probable K^+/H^+ antiporters in the *P. aeruginosa* genome, suggesting that the K^+ transport activity measured in these mutants is an accumulation of activities rather than the independent activity of the indicated Na^+/H^+ antiporters.

4.2.4 Cation/H^+ Antiport Activity in Δ*nhab*Δ*nhap*Δ*nhap2*Δ*mrpA*

To assess the Na^+ extrusion capacity of the Δ*nhab*Δ*nhap*Δ*nhap*2Δ*mrpA* strain, as well as probe for additional antiporters in *P. aeruginosa*, cation/H^+ antiporter activity was measured in this mutant. As described above, everted membrane vesicles were prepared from stationary phase cells and Na^+/H^+ antiport activity was measured by the acridine orange fluorescence quenching method.[64] Fluorescence scans collected from this assay are shown in Figure 4.6A. The black arrows indicate the addition of the NaCl solution to stimulate Na^+/H^+ antiport. As seen in the wildtype trace, the addition of NaCl stimulates a large response in fluorescence dequenching, indicating a significant amount of Na^+/H^+ antiport activity is taking place. In the trace shown for the quadruple deletion mutant, the addition of Na^+ does not elicit the same response, but rather induces a slight drop in fluorescence intensity followed by a slight recovery to the fluorescence intensity prior to addition of the substrate. The assay is terminated by addition of NH^4Cl to establish a reference endpoint and ensure that the membrane vesicles are properly sealed. The absence of fluorescence dequenching following the addition of NaCl confirms the removal of all

Na^+/H^+ antiporters from the cell. The same result is achieved when LiCl is added as a substrate, confirming as well that all of the enzymes capable of Li^+/H^+ antiport have been removed from the cell as well. However, when KCl is added as a substrate, there is still considerable K^+/H^+ antiport activity (Figure 4.5B), indicating that there are additional K^+/H^+ antiporters present. We have identified three putative K^+/H^+ antiporters remaining in the genome: PA3660, PA3739, and PA5529, which are likely responsible for this activity.

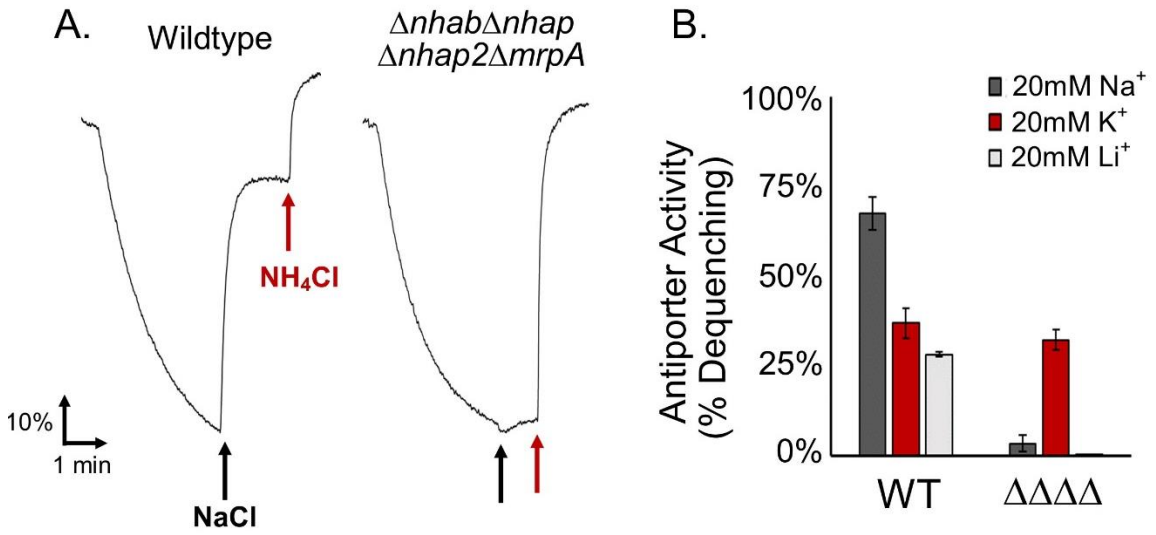

Figure 4.6: Antiporter activity in the wildtype and quadruple antiporter deletion mutant Δ*nhab*Δ*nhap*Δ*nhap2*Δ*mrpA*. (A) Fluorescence scans of Na^+/H^+ antiport activity in wildtype PAO1 and the Δ*nhab*Δ*nhap*Δ*nhap2*Δ*mrpA* mutant which is devoid of Na^+/H^+ antiporters. Antiport activity was measured following the fluorescence quenching method outlined previously (see 2.4.1.1). (B) Cation/H^+ antiport activity in wildtype PAO1 and the Δ*nhab*Δ*nhap*Δ*nhap2*Δ*mrpA* mutant using Na^+ (black), K^+ (red) and Li^+ (grey) as substrates. Antiporter activities are averaged from three biological replicates and error bars represent the standard deviation.

4.2.5 Transcriptional Changes in Δ*nhab*Δ*nhap*Δ*nhap2*Δ*mrpA*

To understand the physiological repercussions of eliminating all of the Na^+/H^+ antiporters from *P. aeruginosa*, we characterized the transcriptome of the quadruple deletion mutant compared with the wildtype strain. Cultures were grown in nutrient rich LB broth at 50mM NaCl and cells were harvested during mid-exponential (4 h) and stationary (15 h) phases. Comparison of the

transcriptome of wildtype and Δ*nhab*Δ*nhap*Δ*nhap2*Δ*mrpA* revealed the expression-level changes taking place in the quadruple mutant and provided insights into the means by which this mutant survives without and Na^+/H^+ antiporters. As shown in Figure 4.7, the greatest transcriptional changes are experienced during exponential growth, with 202 genes having significantly increased expression and 269 genes having significantly decreased expression in the quadruple mutant with respect to wildtype. This is compared with only 45 significantly increased and 17 significantly decreased genes during stationary phase growth in the quadruple mutant compared with wildtype.

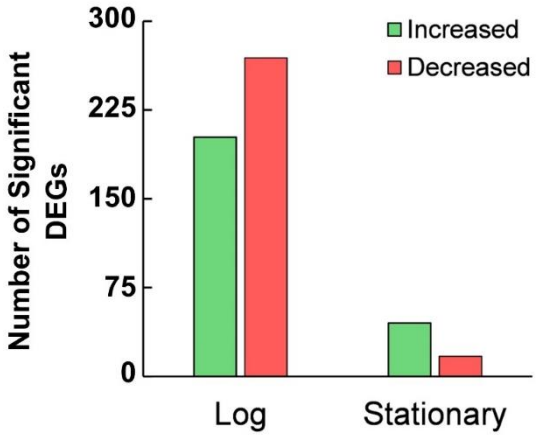

Figure 4.7: Total number of differentially expressed genes (DEGs) with significant changes in expression in Δ*nhab*Δ*nhap*Δ*nhap2*Δ*mrpA* compared with wildtype PAO1.

Among those differentially expressed genes (DEGs) featuring significant changes in expression in the quadruple deletion mutant were genes responsible for virulence factor production, quorum sensing, biofilm formation, and metabolism.

4.2.5.1 PQS Signaling and Pyocyanin Production

Significant changes in expression of the genes encoding for the *Pseudomonas* quinolone signal (PQS)- and pyocyanin synthesis pathways were present in both exponential and stationary phase Δ*nhab*Δ*nhap*Δ*nhap2*Δ*mrpA* cells. During exponential growth, components of both pathways had significantly reduced expression compared with wildtype. Figure 4.8A represents the log2-fold

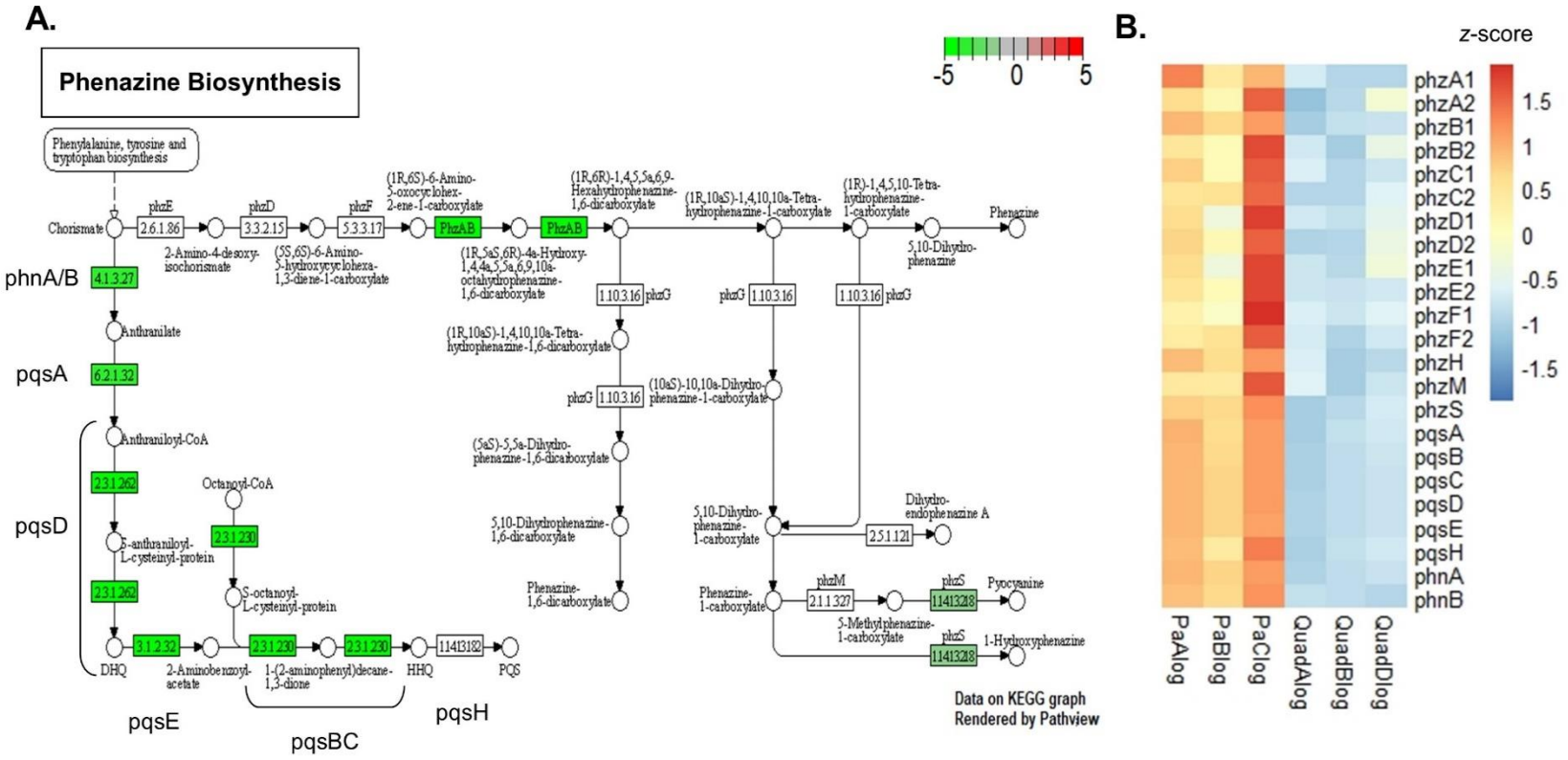

Figure 4.8: Expression of PQS and pyocyanin synthesis pathways in Δ*nhab*Δ*nhap*Δ*nhap2*Δ*mrpA* compared with wildtype during exponential phase growth. (A) Pathway view of expression changes during exponential phase growth. Green indicates a negative change in expression (log2-foldchange) in the Δ*nhab*Δ*nhap*Δ*nhap2*Δ*mrpA* mutant compared with WT. Images are rendered using the Pathview function in Rstudio. (B) Heatmap showing levels of transcripts of relevant genes in the quadruple mutant and WT during exponential growth. Total reads for each transcript were normalized and log transformed using the DESeq2 rlog function in Rstudio and are *z*-scored by row. Columns labeled with 'Pa' and 'Quad' represent biological replicate growths.

change of significant DEGs from exponential phase cells overlaid onto the relevant KEGG pathways. Genes highlighted in green are expressed at significantly lower levels in the quadruple mutant compared with WT. From this figure, we can see that the genes encoding the PQS synthesis pathway, up until the 2-heptyl-4-quinolone (HHQ) intermediate, are expressed at significantly lower levels in the quadruple deletion mutant relative to wildtype. This trend can be corroborated by assessing the levels of transcripts in each sample analyzed, shown here in Figure 4.8B. The relative homogeneity between samples can be assessed as well, represented here as color-coded *z*-scores.

In the pyocyanin synthesis pathway, the two sets of *phzA* and *phzB* genes responsible for catalyzing early steps in the pathway have significantly reduced expressed, as well as *phzS* which encodes the last step of the pathway.[88] The genes composing the rest of the pathway follow a similar trend in total transcript levels relative to WT (Figure 4.8B), however the changes do not meet the criteria for significance.

During stationary growth, there are again significant changes in the expression of these two pathways. Unlike the exponential phase cells, in the stationary phase quadruple mutant expression of the PQS synthesis pathway is significantly increased with respect to WT (Figure 4.9A). The changes again are only up until the HHQ intermediate. The final step in this pathway is catalyzed by PqsH,[102] which is not expressed at levels significantly different from WT. Expression of the pyocyanin synthesis pathway is again decreased with respect to wildtype, with the entire pathway being significantly reduced in stationary phase cells. This is a notable contrast as it is thought that phenazine biosynthesis is positively regulated by PQS, which composes a branch of the quorum sensing systems in *P. aeruginosa*.[103] However, in the Δ*nhab*Δ*nhap*Δ*nhap2*Δ*mrpA* mutant, the significant increase in expression of all the genes preceding the final PQS synthesis step does not

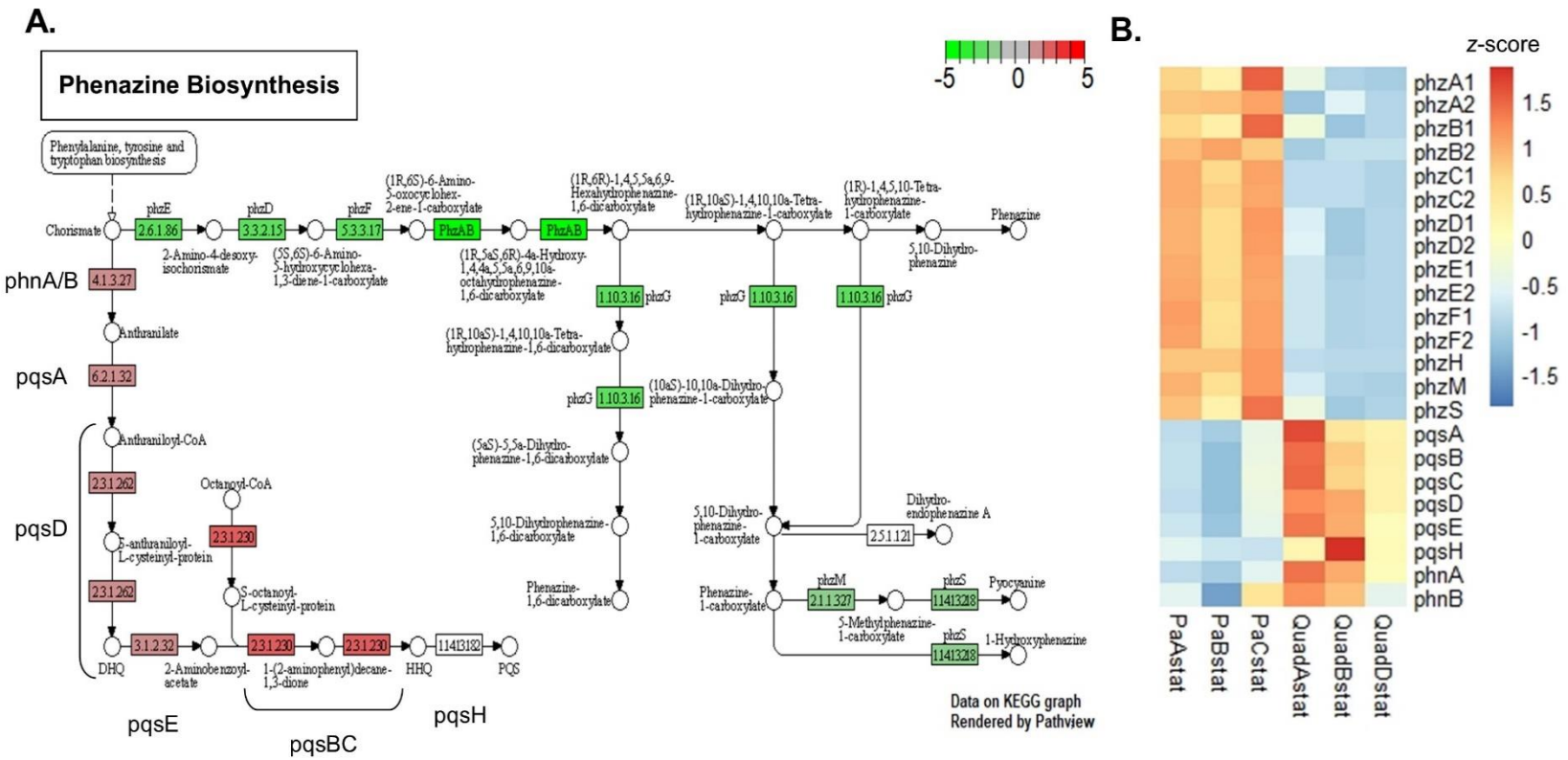

Figure 4.10: Expression of PQS and pyocyanin synthesis pathways in Δ*nhab*Δ*nhap*Δ*nhap2*Δ*mrpa* compared with wildtype during stationary phase growth. (A) Pathway view of expression changes during stationary phase growth. Green indicates a negative log2-fold change in expression and red indicates a positive log2-fold change in expression in Δ*nhab*Δ*nhap*Δ*nhap2*Δ*mrpA* compared with WT. Images are rendered using the Pathview function in Rstudio. (B) Heatmap showing levels of transcripts of relevant genes in the quadruple mutant and WT during stationary growth. Total reads for each transcript were normalized and log transformed using the DESeq2 rlog function in Rstudio and are *z*-scored by row. Columns labeled with 'Pa' and 'Quad' represent biological replicate growths.

translate to increased pyocyanin synthesis, but rather this mutant has significantly decreased expression of that pathway.

4.2.5.2 Virulence Traits

The *Pseudomonas* quinolone signal (PQS) regulates many virulence traits in *P. aeruginosa: pqs*-null mutants have decreased biofilm development and reduced production of virulence factors, including pyocyanin, elastase, lectin, and rhamnolipids.[103] Given the changes in PQS synthesis, we went on to investigate the expression of other virulence traits in the quadruple deletion mutant. Pathway analysis revealed significant changes in a variety of virulence traits and some shifts in other quorum sensing pathways during exponential growth (Figure 4.10). In addition to the PQS signaling pathway, the quadruple mutant also has decreased expression of the LasI/R quorum sensing system. The decreased expression of these two regulatory systems is likely responsible for the accompanying decrease in exponential phase expression of genes encoding lectin (*lecB*), rhamnolipids (*rhlC*) and elastases (expression of *lasA*/*B* was decreased 2.6 and 1.7-fold, respectively) (Figure 4.11).

However, contrary to the observed decrease in the production of virulence traits, biofilm production in the quadruple deletion mutant is significantly increased with respect to wildtype. Specifically, genes encoding for production of the Psl and Pel polysaccharides, but not alginate, were expressed at significantly greater levels in the quadruple mutant.[104] It is interesting that the trend in biofilm formation runs contrary to that seen in the production of other virulence traits, as the production of biofilm is thought to be regulated by the same QS pathways.[55] The divergence in expression profiles indicates that the production of biofilm is being stimulated by other means in the quadruple deletion mutant, however the mechanism underlying this process is not clear at this time.

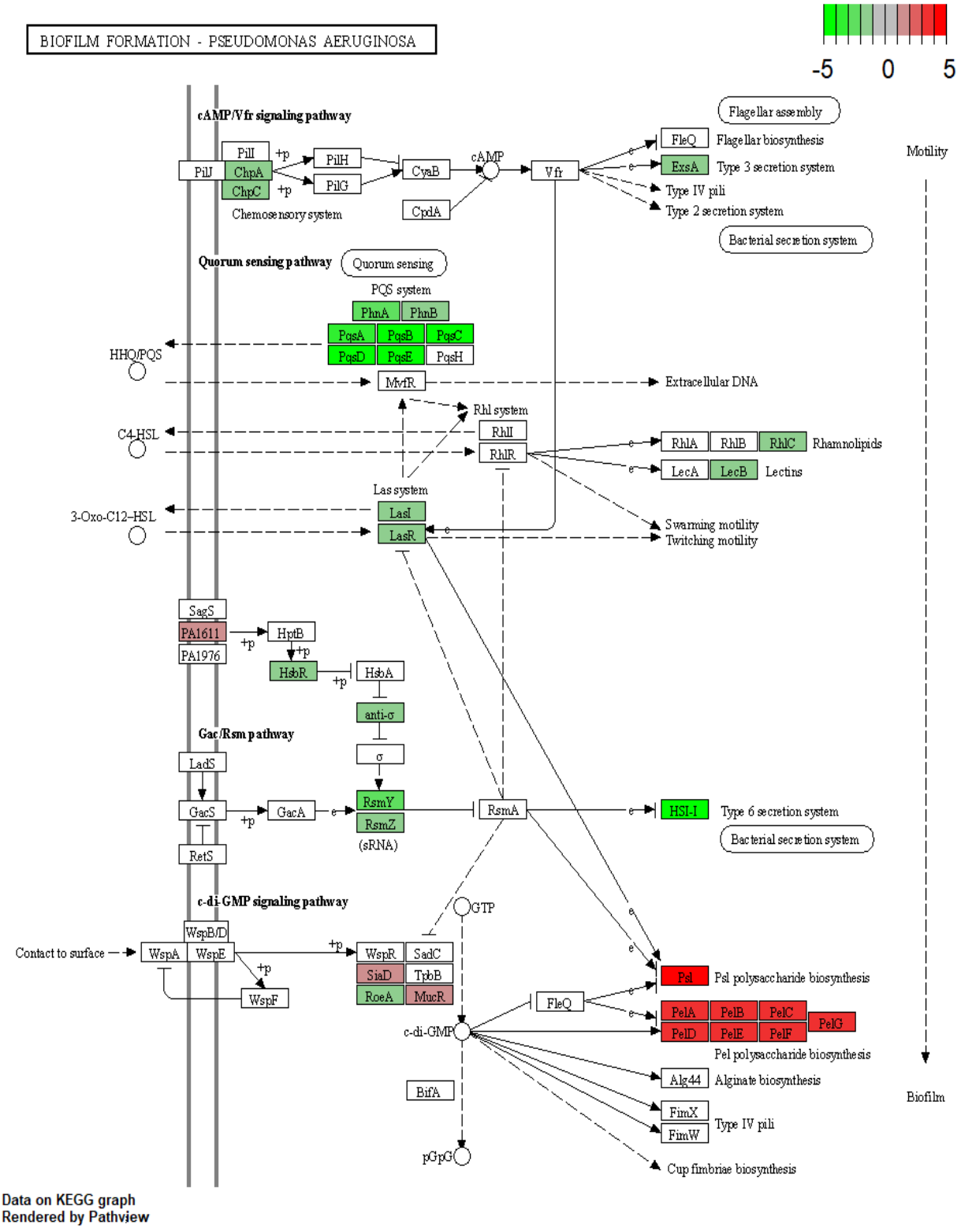

Figure 4.12: Transcriptional changes in quorum sensing, virulence trait production and biofilm formation in the Δ*nhab*Δ*nhap*Δ*nhap2*Δ*mrpA* mutant. (A) Pathway view of expression changes during exponential phase growth. Green indicates a negative log2-fold change in expression and red indicates a positive log2-fold change in expression relative to WT. Images are rendered using the Pathview function in Rstudio.

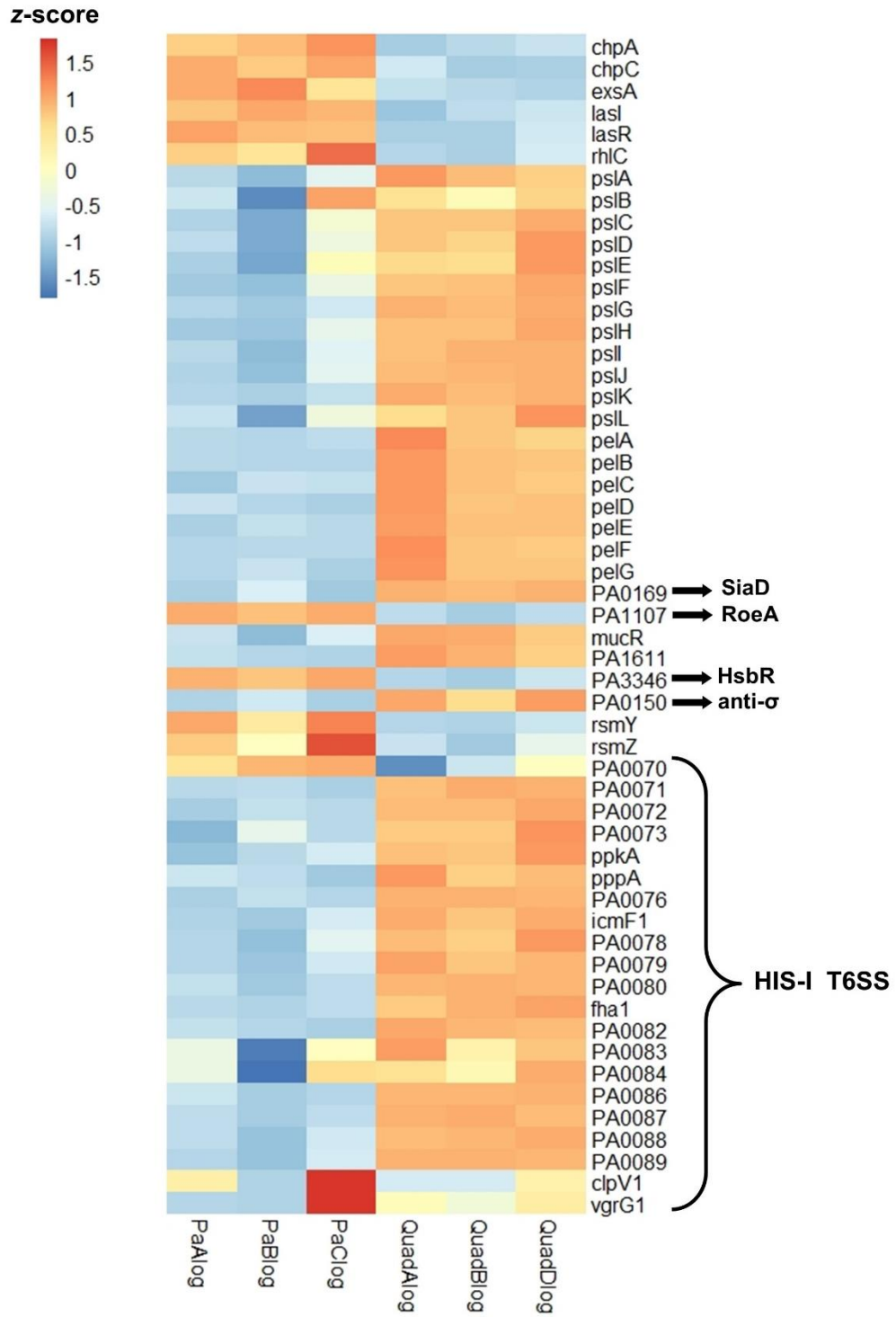

Figure 4.13: Heatmap showing levels of transcripts of relevant genes in the quadruple mutant and WT during exponential growth. Total reads for each transcript were normalized and log transformed using the DESeq2 rlog function in Rstudio and are *z*-scored by row. Columns labeled with 'Pa' and 'Quad' represent biological replicate growths.

4.2.5.3 ANR Regulon

Upon analysis of the genes with the greatest increase and greatest decrease in expression in Δ*nhab*Δ*nhap*Δ*nhap2*Δ*mrpA* compared with WT, we noted significant changes in expression of the genes encoding the denitrification pathway during exponential growth, an unexpected result as our cells were grown in fully aerated conditions. Upon further analysis, it was noted that several genes previously shown to be regulated by the presence of oxygen had significant changes in the quadruple mutant. These genes are regulated by ANR, and oxygen sensitive transcriptional regulator which is thought to control transcription of cellular components optimized for growth in low oxygen and anaerobic conditions.[105] To assess the perceived relationship between the ANR regulon and the expression profile of our quadruple deletion mutant, we cross-references the genes featuring significant changes in the Δ*nhab*Δ*nhap*Δ*nhap2*Δ*mrpA* to genes shown to be differentially expressed in a Δ*Anr P. aeruginosa* mutant.

Of the 134 differentially expressed genes identified in the Δ*Anr* mutant as regulated by ANR,[106] 90 have significant changes in expression (log2FC > 1.5, adjusted p-value << 0.01) in the Δ*nhab*Δ*nhap*Δ*nhap2*Δ*mrpA* mutant (Figure 4.12). Of the 44 genes which were not differentially expressed in the quadruple mutant, 13 encode enzymes responsible for anthranilate metabolism (*antR, antABC, catR, catABC, xylXYZ*).[107,108] This is notable, as anthranilate is the precursor of the PQS synthesis pathway.[107] Given the observed decrease in the expression of the PQS pathway, it is possible that the anthranilate degradation pathways are preserved as (i) a means of redirecting anthranilate away from the PQS synthesis pathway and towards the TCA cycle or (ii) that the reduced activity of the PQS pathway causes an accumulation of anthranilate, necessitating the expression of the pathways catalyzing its degradation. This trend is reversed during stationary phase, with the expression of *antABC* being significantly reduced in the quadruple mutant and an

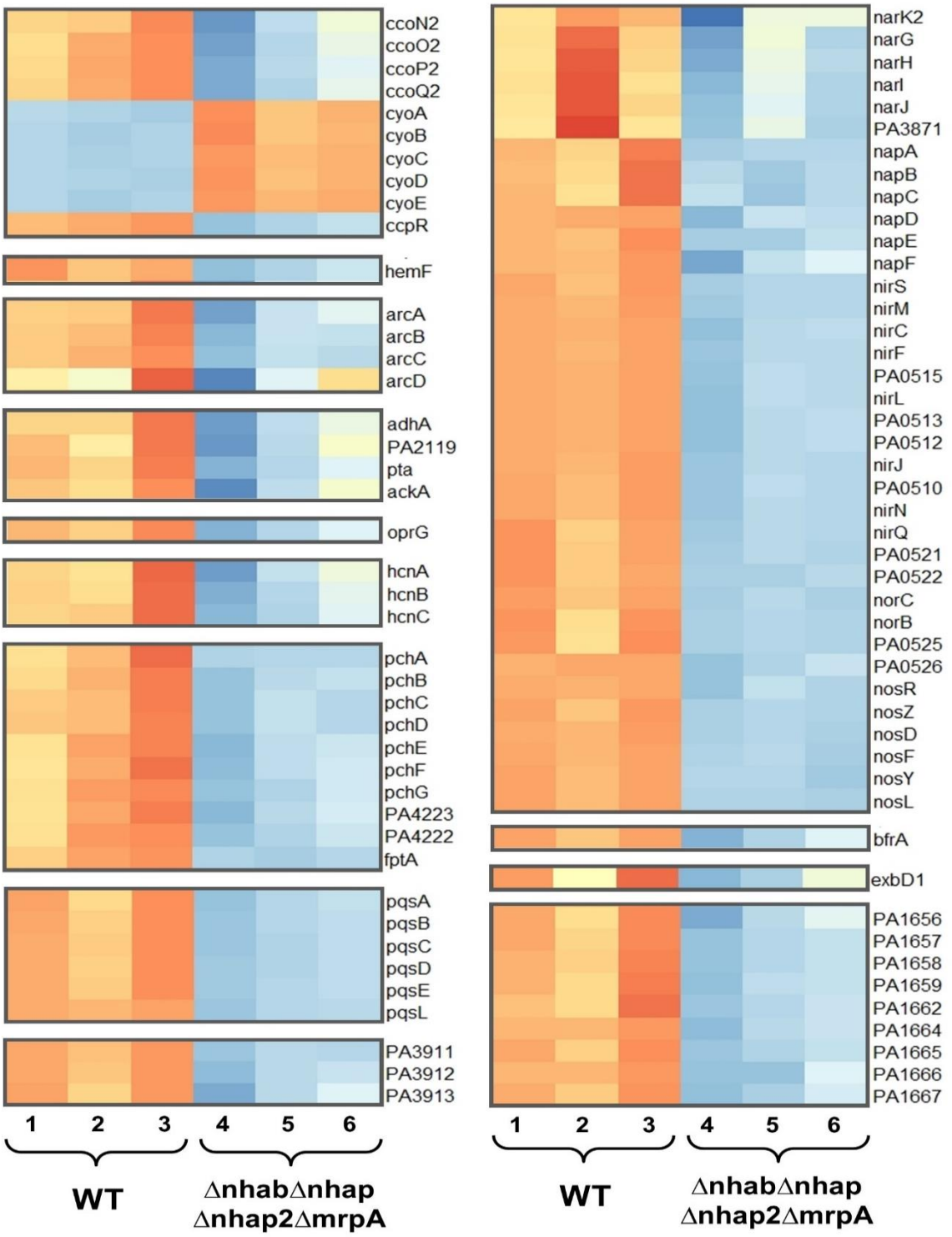

Figure 4.14: Heatmap showing levels of transcripts of ANR-regulated genes in wildtype and Δ*nhab*Δ*nhap*Δ*nhap2*Δ*mrpA* during exponential phase growth. Total reads for each transcript were normalized and log transformed using the DESeq2 rlog function in Rstudio and are *z*-scored by row. Columns 1, 2, and 3 are WT biological replicate growths and columns 4, 5, and 6 are quadruple deletion mutant biological replicate growths.

increase in the expression of the enzymes composing the PQS synthesis pathway.

For all 90 of the identified differentially expressed genes under ANR regulation, the changes in expression in the Δ*nhab*Δ*nhap*Δ*nhap2*Δ*mrpA* mutant followed the same trend as shown for the Δ*anr* mutant,[106] suggesting that the ANR transcriptional regulator may be similarly disrupted in the quadruple mutant. Many of the most significant changes in expression in the quadruple mutant were found in the genes of the denitrification pathways. The genes encoding the denitrification pathways in *P. aeruginosa*: two nitrate reductases (*narGHJI*, *napEFDABC*), a nitrite reductase and donor cytochrome c_{551} (*nirSMCFLGHJEN*), *nirQ*, a nitric oxide reductase (*norBC)*, and a nitrous oxide reductase (*nosRZDFLY*,) as well as co-operonic genes encoding hypothetical proteins, were all expressed at significantly lower levels in the quadruple mutant than in wildtype.[2,106] Two of the five terminal oxidase complexes, cytochrome cbb_3-2 (*ccoN2O2P2Q2*) and cytochrome bo_3 (*cyoABCDE*), are differentially expressed in the quadruple mutant. Cytochrome cbb_3-2 is known for being ANR-regulated, therefore the significant loss of *cco2* operon transcription is a further indication that ANR is dysfunctional in this strain.[17]

4.2.5.4 Choline and Glycerol Metabolism

Significant changes were seen in the expression of choline and glycerol uptake transporters in the quadruple deletion mutant transcriptome (Figure 4.13). This is notable as both components can yield osmoprotectants in the cell,[109,110] a feature which might be increasingly important to the quadruple mutant. In the case of glycerol, it can itself act as an osmoprotectant,[109] and in the process of choline degradation, the intermediate glycine betaine is produced which is known for its role in osmoprotection in bacteria.[110] Further, the activity of the *P. aeruginosa* hemolytic phospholipase C (PlcH), a hydrolase which is secreted by this bacterium to degrade extracellular

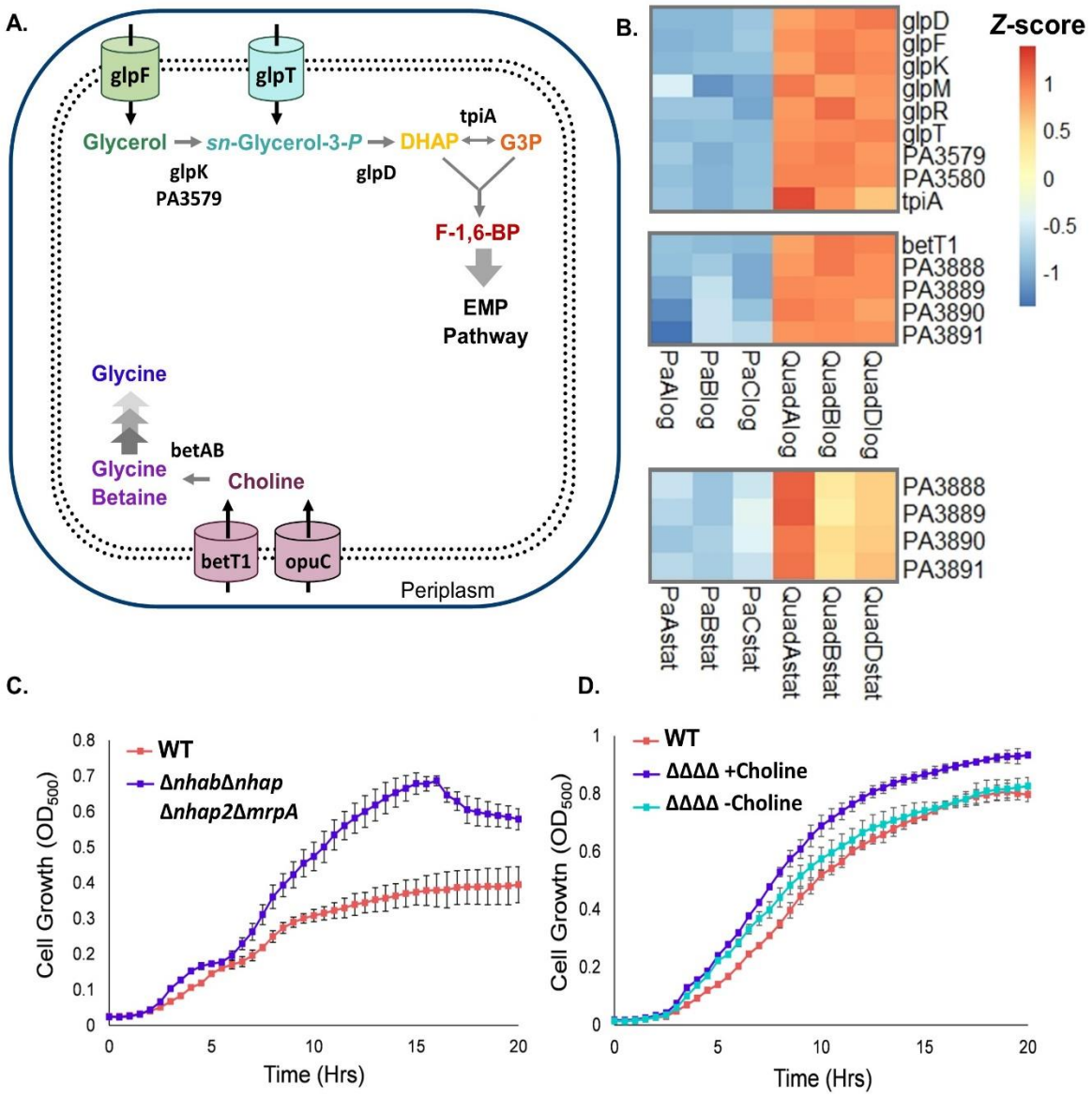

Figure 4.15: Glycerol and choline metabolism in *P. aeruginosa*. (A) Simplified pathways representing the metabolism of glycerol and choline in *P. aeruginosa*, along with the relevant transporters. Dihydroxyacetone phosphate (DHAP), glyceraldehyde-3-P (G3P), fructose-1,6-bis-P (F-1,6-BP). (B) Heatmap showing levels of transcription of the significant DEGs related to glycerol and choline utilization in *P. aeruginosa*. Total reads for each transcript were normalized and log transformed using the DESeq2 rlog function in Rstudio and are *z*-scored by row. Columns labeled with 'Pa' and 'Quad' represent biological replicates from exponential (log) or stationary (stat) growth phase. (C) Growth of wildtype (red) and Δ*nhab*Δ*nhap*Δ*nhap2*Δ*mrpA* (purple) in M9 minimal medium at 50mM NaCl supplemented with 20mM glycerol. (D) Growth of wildtype (red) and Δ*nhab*Δ*nhap*Δ*nhap2*Δ*mrpA* in M9 medium +glucose at 170mM NaCl with 2mM choline (purple) and without (blue). Growth curves are the averages of three technical replicate growths, with error bars calculated accordingly.

phosphatidylcholine (PC) and yield available choline and glycerol, has previously been implicated in the stimulation of ANR activity.[111] Specifically, the stimulation of ANR activity requires the cell to be actively degrading choline, although the mechanisms governing this relationship have yet to be defined.[111] In the quadruple deletion mutant, expression of plcH was not itself increased in expression during exponential growth, but the expression of both the glycerol (glpF) and sn-glycerol-3-P (glpT) transport proteins as well as two choline transport proteins (betT1, PA3888-3891 encoding protein complex OpuC) was significantly greater compared with their expression in wildtype (Figure 4.12B). Upon further analysis, we found that the entire suite of genes responsible for the glycerol degradation pathway,[112] up until fructose-1,6-bisphosphate (F-1,6-BP), were expressed at significantly higher rates during exponential growth in the quadruple deletion mutant (Figure 4.13A). However, expression returned to wildtype-levels during stationary phase growth, suggesting that the quadruple mutant has some use for glycerol during exponential growth specifically.

To assess the utility of glycerol and choline in the Δ*nhab*Δ*nhap*Δ*nhap2*Δ*mrpA* we conducted growth curves in defined M9 minimal medium supplemented with both components. In 50mM NaCl M9 supplemented with 20mM glycerol as the sole carbon source (Figure 4.13C), the quadruple mutant was shown to have an advantage over the wildtype strain, maintaining a longer exponential growth phase and reaching significantly higher stationary phase culture density. This suggests that the quadruple mutant is utilizing glycerol more effectively that wildtype, a result which is likely due to increased expression of the enzymes composing the glycerol metabolic pathway. Furthermore, this growth shows a significant reversal of the pattern of growth shown in rich LB medium. Even though the quadruple mutant is without its four Na^+/H^+ antiporters, this strain can grow much better than its wildtype counterpart in M9 medium with 50mM NaCl. It is

possible that the quadruple mutant is better adapted to maintain efficient metabolism in nutrient-limited conditions than the wildtype.

In M9 medium supplemented with 20mM glucose and 2mM choline, a similar trend in quadruple deletion mutant growth is found. Shown in Figure 4.13D, the presence of choline does improve the growth of the quadruple mutant compared with its growth in the absence of choline, with +choline cultures having a slightly prolonged exponential phase and reaching higher stationary phase culture density. Notably, the quadruple again grows better than the wildtype in the same conditions, although to a lesser extent than was shown in glycerol supplemented medium. Again it is possible that the increased growth in the quadruple mutant is a product of this strain being better adapted to efficiently utilize the components provided in the M9 medium than wildtype, however it is clear that the presence of choline does benefit the quadruple mutant to some degree.

4.3 Discussion

In this study, we have characterized each of the four Na^+/H^+ antiporters present in *P. aeruginosa* and provided insight into the physiological repercussions of their loss. Through the creation of triple antiporter deletion mutants, we were able to functionally isolate each of the Na^+-transporters in their native organism and determine the enzyme kinetics of Na^+ translocation. We have also defined the Li^+-extrusion pathways employed in *P. aeruginosa* and confirmed the presence of additional K^+/H^+ antiporters in the genome. A quadruple deletion mutant was generated which featured the deletion of all four Na^+/H^+ antiporters from the *P. aeruginosa* genome. Creation of this mutant allowed us to confirm the absence of any additional Na^+/H^+ antiporters in the *P. aeruginosa* genome and provided the opportunity to assess the physiological impacts that the deletion of all Na^+/H^+ antiporters has on the cell. This analysis revealed

connections between ion management and virulence trait production, quorum sensing, central metabolism and ANR regulation in the cell. The profound impact of Na^+/H^+ antiporter deletion demonstrates the importance of these transporters to cell functionality, but also provide infection-relevant insights into *P. aeruginosa* physiology.

4.3.1 Growth of the Single and Triple Na^+/H^+ Antiporter Deletion Mutants

Single deletion mutants lacking the NhaB or NhaP antiporters were able to grow as well as wildtype in all of the pH and [Na^+] conditions tested, indicating that the absence of these transporters can be sufficiently compensated for by the remaining antiporters in the growth conditions assessed. In the Δ*nhap2* single deletion mutant, the absence of NhaP2 causes a stationary phase growth defect at pH 8.5 with a progressive exponential phase growth defect as the concentration of sodium is increased. The most significant growth defect is experienced by the Δ*mrpA* single deletion mutant. In conditions of moderate pH and low sodium, this strain can grow just as well as wildtype, but when the pH or [Na^+] are increased the strain experiences a significantly longer lag phase and appears unable to grow above 170mM NaCl at pH 8.5. However, following the prolonged lag phase, the Δ*mrpA* mutant eventually begins to grow at rates similar to wildtype, indicating that this mutant does eventually overcome the absence of a functional Mrp antiporter. Compared with the successful growth of the triple antiporter deletion mutants, of which three similarly had *mrpA* deleted, in the same conditions, we believed that there is a period of physiological adjustment taking place in the Δ*mrpA* mutant that is not present in the triple antiporter deletion strains having the same mutation. While the deletion of the MrpA subunit is sufficient to disrupt Mrp Na^+/H^+ antiporter activity,[39] the remainder of the Mrp operon is still present in the genome and likely being transcribed at wildtype levels. It is possible that the expression and partial assembly of the remaining Mrp subunits prolongs the process of the cell

adapting to the loss of antiporter function, accounting for the prolonged lag phase and eventual growth demonstrated by the Δ*mrpA*, while in the cloning of the triple antiporter deletion mutants we have isolated strains which are adapted to tolerate the loss of three of their four Na^+/H^+ antiporters, and are therefore primed to respond to environmental pH and [Na^+] challenge. This hypothesis remains to be substantiated; however, the adaptive capacities of this bacterium make it a possibility.

From the growth profiles of the triple antiporter deletion mutants we can begin to ascertain the unique functional capacity of each of the individual antiporters. Once all four of the Na^+/H^+ antiporters have been removed, as is the case in the quadruple antiporter deletion mutant, the cells becomes incredibly Na^+- and pH-sensitive, indicating that the attributes of Na^+ and pH tolerance demonstrated in each of the triple deletion mutants can be attributed to the Na^+/H^+ antiporter present. Both Mrp and NhaB alone provide sufficient Na^+/H^+ antiport activity to support normal growth in all conditions tested, including those of pH and Na^+ stress. NhaP2 alone can provide adequate Na^+ tolerance at pH 7.5, maintaining normal growth up to 300 mM NaCl. At high concentrations of sodium and pH 8.5 this mutant has a prolonged lag phase, although final culture densities are comparable to wildtype. The mutant that has NhaP only is much less robust than the previous three mutants. It suffers a significant stationary phase growth defect at even 50mM NaCl, which progresses as the sodium concentration is increased. This mutant is entirely unable to grow in conditions of 300mM NaCl and above at pH 8.5, revealing that, on its own, NhaP cannot meet the ionic requirements of the cell in these conditions. The contrast between the ability of the Mrp and NhaB antiporters to support growth in these conditions with the inability of NhaP to do the same highlights the differences in the properties of each of these transporters.

4.3.2 Assessing the Kinetic Parameters and Physiological Contributions of the Na^+/H^+ Antiporters in *P. aeruginosa*

When growth of each strain was compared with the measured activity of each antiporter, we identified a trend which might account for the greater pH and Na^+ tolerance of NhaB and Mrp. Analysis of the extrapolated kinetic parameters reveals that, according to Vmax, the NhaP antiporter has the highest rate of turnover of the four transporters pH 7.5, followed by NhaB and NhaP2, with Mrp having the lowest rate of turnover, a trend which seems inconsistent with the observed phenotype for each triple mutant (Table 4.1). If we however consider the antiporters by Km, we can see that the pattern of Na^+ efficiency better aligns with the growth measured for each strain. NhaB has the lowest Km of ~0.7 mM, followed by Mrp and NhaP2, with NhaP having the highest Km and thus the lowest affinity for Na^+. The trends triple mutant growth at pH 7.5 suggest that Na^+ affinity, rather than a maximum rate of turnover, is of greater importance to Na^+-tolerance *in vivo* at this pH.

Another notable differences between these antiporters is the proposed stoichiometry of exchange catalyzed by each. NhaP catalyzes the exchange of 1 H^+ for 1 Na^+,[37] while both NhaB and Mrp are thought to catalyze electrogenic exchange ($3H^+/2Na^+$ and $2H^+/1Na^+$, respectively).[41,44] In this case NhaB and Mrp will be much more efficient moderators of cytosolic pH when grown in conditions of high external pH. At pH 8.5, NhaB has both the highest Vmax and the lowest Km of the four antiporters, indicating that this transporter is well equipped to support ion homeostasis at high pH (Table 4.1), as we are shown by the growth of this mutant at pH 8.5 500 mM NaCl. However. it is followed by NhaP, which has a near 3-fold increase in Na^+ affinity at pH 8.5, and then Mrp, which has the lowest measured Na^+ affinity at pH 8.5. Therefore, it is likely that during growth at high pH, the efficiency of pH management (stoichiometry) becomes more important to

cell survival than Na^+-affinity.

At pH 8.5, NhaP2 activity was significantly lower than at pH 7.5. This is consistent with results in NhaP2 homologs, which indicate that this antiporter is essential for growth at low pH.[42] The substrate binding curve generated for NhaP2 indicated that the Km for Na^+ at this pH was much lower than pH 7.5 (Figure 4.4), however sub-saturating concentrations of NaCl were not available for this assay, and thus the Km could not be reliably determined. In addition to Na^+/H^+ antiport, NhaP2 is thought to catalyze K^+/H^+ antiport as well. From this analysis it is difficult to conclusively confirm it's K^+/H^+ activity as the quadruple deletion mutant had substantial K^+/H^+ antiport activity as well (Figure 4.6), likely performed by K^+-selective antiporters encoded for by PA3660, PA3739 and PA5529. However the inability of NhaP2 to transport Li^+ suggests that the binding site of this enzyme cannot accommodate the small Li^+ ion; a result which would be expected for a transporter with a large substrate binding site designed to coordinate much larger K^+ ions (Figure 4.7). Conversely, the significant Li^+/H^+ antiport activity of NhaB has inverse implications for the substrate binding site(s) available in this protein, which appear to be ideally structured to accommodate the Li^+ ion size. The observed Li^+ activity for each of the four antiporters may provide insights into the size of each enzyme's substrate binding site (Figure 4.7).

4.3.3 Transcriptome of the Δ*nhab*Δ*nhap*Δ*nhap2*Δ*mrpA* Mutant: Implications in Virulence

Antiporter activity measurements in the quadruple deletion mutant confirm that the strain possess no Na^+/H^+ antiporters (Figure 4.6) and is therefore severely limited in its ion management capacities. To understand the impact that this defect will have on cell physiology we analyzed the transcriptome of this mutant in comparison with wildtype during both exponential and stationary phase growth. The greatest changes in expression were measured during exponential growth, with

a total of 471 genes having significant changes in expression in the quadruple deletion mutant (Figure 4.7). Given the pathogenicity of *P. aeruginosa*, we first investigated the changes in expression of genes known to contribute to *P. aeruginosa* virulence.

During exponential growth, the quadruple mutant has significant decreases in genes encoding two of the four quorum sensing (QS) pathways, the *Pseudomonas* quinolone system (PQS) and the LasI/R two component system (Figure 4.11).[55] These QS pathways are responsible for controlling the expression of several virulence traits including elastases, rhamnolipids, and the characteristic pigmented toxin pyocyanin.[78] Consequently, the expression of each of these virulence traits was also significantly decreased during exponential growth in the quadruple mutant. The production of biofilm, another characteristic trait of *P. aeruginosa*, is also controlled by these QS pathways; however the expression of genes encoding for the synthesis of the extracellular polysaccharides which compose the biofilm matrix (Psl and Pel)[104] were significantly increased in expression in the quadruple mutant (Figure 4.11). This result is inconsistent with the reduction of QS signaling, indicating that the production of biofilm is being regulated through other means. This mutant also has a significant increase in the exponential phase expression of the genes encoding for the peptidoglycan biosynthetic pathway (see Figure B.1 for pathway view). This is notable as both processes of biofilm formation and peptidoglycan biosynthesis represent an effort by the cell to fortify the barriers between the cell and the exterior environment and have been implicated in antibiotic resistance in *P. aeruginosa*.[113,114] It is possible that these two processes may be linked in this mutant, however the utility of these processes in the face of Na^+ and H^+ imbalance is not clear.

During stationary phase growth, the expression of the genes encoding the PQS synthesis pathway is significantly increased in the quadruple deletion mutant, with the exception of the

pqsH, which catalyzes the final step in the pathway and converts HHQ to PQS via an NADH-dependent reaction.[102] As explained above, the PQS signaling cascade is thought to regulate the production of pyocyanin in *P. aeruginosa*. However, the expression of the genes encoding the pyocyanin synthesis pathway remains significantly decreased with respect to wildtype, indicating that, although the PQS signaling cascade is likely functioning, it is not eliciting the expected effect on pyocyanin production. The reduction in pyocyanin production during both exponential and stationary phase growth in the quadruple mutant represents an interesting correlation between the quadruple mutant and the Δ*nqrF* mutant discussed in Chapter 3. Although it remains to be conclusively demonstrated, we believe that the NADH dehydrogenase NQR couples the transfer of electrons from NADH to quinone with the translocation of Na^+ ions out of the cell. If this is the case, it would make the activity of NQR very important in the quadruple mutant, as it may be the only means left by which the cell can extrude Na^+.

The relationship between NQR and pyocyanin synthesis in the Δ*nqrF* mutant is argued to be a function of redox balancing by the cell, with excess NADH being shuttled to pyocyanin synthesis to restore the cellular NAD^+/NADH ratio. Therefore, the reduction in pyocyanin synthesis in the quadruple mutant may be evidence of an inverse relationship, in which the synthesis of pyocyanin is sacrificed in favor of providing NQR with NADH to support maximum Na^+ extrusion. In addition, the final step in the PQS synthesis pathway, catalyzed by PqsH, is also NADH-dependent,[102] presenting that possibility that the exponential phase expression of both pathways is significantly reduced in the quadruple mutant for the sake of redirecting NADH to NQR. There is some evidence for the prioritization of NQR over its H^+-translocating counterpart NUO in the quadruple mutant (see Figure B.2), however this trend in expression needs to be corroborated with measurement of NADH:quinone oxidoreductase activities. The role for NADH

in virulence regulation has been demonstrated previously,[24] however the role for NQR, and by extension the Na+/H+ antiporters, has not been well defined. These results suggest that the efficient management of cellular Na^+ is critical to *P. aeruginosa* pathogenesis.

4.3.4 Transcriptome of the Δ*nhab*Δ*nhap*Δ*nhap2*Δ*mrpA* Mutant: ANR Regulon

Another notable feature of the quadruple mutant transcriptome is the reduction in expression of reportedly ANR-regulated genes. Upon cross referencing the quadruple mutant transcriptome with the transcriptome of a *P. aeruginosa* Δ*anr* mutant,[106] it was revealed that not only are a significant number of the DEGs shared between the two lists, but that the changes in expression experienced in both strains are analogous. This complementarity signals that the quadruple mutant may be experiencing a disruption in ANR activity, and therefore the genes controlled by this transcriptional regulator are not being expressed. The role of ANR in the cell is to work as a regulator of genes required for anaerobic growth.[105] Similar to the FNR regulator of *E. coli*, this protein requires an assembled $[4Fe\text{-}4S]^{2+}$ cluster to dimerize and bind DNA.[115] When oxygen is present, the Fe-S cluster will be oxidized and the ANR protein will become inactive, thus 'turning off' expression of the genes within its regulon.[105] However, the cells grown for RNA sequencing were grown in fully aerated conditions, raising the question of how ANR is active in the oxic wildtype cells.

The changes to expression of the ANR regulon in the quadruple mutant indicates that some consequence of Na^+/H^+ antiporter deletion is interrupting ANR function. In addition to being oxygen sensitive, the activity of ANR is redox sensitive as well.[116] Given the proposed compensatory role of NQR in the quadruple mutant, it is possible that the cell is suffering a redox imbalance which impedes ANR function. If this is the case, these cells would likely be incapable of anaerobic growth, however this hypothesis remains to be tested. Nonetheless the disruption of

ANR has important implications for metabolism and virulence in *P. aeruginosa.* Among the ANR regulon are several respiratory enzymes, most prominently a series of terminal electron acceptors including cytochrome cbb_3-2, cytochrome bo_3, nitrate reductase, nitrite reductase, nitric oxide reductase and nitrous oxide reductase. The implications for *P. aeruginosa* respiration are therefore quite significant in the quadruple deletion mutant. In addition, evidence suggests that the ANR regulon and related pathways are important to *P. aeruginosa* adaptation and long-term colonization of the CF airway.[7,111,117] Δ*anr* mutants were shown to have signification attenuation of virulence during respiratory infection in mice, with bacteria being largely cleared from the mouse lung just 24 hours post-inoculation.[111] Therefore the cellular processes influencing and dictating ANR activity may play a role in the progression of *P. aeruginosa* infection, making a case for the importance of Na^+ and H^+ homeostasis to *P. aeruginosa* pathogenicity.

4.3.5 Transcriptome of the Δ*nhab*Δ*nhap*Δ*nhap2*Δ*mrpA* Mutant: Choline and Glycerol Degradation

Genes encoding choline and glycerol transporters were expressed at significantly higher levels in the quadruple deletion mutant compared with wildtype. It is possible that this phenotype is just an attempt by the cell to encourage the uptake of these compounds for the osmoprotection that they provide.[109] The deletion of all of the Na^+/H^+ antiporters has likely left the cells more susceptible to osmotic stress and thus the increase in expression of the choline and glycerol transporters may simply be a means of osmoadaptation in the mutant. This is likely the case during stationary phase growth. While there are several genes related to choline and glycerol processing which are increased in expression during exponential growth, during stationary growth the OpuC transporter, which has been shown to play a primarily osmoregulatory role in the species,[118] is the only enzyme still being expressed at significantly greater levels in the quadruple mutant.

However, during exponential phase growth the uptake of these compounds can have greater implications in *P. aeruginosa* physiology.

Choline and glycerol uptake has been shown to be important during *P. aeruginosa* colonization of the lung, likely in relation to the activity of the hemolytic phospholipase C (PlcH) secreted by *P. aeruginosa*. PlcH catalyzes the degradation of extracellular phosphatidylcholine (PC) into its component parts, including both choline and glycerol, which the cell will take in and utilize.[119] PC is the major phospholipid component of pulmonary surfactant and is thought to be an important nutrient for *P. aeruginosa* during lung colonization. Mutants having defective choline and/or glycerol degradation pathways were shown to have attenuated virulence in mouse lung infection models,[119] indicating the importance of the metabolism of these two components to infectious success in *P. aeruginosa.* Given the results of quadruple mutant growth on both glycerol and choline, it is clear that the mutant is primed to utilize these components. The increase in expression of both choline and glycerol uptake proteins, as well as the genes encoding the glycerol degradation pathway, may suggest that there is a relationship between Na^+ and H^+ ion gradients and the excretion and activity of PlcH, or alternatively the cells ability to metabolize of the products of PlcH activity.

In addition, evidence suggests that the activity of PlcH and subsequent choline degradation by the cell are essential for the activation of ANR.[111] Specifically, it was found that the choline degradation pathway needs to be active in *P. aeruginosa* to stimulate ANR. Although the expression of *plcH* is unchanged in the quadruple mutant, the relationship between choline metabolism and ANR activity presents the possibility that the increase in choline uptake proteins may be in an effort to stimulate ANR activity in the ANR-defective cells.

4.4 Conclusion

In this study we have shown that *P. aeruginosa* possesses four Na^+/H^+ antiporters, each with unique properties of ion affinity, pH-dependence, and ion specificity. This work presents the first enzyme activity characterization of the NhaP2 antiporter in *P. aeruginosa*, revealing that this enzyme is unable to transport Li^+ and is likely a contributor to Na^+ and K^+-extrusion during growth at low pH. In employing so many complementary enzymes, *P. aeruginosa* can maintain efficient ion homeostasis across a wide range of [Na^+] and pH conditions, an attribute which enables the environmental ubiquity of this microbe. In addition to defining the properties of the individual Na^+/H^+ antiporters, we have also assessed the role of ion management in the physiology and pathogenesis of *P. aeruginosa*. Deletion of all four of the Na^+/H^+ antiporters from *P. aeruginosa* resulted in significant transcriptional changes in the mutant, most notably in processes of quorum sensing, virulence trait production, ANR activity and metabolism. The greatest changes in cell physiology are seen during exponential phase, at which time the cell is expected to metabolically active. The changes experienced in the quadruple mutant suggest that the central metabolism of the bacterium is shifted significantly from wildtype. The quadruple deletion mutant has a significant reduction in the expression of several cell traits that are thought to be important to infectious success in the CF lung, indicating that the ion management provided by the four Na^+/H^+ antiporters may be of increased importance during respiratory infection. The proposed relationship between the Na^+/H^+ antiporters, the NADH dehydrogenase NQR and pyocyanin production presents a very interesting intersection between ionic homeostasis and redox balance which has important, infection relevant implications in *P. aeruginosa* physiology. Further investigation should be carried out to better define this relationship and discern the role which is plays in *P. aeruginosa* pathogenicity.

5. CONCLUDING REMARKS AND FUTURE DIRECTIONS

In this study we have presented a complete characterization of the enzymes responsible for Na^+ and H^+ gradient generation and regulation in *Pseudomonas aeruginosa*. We have elucidated the 'hierarchy' of NADH dehydrogenases present in *P. aeruginosa* and determined NQR to be the major NADH dehydrogenase in this bacterium. We have identified the four Na^+/H^+ antiporters present in *P. aeruginosa* and revealed that there are additional K^+/H^+ antiporters present in the genome which remain to be characterized. And most intriguingly, we have begun to uncover a dynamic system of ionic, metabolic and pathogenic cooperation in *P. aeruginosa* which may provide infection-relevant insights in the development of new antibacterial strategies against *P. aeruginosa*. From the data presented here, it appears that there is a relationship between ion regulation, NADH metabolism, and pyocyanin production/virulence signaling in *P. aeruginosa*. Upon deletion of NQR, there is a significant shift in the onset of virulence to an earlier timepoint and a significant increase in the production of pyocyanin by the strain. It is hypothesized that this shift in virulence activation and pyocyanin production is due to an imbalance of NAD^+/NADH introduced by the NQR deletion. Interestingly, the phenotype in the quadruple antiporter deletion mutant is the inverse, with virulence trait production significantly decreased with respect to wildtype. This is notable as NQR is believed to couple electron transfer to the translocation of Na^+ across the membrane. In the quadruple deletion mutant, which has lost four of its primary Na^+-efflux enzymes, the activity of NQR will be critical to cellular management of Na^+ and therefore it is proposed that NADH would be redirected to NQR to preferentially fuel its Na^+-pumping activity. The proposal that NADH is regulating virulence initiation in *P. aeruginosa* is supported by the observed reciprocal phenotypes in the Δ*nqr* and Δ*nhab*Δ*nhap*Δ*nhap2*Δ*mrpA*, however

further characterization of these mechanisms is required to fully define this regulatory mechanism in *P. aeruginosa*.

To further test the proposed hypotheses, it will be beneficial to construct a double mutant strain which has both NQR and the genes responsible for pyocyanin synthesis deleted and observe the virulence and virulence trait production of this strain in comparison with wildtype and a strain which retains NQR but is defective in pyocyanin synthesis. If it is the case that the increased production of pyocyanin is giving rise to the hypervirulence in the Δ*nqr* strain, then we would expect this double mutant strain to be no more virulent than wildtype. Fluorescence-lifetime imaging microscopy methods exist for the monitoring of NADH in *P. aeruginosa*. Measuring the NADH dynamics in the wildtype, Δ*nqr, and* Δ*nhab*Δ*nhap*Δ*nhap2*Δ*mrpA* may provide insights into the redox state of each mutant. Time based experiments may reveal the shifts in redox state at different time points in growth, which may allow for the determination of discrete virulence-transitions for each mutant, providing evidence on the regulation of virulence in each strain. This information will provide insights critical to our understanding of the relationships between ion management, biochemistry and pathogenicity in *P. aeruginosa*.

REFERENCES

(1) Komagata, K. Differentiation of Genus Pseudomonas and Related Aerobic Bacteria. *J. Gen. Appl. Microbiol.* **1961**, *7* (4), 282–299.

(2) Williams, H. D.; Zlosnik, J. E. A.; Ryall, B. Oxygen, Cyanide and Energy Generation in the Cystic Fibrosis Pathogen Pseudomonas Aeruginosa. *Adv. Microb. Physiol.* **2006**, *52*, 1–71.

(3) Green, S. K.; Schroth, M. N.; Cho, J. J.; Kominos, S. D.; Vitanza-Jack, V. B. Agricultural Plants and Soil as a Reservoir for Pseudomonas Aeruginosa. *Appl. Microbiol.* **1974**, *28* (6), 987–991.

(4) Khan, N. H.; Ishii, Y.; Kimata-Kino, N.; Esaki, H.; Nishino, T.; Nishimura, M.; Kogure, K. Isolation of Pseudomonas Aeruginosa from Open Ocean and Comparison with Freshwater, Clinical, and Animal Isolates. *Microb. Ecol.* **2007**, *53* (2), 173–186.

(5) Choudhary, S.; Sar, P. Uranium Biomineralization by a Metal Resistant Pseudomonas Aeruginosa Strain Isolated from Contaminated Mine Waste. *J. Hazard. Mater.* **2011**, *186* (1), 336–343.

(6) Wang, C. L.; Ozuna, S. C.; Clark, D. S.; Keasling, J. D. A Deep-Sea Hydrothermal Vent Isolate, Pseudomonas Aeruginosa CW961, Requires Thiosulfate for Cd2+ Tolerance and Precipitation. *Biotechnol. Lett.* **2002**, *24* (8), 637–641.

(7) Trautmann, M.; Lepper, P. M.; Haller, M. Ecology of Pseudomonas Aeruginosa in the Intensive Care Unit and the Evolving Role of Water Outlets as a Reservoir of the Organism. *Am J Infect Control*. **2005**, *33* (5 Suppl 1), S41–S49.

(8) Grosso-Becerra, M. V.; Santos-Medellín, C.; González-Valdez, A.; Méndez, J. L.; Delgado, G.; Morales-Espinosa, R.; Servín-González, L.; Alcaraz, L. D.; Soberón-Chávez, G. Pseudomonas Aeruginosa Clinical and Environmental Isolates Constitute a Single Population with High Phenotypic Diversity. *BMC Genomics* **2014**, *15* (1), 318.

(9) Morrison, A. J.; Wenzel, R. P. Epidemiology of Infections Due to Pseudomonas Aeruginosa. *Rev. Infect. Dis*. **1984**, *6* (Suppl 3), S627–S642.

(10) Mittal, R.; Aggarwal, S.; Sharma, S.; Chhibber, S.; Harjai, K. Urinary Tract Infections Caused by Pseudomonas Aeruginosa: A Minireview. *J. Infect. Public Health*. **2009**, *2* (3), 101–111.

(11) Pachori, P.; Gothalwal, R.; Gandhi, P. Emergence of Antibiotic Resistance Pseudomonas Aeruginosa in Intensive Care Unit; a Critical Review. *Genes Dis*. **2019**, *6* (2), 109–119.

(12) Weiner-Lastinger MPH, L. M.; Abner, S.; Edwards MStat, J. R.; Kallen, A. J.; Karlsson, M.; Magill, S. S.; Pollock, D.; See, I.; Soe MBBS, M. M.; Walters, M. S.; Dudeck MPH, M. A. Antimicrobial-Resistant Pathogens Associated with Adult Healthcare-Associated Infections: Summary of Data Reported to the National Healthcare Safety Network, 2015-2017. *Infect. Control Hosp. Epidemiol.* **2020**, *41* (1), 1–18.

(13) Davies, J. C. Pseudomonas Aeruginosa in Cystic Fibrosis: Pathogenesis and Persistence. *Paediatr. Respir. Rev.* **2002**, *3* (2), 128–134.

(14) Stover, C. K.; Pham, X. Q.; Erwin, A. L.; Mizoguchi, S. D.; Warrener, P.; Hickey, M. J.; Brinkman, F. S. L.; Hufnagle, W. O.; Kowallk, D. J.; Lagrou, M.; Garber, R. L.; Goltry, L.; Tolentino, E.; Westbrock-Wadman, S.; Yuan, Y.; Brody, L. L.; Coulter, S. N.; Folger, K. R.; Kas, A.; Larbig, K.; Lim, R.; Smith, K.; Spencer, D.; Wong, G. K. S.; Wu, Z.; Paulsen, I. T.; Relzer, J.; Saler, M. H.; Hancock, R. E. W.; Lory, S.; Olson, M. V. Complete Genome Sequence of Pseudomonas Aeruginosa PAO1, an Opportunistic Pathogen. *Nature* **2000**, *406* (6799), 959–964.

(15) Oberhardt, M. A.; Puchałka, J.; Fryer, K. E.; Martins Dos Santos, V. A. P.; Papin, J. A. Genome-Scale Metabolic Network Analysis of the Opportunistic Pathogen Pseudomonas Aeruginosa PAO1. *J. Bacteriol.* **2008**, *190* (8), 2790–2803.

(16) Frimmersdorf, E.; Horatzek, S.; Pelnikevich, A.; Wiehlmann, L.; Schomburg, D. How Pseudomonas Aeruginosa Adapts to Various Environments: A Metabolomic Approach. *Environ. Microbiol.* **2010**, *12* (6), 1734–1747.

(17) Alvarez-Ortega, C.; Harwood, C. S. Responses of Pseudomonas Aeruginosa to Low Oxygen Indicate That Growth in the Cystic Fibrosis Lung Is by Aerobic Respiration. *Mol. Microbiol.* **2007**, *65* (1), 153–165.

(18) Arai, H. Regulation and Function of Versatile Aerobic and Anaerobic Respiratory Metabolism in Pseudomonas Aeruginosa. *Front. Microbiol.* **2011**, *2*, 103.

(19) Jo, J.; Price-Whelan, A.; Cornell, W. C.; Dietrich, L. E. P. Interdependency of Respiratory Metabolism and Phenazine-Associated Physiology in Pseudomonas Aeruginosa PA14. *J. Bacteriol.* **2020**, *202* (4), e00700-19.

(20) Dolan, S. K.; Kohlstedt, M.; Trigg, S.; Vallejo Ramirez, P.; Kaminski, C. F.; Wittmann, C.; Welch, M. Contextual Flexibility in Pseudomonas Aeruginosa Central Carbon Metabolism during Growth in Single Carbon Sources. *MBio* **2020**, *11* (2), e02684-19.

(21) Wurtzel, O.; Yoder-Himes, D. R.; Han, K.; Dandekar, A. A.; Edelheit, S.; Greenberg, E. P.; Sorek, R.; Lory, S. The Single-Nucleotide Resolution Transcriptome of Pseudomonas Aeruginosa Grown in Body Temperature. *PLoS Pathog.* **2012**, *8* (9), e1002945.

(22) Thomas, K. L.; Lloyd, D.; Boddy, L. Effects of Oxygen, PH and Nitrate Concentration on Denitrification by *Pseudomonas* Species. *FEMS Microbiol. Lett.* **1994**, *118* (1–2), 181–186.

(23) Folkesson, A.; Jelsbak, L.; Yang, L.; Johansen, H. K.; Ciofu, O.; Hoiby, N.; Molin, S. Adaptation of Pseudomonas Aeruginosa to the Cystic Fibrosis Airway: An Evolutionary Perspective. *Nat. Rev. Microbiol.* **2012,** *10* (12), 841–851.

(24) Perinbam, K.; Chacko, J. V.; Kannan, A.; Digman, M. A.; Siryaporn, A. A Shift in Central Metabolism Accompanies Virulence Activation in Pseudomonas Aeruginosa. *MBio* **2020**, *11* (2), e02730-18.

(25) Yagi, T. Bacterial NADH-Quinone Oxidoreductases. *J. Bioenerg. Biomembr.* **1991**, *23* (2), 211–225.
(26) Friedrich, T.; Scheide, D. The Respiratory Complex I of Bacteria, Archaea and Eukarya and Its Module Common with Membrane-Bound Multisubunit Hydrogenases. *FEBS Lett.* **2000**, *479* (1–2), 1–5.
(27) Wikström, M.; Hummer, G. Stoichiometry of Proton Translocation by Respiratory Complex I and Its Mechanistic Implications. *Proc. Natl. Acad. Sci. U. S. A.* **2012**, *109* (12), 4431–4436.
(28) Raba, D. A.; Rosas-Lemus, M.; Menzer, W. M.; Li, C.; Fang, X.; Liang, P.; Tuz, K.; Minh, D. D. L.; Juárez, O. Characterization of the Pseudomonas Aeruginosa NQR Complex, a Bacterial Proton Pump with Roles in Autopoisoning Resistance. *J. Biol. Chem.* **2018**, *293* (40), 15664–15677.
(29) Bertsova, Y. V.; Baykov, A. A.; Bogachev, A. V. A Simple Strategy to Differentiate between H+- and Na+-Transporting NADH:Quinone Oxidoreductases. *Arch. Biochem. Biophys.* **2020**, *681*, 108266.
(30) Barquera, B. The Sodium Pumping NADH:Quinone Oxidoreductase (Na+-NQR), a Unique Redox-Driven Ion Pump. *J. Bioenerg. Biomembr.* **2014**, *46* (4), 289–298.
(31) Vamshi Krishna, K.; Venkata Mohan, S. Purification and Characterization of NDH-2 Protein and Elucidating Its Role in Extracellular Electron Transport and Bioelectrogenic Activity. *Front. Microbiol.* **2019**, *10* (MAY), 880.
(32) Mitchell, P. Coupling of Phosphorylation to Electron and Hydrogen Transfer by a Chemi-Osmotic Type of Mechanism. *Nature* **1961**, *191* (4784), 144–148.
(33) Häse, C. C.; Fedorova, N. D.; Galperin, M. Y.; Dibrov, P. A. Sodium Ion Cycle in Bacterial Pathogens: Evidence from Cross-Genome Comparisons. *Microbiol. Mol. Biol. Rev.* **2001**, *65* (3), 353–370.
(34) Krulwich, T. A.; Hicks, D. B.; Ito, M. Cation/Proton Antiporter Complements of Bacteria: Why so Large and Diverse? *Mol. Microbiol.* **2009**, *74* (2), 257–260.
(35) Padan, E.; Venturi, M.; Gerchman, Y.; Dover, N. Na(+)/H(+) Antiporters. *Biochim. Biophys. Acta* **2001**, *1505* (1), 144–157.
(36) Kuroda, T.; Fujita, N.; Utsugi, J.; Kuroda, M.; Mizushima, T.; Tsuchiya, T. A Major Li(+) Extrusion System NhaB of Pseudomonas Aeruginosa : Comparison with the Major Na(+) Extrusion System NhaP. *Microbiol. Immunol.* **2004**, *48* (4), 243–250.
(37) Utsugi, J.; Inaba, K.; Kuroda, T.; Tsuda, M.; Tsuchiya, T. Cloning and Sequencing of a Novel Na+/H+ Antiporter Gene from Pseudomonas Aeruginosa. *Biochim. Biophys. Acta - Gene Struct. Expr.* **1998**, *1398* (3), 330–334.
(38) Ueda, A.; Wood, T. K. Potassium and Sodium Transporters of Pseudomonas Aeruginosa Regulate Virulence to Barley. *Appl. Microbiol. Biotechnol.* **2008**, *79* (5), 843–858.
(39) Kosono, S.; Haga, K.; Tomizawa, R.; Kajiyama, Y.; Hatano, K.; Takeda, S.; Wakai, Y.; Hino, M.; Kudo, T. Characterization of a Multigene-Encoded Sodium/Hydrogen

Antiporter (Sha) from Pseudomonas Aeruginosa: Its Involvement in Pathogenesis. *J. Bacteriol.* **2005**, *187* (15), 5242–5248. https://doi.org/10.1128/JB.187.15.5242-5248.2005.

(40) Padan, E.; Landau, M. Sodium-Proton (Na+/H+) Antiporters: Properties and Roles in Health and Disease. *Met Ions Life Sci.* **2016**, 16, 391–458.

(41) Pinner, E.; Padan, E.; Schuldiner, S. Kinetic Properties of NhaB, a Na+/H+ Antiporter from Escherichia Coli. *J. Biol. Chem.* **1994**, *269* (42), 26274–26279.

(42) Resch, C. T.; Winogrodzki, J. L.; Patterson, C. T.; Lind, E. J.; Quinn, M. J.; Dibrov, P.; Häse, C. C. The Putative Na+/H+ Antiporter of Vibrio Cholerae, Vc-NhaP2, Mediates the Specific K+/H+ Exchange in Vivo. *Biochemistry* **2010**, *49* (11), 2520–2528.

(43) Ito, M.; Morino, M.; Krulwich, T. A. Mrp Antiporters Have Important Roles in Diverse Bacteria and Archaea. *Front. Microbiol.* **2017**, *8*, 2325.

(44) Steiner, J.; Sazanov, L. Structure and Mechanism of the MRP Complex, an Ancient Cation/Proton Antiporter. *Elife* **2020**, *9*, e59407.

(45) Häse, C. C.; Barquera, B. Role of Sodium Bioenergetics in Vibrio Cholerae. *Biochim. Biophys. Acta - Bioenerg.* **2001**, *1505* (1), 169–178.

(46) Minato, Y.; Fassio, S. R.; Reddekopp, R. L.; Häse, C. C. Inhibition of the Sodium-Translocating NADH-Ubiquinone Oxidoreductase [Na+-NQR] Decreases Cholera Toxin Production in Vibrio Cholerae O1 at the Late Exponential Growth Phase. *Microb. Pathog.* **2014**, *66*, 36–39.

(47) Vilchèze, C.; Weinrick, B.; Leung, L. W.; Jacobs, W. R. Plasticity of Mycobacterium Tuberculosis NADH Dehydrogenases and Their Role in Virulence. *Proc. Natl. Acad. Sci. U. S. A.* **2018**, *115* (7), 1599–1604.

(48) Velmurugan, K.; Chen, B.; Miller, J. L.; Azogue, S.; Gurses, S.; Hsu, T.; Glickman, M.; Jacobs, W. R.; Porcelli, S. A.; Briken, V. Mycobacterium Tuberculosis NuoG Is a Virulence Gene That Inhibits Apoptosis of Infected Host Cells. *PLoS Pathog.* **2007**, *3* (7), e110.

(49) Milelr, J. L.; Velmurugan, K.; Cowan, M. J.; Briken, V. The Type I NADH Dehydrogenase of Mycobacterium tuberculosis Counters Phagosomal NOX2 Activity to Inhibit TNF-α-Mediated Host Cell Apoptosis. *PLoS Pathog.* **2010**, *6* (4), e1000864.

(50) Camacho Carvajal, M. M.; Wijfjes, A. H. M.; Mulders, I. H. M.; Lugtenberg, B. J. J.; Bloemberg, G. V. Characterization of NADH Dehydrogenases of Pseudomonas Fluorescens WCS365 and Their Role in Competitive Root Colonization. *Mol. Plant-Microbe Interact.* **2002**, *15* (7), 662–671.

(51) Schurig-Briccio, L. A.; Parraga Solorzano, P. K.; Lencina, A. M.; Radin, J. N.; Chen, G. Y.; Sauer, J.; Kehl-Fie, T. E.; Gennis, R. B. Role of Respiratory NADH Oxidation in the Regulation of *Staphylococcus Aureus* Virulence. *EMBO Rep.* **2020**, *21* (5), e45832.

(52) Vaish, M.; Price-Whelan, A.; Reyes-Robles, T.; Liu, J.; Jereen, A.; Christi, S.; Alonzo, F.; Benson, M. A.; Torres, V. J.; Krulwicha, T. A. Roles of Staphylococcus Aureus Mnh1 and Mnh2 Antiporters in Salt Tolerance, Alkali Tolerance, and Pathogenesis. *J. Bacteriol.* **2018**, *200* (5), e00611-17.

(53) (1) Minato, Y.; Ghosh, A.; Faulkner, W. J.; Lind, E. J.; Bartra, S. S.; Plano, G. V.; Jarrett, C. O.; Hinnebusch, B. J.; Winogrodzki, J.; Dibrov, P.; Häse, C. C. Na+/H+ Antiport Is Essential for Yersinia Pestis Virulence. *Infect. Immun.* **2013**, *81* (9), 3163–3172.

(54) Torres, A.; Kasturiarachi, N.; DuPont, M.; Cooper, V. S.; Bomberger, J.; Zemke, A. NADH Dehydrogenases in Pseudomonas Aeruginosa Growth and Virulence. *Front. Microbiol.* **2019**, *10* (FEB), 1–10.

(55) Lee, J.; Zhang, L. The Hierarchy Quorum Sensing Network in Pseudomonas Aeruginosa. *Protein Cell* **2014**, *6* (1), 26–41.

(56) Moradali, M. F.; Ghods, S.; Rehm, B. H. A. Pseudomonas Aeruginosa Lifestyle: A Paradigm for Adaptation, Survival, and Persistence. *Front. Cell. Infect. Microbiol.* **2017**, *7*, 39.

(57) Palmer, K. L.; Aye, L. M.; Whiteley, M. Nutritional Cues Control Pseudomonas Aeruginosa Multicellular Behavior in Cystic Fibrosis Sputum. *J. Bacteriol.* **2007**, *189* (22), 8079–8087.

(58) Hall, B. G.; Acar, H.; Nandipati, A.; Barlow, M. Growth Rates Made Easy. *Mol. Biol. Evol.* **2013**, *31* (1), 232-238.

(59) Petzoldt T. growthrates: Estimate growth rates from experimental data. R package version 0.8.1. https://CRAN.R-project.org/package=growthrates (accessed July 28, 2020).

(60) Jacobs, M. A.; Alwood, A.; Thaipisuttikul, I.; Spencer, D.; Haugen, E.; Ernst, S.; Will, O.; Kaul, R.; Raymond, C.; Levy, R.; Chun-Rong, L.; Guenthner, D.; Bovee, D.; Olson, M. V.; Manoil, C. Comprehensive Transposon Mutant Library of Pseudomonas Aeruginosa. *Proc. Natl. Acad. Sci. U. S. A.* **2003**, *100* (SUPPL. 2), 14339–14344.

(61) Hmelo, L. R.; Borlee, B. R.; Almblad, H.; Love, M. E.; Randall, T. E.; Tseng, B. S.; Lin, C.; Irie, Y.; Storek, K. M.; Yang, J. J.; Siehnel, R. J.; Howell, P. L.; Singh, P. K.; Tolker-Nielsen, T.; Parsek, M. R.; Schweizer, H. P.; Harrison, J. J. Precision-Engineering the Pseudomonas Aeruginosa Genome with Two-Step Allelic Exchange. *Nat. Protoc.* **2015**, *10* (11), 1820–1841.

(62) Vogel, H. J.; Bonner, D. M. Acetylornithinase of Escherichia coli: partial purification and some properties. *J. Biol. Chem.* **1956**, *218* (1), 97-106.

(63) Barquera, B.; Nilges, M. J.; Morgan, J. E.; Ramirez-Silva, L.; Zhou, W.; Gennis, R. B. Mutagenesis Study of the 2Fe-2S Center and the FAD Binding Site of the Na+-Translocating NADH:Ubiquinone Oxidoreductase from Vibrio Cholerae. *Biochemistry* **2004**, *43* (38), 12322–12330.

(64) Rosen, B. P. Ion Extrusion Systems in Escherichia Coli. *Methods Enzymol.* **1986**, *125* (26), 328–336.

(65) Bolger, A. M.; Lohse, M.; Usadel, B. Trimmomatic: a flexible trimmer for Illumina sequence data. *Bioinformatics.* **2014**, *30* (15), 2114-2120.

(66) Langmean, B.; Salzberg, S. Fast gapped-read alignment with Bowtie 2. *Nat Methods*.

2012, *9*, 357–359.
(67) Liao, Y.; Smyth, G. K.; Shi, W. featureCounts: an efficient general purpose program for assigning sequence reads to genomic features. *Bioinformatics.* **2014**, *30* (7), 923-930.
(68) Love, M. I.; Huber, W.; Anders, S. Moderated estimation of fold change and dispersion for RNA-seq data with DESeq2. *Genome Biol.* **2014**, *15*, 550.
(69) Berger, A.; Dohnt, K.; Tielen, P.; Jahn, D.; Becker, J.; Wittmann, C. Robustness and Plasticity of Metabolic Pathway Flux among Uropathogenic Isolates of Pseudomonas Aeruginosa. *PLoS One* **2014**, *9* (4), e88368.
(70) Kerscher, S.; Dröse, S.; Zickermann, V.; Brandt, U. The Three Families of Respiratory NADH Dehydrogenases. *Results Probl. Cell Differ.* **2008**, *45*, 185–222.
(71) Liang, P.; Fang, X.; Hu, Y.; Yuan, M.; Raba, D. A.; Ding, J.; Bunn, D. C.; Sanjana, K.; Yang, J.; Rosas-Lemus, M.; Häse, C. C.; Tuz, K.; Juárez, O. The Aerobic Respiratory Chain of Pseudomonas Aeruginosa Cultured in Artificial Urine Media: Role of NQR and Terminal Oxidases. *PLoS One* **2020**, *15* (4), e0231965.
(72) Choi, K. H.; Kumar, A.; Schweizer, H. P. A 10-Min Method for Preparation of Highly Electrocompetent Pseudomonas Aeruginosa Cells: Application for DNA Fragment Transfer between Chromosomes and Plasmid Transformation. *J. Microbiol. Methods* **2006**, *64* (3), 391–397.
(73) Iiyama, K.; Lee, J. M.; Kusakabe, T.; Yasunaga-Aoki, C.; Shimizu, S. Improvement in PHERD Vectors to Express Recombinant Proteins Tagged with Hexahistidine at Either the NH2- or COOH- Terminal in Pseudomonas Aeruginosa. *J. Insect Biotechnol. Sericology* **2012**, *80* (2), 57–61.
(74) Datsenko, K. A.; Wanner, B. L. One-Step Inactivation of Chromosomal Genes in Escherichia Coli K-12 Using PCR Products. *Proc. Natl. Acad. Sci. U. S. A.* **2000**, *97* (12), 6640–6645.
(75) Barquera, B.; Hellwig, P.; Zhou, W.; Morgan, J. E.; Häse, C. C.; Gosink, K. K.; Nilges, M.; Bruesehoff, P. J.; Roth, A.; Lancaster, C. R. D.; Gennis, R. B. Purification and Characterization of the Recombinant Na+-Translocating NADH:Quinone Oxidoreductase from Vibrio Cholerae. *Biochemistry* **2002**, *41* (11), 3781–3789.
(76) Koley, D.; Ramsey, M. M.; Bard, A. J.; Whiteley, M. Discovery of a Biofilm Electrocline Using Real-Time 3D Metabolite Analysis. *Proc. Natl. Acad. Sci. U. S. A.* **2011**, *108* (50), 19996–20001.
(77) Tram, G.; Korolik, V.; Day, C. J. MBDS Solvent: An Improved Method for Assessment of Biofilms. *Adv. Microbiol.* **2013**, *3*, 200–204.
(78) Whiteley, M.; Lee, K. M.; Greenberg, E. P. Identification of genes controlled by quorum sensing in Pseudomonas aeruginosa. *Proc Natl Acad Sci U S A.* **1999**, *96* (24), 13904-13909
(79) Heydorn, A.; Nielsen, A. T.; Hentzer, M.; Sternberg, C.; Givskov, M.; Ersboll, B. K.; Molin, S. Quantification of Biofilm Structures by the Novel Computer Program COMSTAT. *Microbiology* **2000**, *146* (10), 2395–2407.
(80) Vorregaard, M. Comstat2-a Modern 3D Image Analysis Environment for Biofilms. In *Informatics and Mathematical Modelling.* Technical University of Denmark: Kongens Lyngby, Denmark. 2008.
(81) Matsushita, K.; Ohnishi, T.; Kaback, H. R. NADH-Ubiquinone Oxidoreductases of the Escherichia Coli Aerobic Respiratory Chain. *Biochemistry* **1987**, *26* (24), 7732–7737.

(82) Zambrano, M. M.; Kolter, R. Escherichia Coli Mutants Lacking NADH Dehydrogenase I Have a Competitive Disadvantage in Stationary Phase. *J. Bacteriol.* **1993**, *175* (17), 5642–5647.

(83) Zhou, W.; Bertsova, Y. V.; Feng, B.; Tsatsos, P.; Verkhovskaya, M. L.; Gennis, R. B.; Bogachev, A. V.; Barquera, B. Sequencing and Preliminary Characterization of the Na+-Translocating NADH:Ubiquinone Oxidoreductase from Vibrio Harveyi. *Biochemistry* **1999**, *38* (49), 16246–16252.

(84) Price-Whelan, A.; Dietrich, L. E. P.; Newman, D. K. Pyocyanin Alters Redox Homeostasis and Carbon Flux through Central Metabolic Pathways in *Pseudomonas aeruginosa* PA14. *J Bacteriol*. **2007**, *189* (17), 6372-6381.

(85) Schurek, K. N.; Marr, A. K.; Taylor, P. K.; Wiegand, I.; Semenec, L.; Khaira, B. K.; Hancock, R. E. W. Novel Genetic Determinants of Low-Level Aminoglycoside Resistance in Pseudomonas Aeruginosa. *Antimicrob. Agents Chemother.* **2008**, *52* (12), 4213–4219.

(86) Friedrich, T.; Van Heek, P.; Leif, H.; Ohnishi, T.; Forche, E.; Kunze, B.; Jansen, R.; Trowitzsch-Kienast, W.; Höfle, G.; Reichenbach, H.; Weiss, H. Two Binding Sites of Inhibitors in NADH:Ubiquinone Oxidoreductase (Complex I): Relationship of One Site with the Ubiquinone-binding Site of Bacterial Glucose:Ubiquinone Oxidoreductase. *Eur. J. Biochem.* **1994**, *219* (1–2), 691–698.

(87) Hall, S.; McDermott, C.; Anoopkumar-Dukie, S.; McFarland, A. J.; Forbes, A.; Perkins, A. V.; Davey, A. K.; Chess-Williams, R.; Kiefel, M. J.; Arora, D.; Grant, G. D. Cellular Effects of Pyocyanin, a Secreted Virulence Factor of Pseudomonas Aeruginosa. *Toxins*. **2016**, *8* (8), 236.

(88) Mavrodi, D. V.; Bonsall, R. F.; Delaney, S. M.; Soule, M. J.; Phillips, G.; Thomashow, L. S. Functional Analysis of Genes for Biosynthesis of Pyocyanin and Phenazine-1-Carboxamide from Pseudomonas Aeruginosa PAO1. *J. Bacteriol.* **2001**, *183* (21), 6454–6465.

(89) Köhler, T.; Michéa-Hamzehpour, M.: Henze, U.; Gotoh, N.; Curty, L. K.; Pechère, J. C. Characterization of MexE-MexF-OprN, a positively regulated multidrug efflux system of Pseudomonas aeruginosa. *Mol Microbiol*. **1997,** *23* (2), 345-354.

(90) Maseda, H.; Yoneyama, H.; Nakae, T. Assignment of the Substrate-Selective Subunits of the MexEF-OprN Multidrug Efflux Pump of Pseudomonas Aeruginosa. *Antimicrob. Agents Chemother.* **2000**, *44* (3), 658–664.

(91) Tseng, J. T.; Bryan, L. E.; Van den Elzen, H. M. Mechanisms and Spectrum of Streptomycin Resistance in a Natural Population of Pseudomonas Aeruginosa. *Antimicrob. Agents Chemother.* **1972**, *2* (3), 136–141.

(92) Hancock, R. E. W.; Raffle, V. J.; Nicas, T. I. Involvement of the Outer Membrane in Gentamicin and Streptomycin Uptake and Killing in Pseudomonas Aeruginosa. *Antimicrob. Agents Chemother.* **1981**, *19* (5), 777–785.

(93) Poole, K. Aminoglycoside Resistance in Pseudomonas Aeruginosa. *Antimicrob. Agents Chemother.* **2005**, *49* (2), 479–487.

(94) Martínez, J. L.; Rojo, F. Metabolic regulation of antibiotic resistance. *FEMS Microbiol Rev.* **2011**, *35* (5), 768-789.

(95) Allen, L.; Dockrell, D. H.; Pattery, T.; Lee, D. G.; Cornelis, P.; Hellewell, P. G.; Whyte, M. K. B. Pyocyanin Production by Pseudomonas Aeruginosa Induces Neutrophil

Apoptosis and Impairs Neutrophil-Mediated Host Defenses In Vivo . *J. Immunol.* **2005**, *174* (6), 3643–3649.

(96) Lau, G. W.; Ran, H.; Kong, F.; Hassett, D. J.; Mavrodi, D. Pseudomonas Aeruginosa Pyocyanin Is Critical for Lung Infection in Mice. *Infect. Immun.* **2004**, *72* (7), 4275–4278.

(97) Chieda, Y.; Iiyama, K.; Lee, J. M.; Kusakabe, T.; Yasunaga-Aoki, C.; Shimizu, S. Inactivation of Pyocyanin Synthesis Genes Has No Effect on the Virulence of *Pseudomonas Aeruginosa* PAO1 toward the Silkworm, *Bombyx Mori*. *FEMS Microbiol. Lett.* **2008**, *278* (1), 101–107.

(98) Fothergill, J. L.; Panagea, S.; Hart, C. A.; Walshaw, M. J.; Pitt, T. L.; Winstanley, C. Widespread Pyocyanin Over-Production among Isolates of a Cystic Fibrosis Epidemic Strain. *BMC Microbiol.* **2007**, *7* (1), 45.

(99) Jeukens, J.; Boyle, B.; Kukavica-Ibrulj, I.; Ouellet, M. M.; Aaron, S. D.; Charette, S. J.; Fothergill, J. L.; Tucker, N. P.; Winstanley, C.; Levesque, R. C. Comparative Genomics of Isolates of a Pseudomonas Aeruginosa Epidemic Strain Associated with Chronic Lung Infections of Cystic Fibrosis Patients. *PLoS One* **2014**, *9* (2), e87611.

(100) O'Brien, S.; Williams, D.; Fothergill, J. L.; Paterson, S.; Winstanley, C.; Brockhurst, M. A. High Virulence Sub-Populations in Pseudomonas Aeruginosa Long-Term Cystic Fibrosis Airway Infections. *BMC Microbiol.* **2017**, *17* (1), 30.

(101) Castro, P. J.; Silva, A. F.; Marreiros, B. C.; Batista, A. P.; Pereira, M. M. Respiratory Complex I: A Dual Relation with H+ and Na+? *Biochim. Biophys. Acta - Bioenerg.* **2016**, *1857* (7), 928–937.

(102) Schertzer, J. W.; Brown, S. A.; Whiteley, M. Oxygen Levels Rapidly Modulate Pseudomonas Aeruginosa Social Behaviours via Substrate Limitation of PqsH. *Mol. Microbiol.* **2010**, *77* (6), 1527–1538.

(103) Lin, J.; Cheng, J.; Wang, Y.; Shen, X. The Pseudomonas Quinolone Signal (PQS): Not Just for Quorum Sensing Anymore. *Front. Cell. Infect. Microbiol.* **2018**, *8*, 230.

(104) Franklin, M. J.; Nivens, D. E.; Weadge, J. T.; Lynne Howell, P. Biosynthesis of the Pseudomonas Aeruginosa Extracellular Polysaccharides, Alginate, Pel, and Psl. *Front. Microbiol*. **2011**, *2*, 167.

(105) Tribelli, P. M.; Lujan, A. M.; Pardo, A.; Ibarra, J. G.; Fernández Do Porto, D.; Smania, A.; López, N. I. Core Regulon of the Global Anaerobic Regulator Anr Targets Central Metabolism Functions in Pseudomonas Species. *Sci. Rep.* **2019**, *9* (1), 1–13.

(106) Hammond, J. H.; Dolben, E. F.; Smith, T. J.; Bhuju, S.; Hogan, D. A. Links between Anr and Quorum Sensing in Pseudomonas Aeruginosa Biofilms. *J. Bacteriol.* **2015**, *197* (17), 2810–2820.

(107) Oglesby, A. G.; Farrow, J. M.; Lee, J. H.; Tomaras, A. P.; Greenberg, E. P.; Pesci, E. C.; Vasil, M. L. The Influence of Iron on Pseudomonas Aeruginosa Physiology: A Regulatory Link between Iron and Quorum Sensing. *J. Biol. Chem.* **2008**, *283* (23), 15558–15567.

(108) Bortolotti, P.; Hennart, B.; Thieffry, C.; Jausions, G.; Faure, E.; Grandjean, T.; Thepaut, M.; Dessein, R.; Allorge, D.; Guery, B. P.; Faure, K.; Kipnis, E.; Toussaint, B.; Le Gouellec, A. Tryptophan Catabolism in Pseudomonas Aeruginosa and Potential for Inter-Kingdom Relationship. *BMC Microbiol.* **2016**, *16* (1), 1–10.

(109) Sleator, R. D.; Hill, C. Bacterial Osmoadaptation: The Role of Osmolytes in Bacterial Stress and Virulence. *FEMS Microbiol. Rev.* **2002**, *26* (1), 49–71.

(110) Wargo, M. J. Homeostasis and Catabolism of Choline and Glycine Betaine: Lessons from Pseudomonas Aeruginosa. *Appl. Environ. Microbiol.* **2013**, *79* (7), 2112–2120.
(111) Jackson, A. A.; Gross, M. J.; Daniels, E. F.; Hampton, T. H.; Hammond, J. H.; Vallet-Gely, I.; Dove, S. L.; Stanton, B. A.; Hogan, D. A. Anr and Its Activation by PlcH Activity in Pseudomonas Aeruginosa Host Colonization and Virulence. *J. Bacteriol.* **2013**, *195* (13), 3093–3104.
(112) Poblete-Castro, I.; Wittmann, C.; Nikel, P. I. Biochemistry, Genetics and Biotechnology of Glycerol Utilization in *Pseudomonas* Species. *Microb. Biotechnol.* **2020**, *13* (1), 32–53.
(113) Dhar, S.; Kumari, H.; Balasubramanian, D.; Mathee, K. Cell-Wall Recycling and Synthesis in Escherichia Coli and Pseudomonas Aeruginosa – Their Role in the Development of Resistance. *J. Med. Microbiol.* **2018**, *67* (1), 1–21.
(114) Taylor, P. K.; Yeung, A. T. Y.; Hancock, R. E. W. Antibiotic Resistance in Pseudomonas Aeruginosa Biofilms: Towards the Development of Novel Anti-Biofilm Therapies. *J. Biotechnol.* **2014**, *191*, 121–130.
(115) Yoon, S. S.; Karabulut, A. C.; Lipscomb, J. D.; Hennigan, R. F.; Lymar, S. V; Groce, S. L.; Herr, A. B.; Howell, M. L.; Kiley, P. J.; Schurr, M. J.; Gaston, B.; Choi, K.-H.; Schweizer, H. P.; Hassett, D. J. Two-Pronged Survival Strategy for the Major Cystic Fibrosis Pathogen, Pseudomonas Aeruginosa, Lacking the Capacity to Degrade Nitric Oxide during Anaerobic Respiration. *EMBO J.* **2007**, *26* (15), 3662–3672.
(116) Unden, G.; Trageser, M.; Duchêne, A. Effect of Positive Redox Potentials (>+400mV) on the Expression of Anaerobic Respiratory Enzymes in *Escherichia Coli*. *Mol. Microbiol.* **1990**, *4* (2), 315–319.
(117) Schobert, M.; Jahn, D. Anaerobic Physiology of Pseudomonas Aeruginosa in the Cystic Fibrosis Lung. *Int. J. Med. Microbiol.* **2010**, *300* (8), 549–556.
(118) Chen, C.; Beattie, G. A. Characterization of the Osmoprotectant Transporter OpuC from Pseudomonas Syringae and Demonstration That Cystathionine-β-Synthase Domains Are Required for Its Osmoregulatory Function. *J. Bacteriol.* **2007**, *189* (19), 6901–6912.
(119) Sun, Z.; Kang, Y.; Norris, M. H.; Troyer, R. M.; Son, M. S.; Schweizer, H. P.; Dow, S. W.; Hoang, T. T. Blocking Phosphatidylcholine Utilization in Pseudomonas Aeruginosa, via Mutagenesis of Fatty Acid, Glycerol and Choline Degradation Pathways, Confirms the Importance of This Nutrient Source In Vivo. *PLoS One* **2014**, *9* (7), e103778.

APPENDICES

Appendix A Supplementary Information for Chapter 3: The Three NADH Dehydrogenases of *Pseudomonas aeruginosa*: Their Roles in Energy Metabolism and Links to Virulence

A.1 *Growth Parameters for PAO1 and NADH Dehydrogenase Mutants*

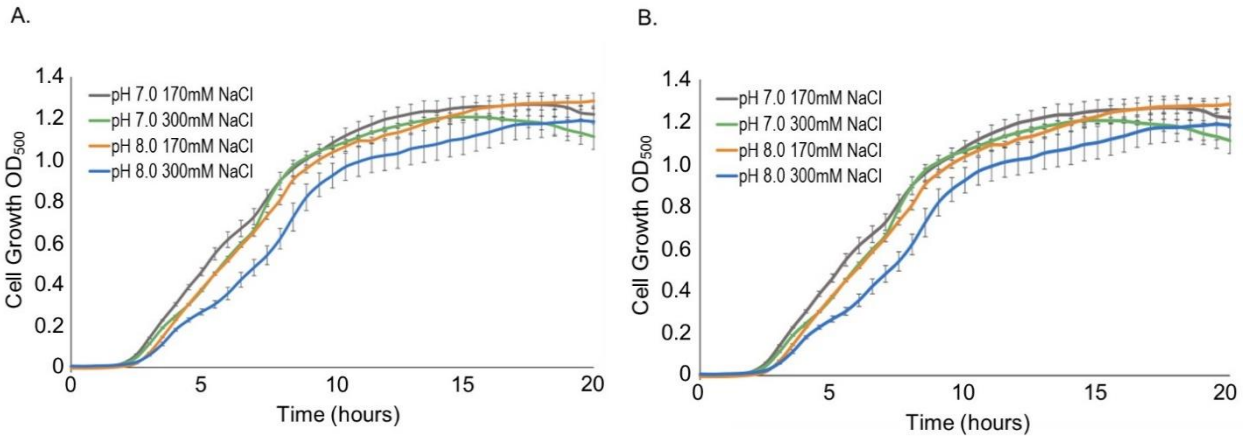

Figure A.1: Growth curves of wild type PAO1 in LB (A) and SCFM (B). Changes in OD_{500} were measured using a Tecan Infinite M1000 Pro plate reader during 20 hours of growth at 37°C with continuous orbital shaking at 217 rpm. Each curve was constructed using two biological replicates with three technical replicates each, with standard deviation calculated accordingly and represented as error bars.

Table A.1: Doubling times[a] for WT PAO1, single, and double NADH dehydrogenase deletion mutants in LB medium[b].

Growth Parameters in LB				
	pH 7.0 170mM NaCl	pH 7.0 300mM NaCl	pH 8.0 170mM NaCl	pH 8.0 300mM NaCl
Strain	Doubling Time (min)	Doubling Time (min)	Doubling Time (min)	Doubling Time (min)
PAO1	26.6 ± 1.8	22.2 ± 2.3	24.9 ± 1.4	30.6 ± 2.4
Δ*ndh*	27.7 ± 1.6	26.5 ± 4.3	25.8 ± 1.7	32.8 ± 2.7
Δ*nuoG*	30.4 ± 2.9*	31.6 ± 6.6*	33 ± 3.2*	41.8 ± 5.6*
Δ*nqrF*	31.2 ± 1.1*	33 ± 1.5*	29.5 ± 2.1*	39 ± 2.1*
Δ*nqrF*Δ*nuoG*	39.5 ± 0.7**	50.5 ± 0.7**	44.2 ± 2.3**	59.1 ± 3.4**
Δ*nqrF*Δ*ndh*	44.9 ± 1.7**	41.5 ± 1.7**	39.3 ± 2.2**	45.8 ± 8.3**
Δ*nuoG*Δ*ndh*	34.4 ± 1.8**	34.8 ± 1.8**	32.8 ± 2.3**	40.4 ± 3.7*

[a] Maximum growth rates and doubling times were determined using the fit_easylinear algorithm provided in the growthrates R package [32, 33].
[b] Above parameters calculated from growth curves depicted in Figures 1 and 2.
* indicates *P*-value ≤ 0.01, ** indicates *P*- value ≤ 0.001.

Table A.2: Doubling times[a] for WT PAO1, single, and double NADH dehydrogenase deletion mutants in SCFM medium[b].

Growth Parameters in SCFM				
	pH 7.0 170mM NaCl	pH 7.0 300mM NaCl	pH 8.0 170mM NaCl	pH 8.0 300mM NaCl
Strain	Doubling Time (min)	Doubling Time (min)	Doubling Time (min)	Doubling Time (min)
PAO1	40.4 ± 3.8	39 ± 7.7	38 ± 2.4	32.8 ± 7.6
Δ*ndh*	33.3 ± 1.4	30.9 ± 3.9*	27.6 ± 1.0**	27.2 ± 3.0*
Δ*nuoG*	40.7 ± 3.6	35.9 ± 2.6	38 ± 1.8	34.4 ± 5.8
Δ*nqrF*	37.9 ± 2.6*	34.9 ± 4.9	32.7 ± 1.8	29.8 ± 4.2
Δ*nqrF*Δ*nuoG*	42.1 ± 4.4	47.8 ± 0.8*	37.9 ± 2.8	42.8 ± 4.6*
Δ*nqrF*Δ*ndh*	42.4 ± 2.3	39.7 ± 8.5	84.6 ± 1.0**	79.4 ± 6.9**
Δ*nuoG*Δ*ndh*	46.7 ± 1.6*	40.7 ± 1.0	46.4 ± 2.4*	43.3 ± 3.3*

[a] Maximum growth rates and doubling times were determined using the fit_easylinear algorithm provided in the growthrates R package [32, 33].
[b] Above parameters calculated from growth curves depicted in Figures 1 and 2.
***** indicates *P*-value ≤ 0.01, ** indicates *P*- value ≤ 0.001.

A.2 *NADH:Quinone Oxidoreductase Activity in PAO1 and NADH Dehydrogenase Mutants*

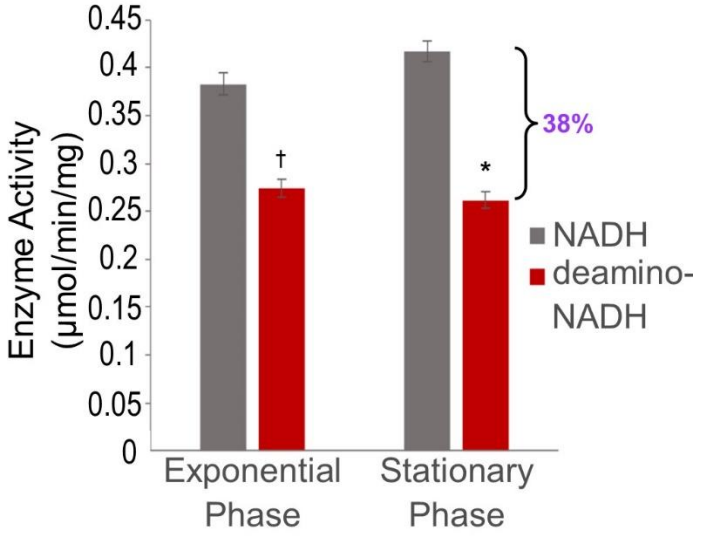

Figure A.2: NADH:quinone oxidoreductase activity in wild type (PAO1) using NADH and deamino-NADH as a substrates. Membranes were harvested in exponential and stationary phase. Enzyme activity is defined as the µmoles of NADH (or deamino-NADH) consumed per minute per mg of membrane protein. The reaction contained: 100µM NADH, 50µM ubiquinone-1 and 100mM NaCl. Changes in absorbance were followed at 340nm (ε_{NADH}= 6.22 mM^{-1} cm^{-1}). Stars indicate p-values of ≤ 0.01 compared to WT according to student's t-test.

Table A.3: NADH dehydrogenase activity[a].

Strain	Enzymes present	Activity (% of WT); Exponential Phase	Activity (% of WT); Stationary Phase
Wild type (PAO1)	NQR, NUO, NDH2	100%	100%
Δ*nuoG*Δ*ndh*	NQR	48%	48%
Δ*nqrF*Δ*ndh*	NUO	15%	46%
Δ*nqrF*Δ*nuoG*	NDH2	37%	49%
Δ*nqrF*	NUO, NDH2	41%	54%
Δ*nuoG*	NQR, NDH2	67%	53%
Δ*ndh*	NQR, NUO	62%	62%
Wild type (PAO1) w/ deamino NADH	NQR, NUO, NDH2*	70%	62%

[a]Activities for each strain represented as a percentage of wild-type activity (100%)

A.3 Surface Images of Biofilm

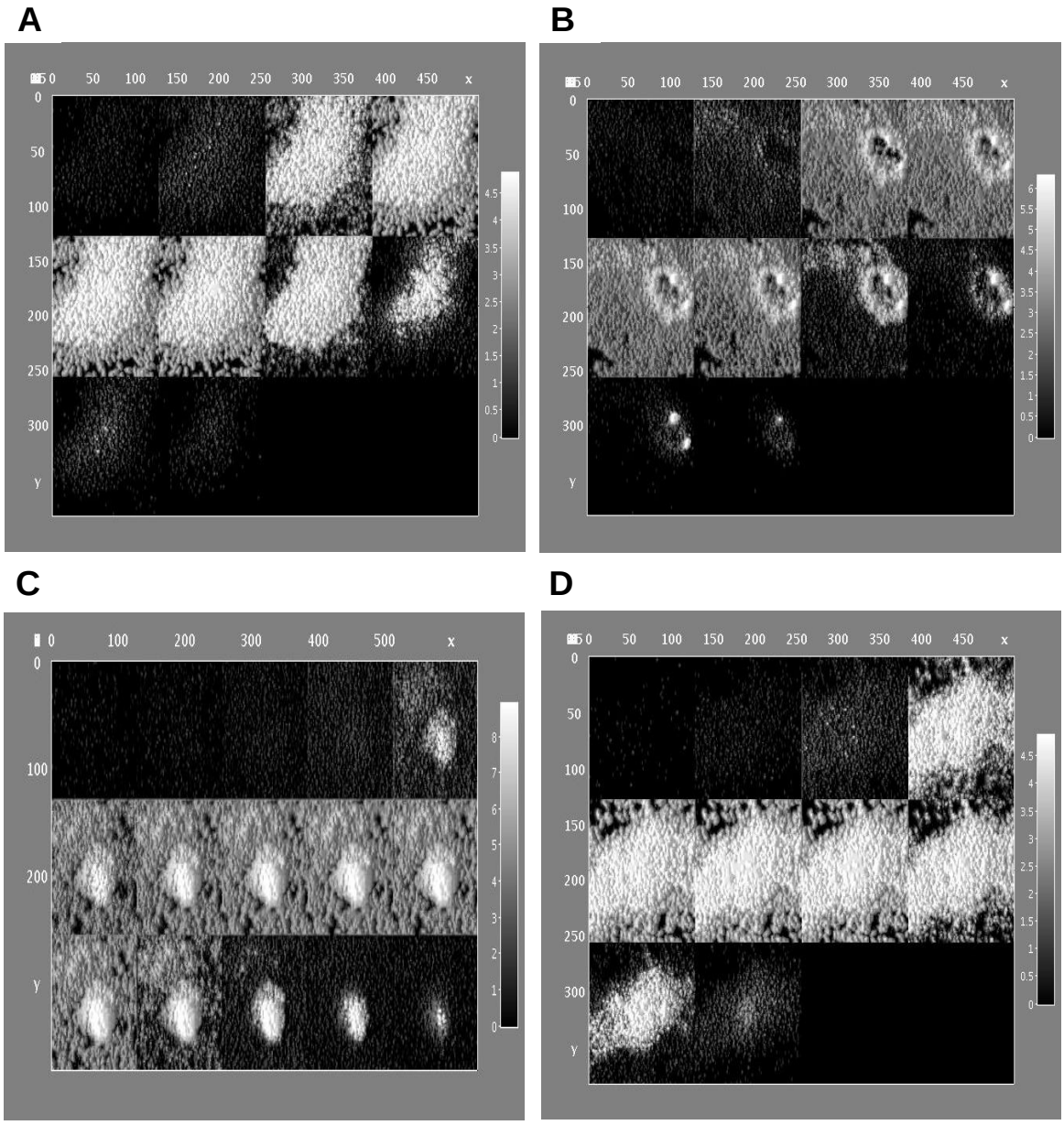

Figure A.3: Surface images of biofilm at mid-attachment. Representative surface images of biofilm produced by WT (A), Δ*ndh* (B), Δ*nuoG* (C), and Δ*nqrF* (D) at the 6-hour timepoint.

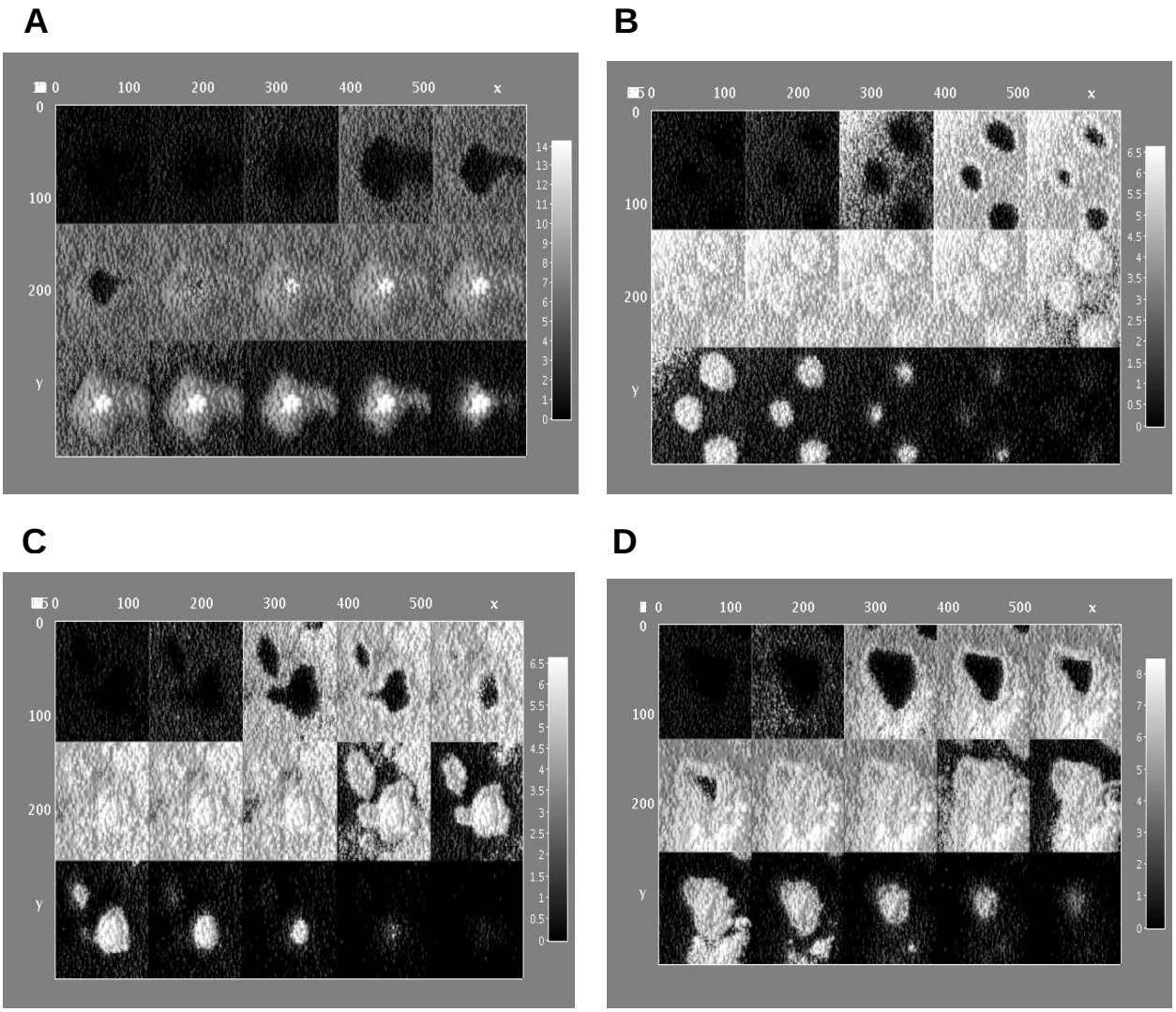

Figure A.5: Surface images of mature biofilm. Representative surface images of biofilm produced by WT (A), Δ*ndh* (B), Δ*nuoG* (C), and Δ*nqrF* (D) at the 24-hour timepoint.

Table A.4: Differential gene expression in the Δ*nqrF* mutant compared to WT in exponential and stationary phases[a].

Gene	Function	Log_2FC Exponential	*P*-value	Log_2FC Stationary	*P*-value
pelA	Encode enzymes involved in Pel exopolysaccharide biosynthesis	0.267369	0.058633	-0.17923	0.219728
pelB		0.24772	0.098497	0.047462	0.792461
pelC		0.422171	0.093354	-0.2708	0.336114
pelD		0.667538	0.00082	-0.00121	0.995712
pelE		0.306455	0.100707	-0.11951	0.50129
pelF		0.101154	0.497763	-0.29852	0.090522
pelG		-0.18566	0.261846	-0.067	0.674183
algD	Encode enzymes involved in alginate biosynthesis	-0.08545	0.629886	-0.10758	0.47636
alg8		-0.02562	0.882777	0.014741	0.931371
alg44		0.165156	0.372885	-0.18843	0.392006
algK		0.238617	0.186971	0.056443	0.798896
algE		0.408082	0.014132	0.010081	0.956702
algG		-0.03058	0.822076	0.149362	0.361075
algX		0.696029	0.000558	0.18302	0.395362
algL		0.600475	0.005554	0.619354	0.012392
algI		0.124164	0.398187	-0.06643	0.666308
algJ		0.340558	0.051811	0.012163	0.962175
algF		0.324613	0.021912	-0.042	0.778684
algA		0.416906	0.002894	0.004878	0.975099
pslA	Encode enzymes involved in Psl exopolysaccharide biosynthesis	1.119932	4.90E-14	0.538923	0.006172
pslB		1.351238	9.45E-13	0.233283	0.159401
pslC		1.230931	1.05E-12	0.21246	0.233326
pslD		1.125739	1.38E-11	0.131871	0.395237
pslE		1.222171	3.64E-11	0.275261	0.093718
pslF		1.352671	1.82E-12	0.295345	0.069601
pslG		1.150325	6.09E-12	0.445182	0.014646
pslH		1.279033	2.71E-14	0.434807	0.015711
pslI		1.234754	1.23E-12	0.392453	0.028786
pslJ		1.154555	1.16E-10	0.36627	0.034244
pslK		1.055982	1.97E-12	0.299122	0.092272
pslL		1.108718	1.88E-17	0.306819	0.047653
lasA	LasA protease precursor	2.724534	8.12E-20	-0.1253	0.315322
mexE	MexEF-OprN Multi-drug Efflux Pump	-9.01185	0	-5.51868	0
mexF		-8.90869	0	-5.06271	0
oprN		-8.40364	0	-4.90324	0
PA2491	MexS, regulator of MexEF-OprN	-3.36747	0	-3.85139	0

mexG		3.253928	4.99E-45	-0.43834	1.45E-05
mexH	MexGHI-OpmD RND	3.220433	1.82E-36	-0.28341	0.092959
mexI	Efflux Pump	3.020968	1.23E-28	-0.50558	0.001162
opmD		3.708842	0	-1.113	1.29E-27

[a]A positive value indicates an increased expression in Δ*nqrF* compared to wild-type. P-values were determined using the calculations outlined in Materials and Methods.

Appendix B Supplementary Information for Chapter 4: Na^+ Management in *Pseudomonas aeruginosa*: Characterization of the Na^+/H^+ Antiporters

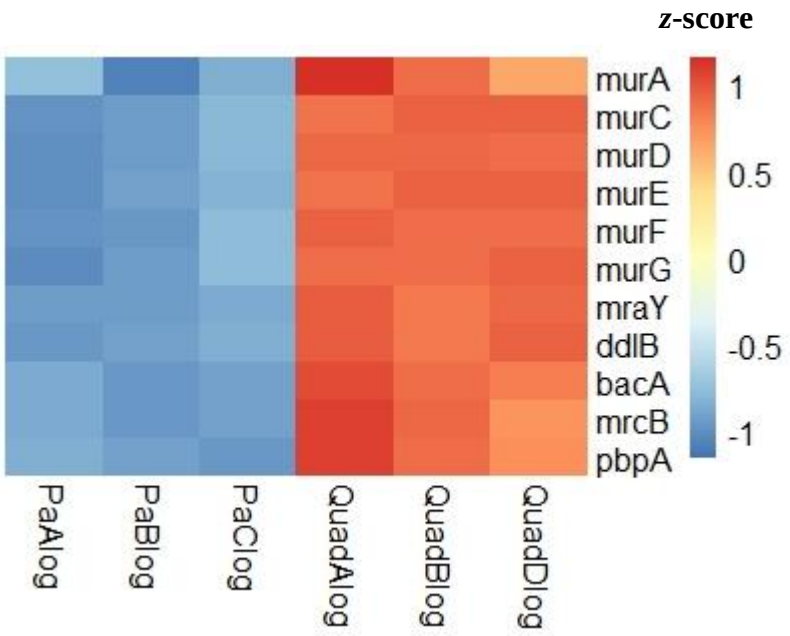

Figure B.1: Exponential phase expression of the peptidoglycan biosynthesis pathways in the Δ*nhab*Δ*nhap*Δ*nhap2*Δ*mrpa* mutant compared with wildtype during exponential phase growth. Heatmap showing levels of transcripts of relevant genes in the quadruple mutant and WT. Total reads for each transcript were normalized and log transformed using the DESeq2 rlog function in Rstudio and are *z*-scored by row. Columns labeled with 'Pa' and 'Quad' represent biological replicate growths.

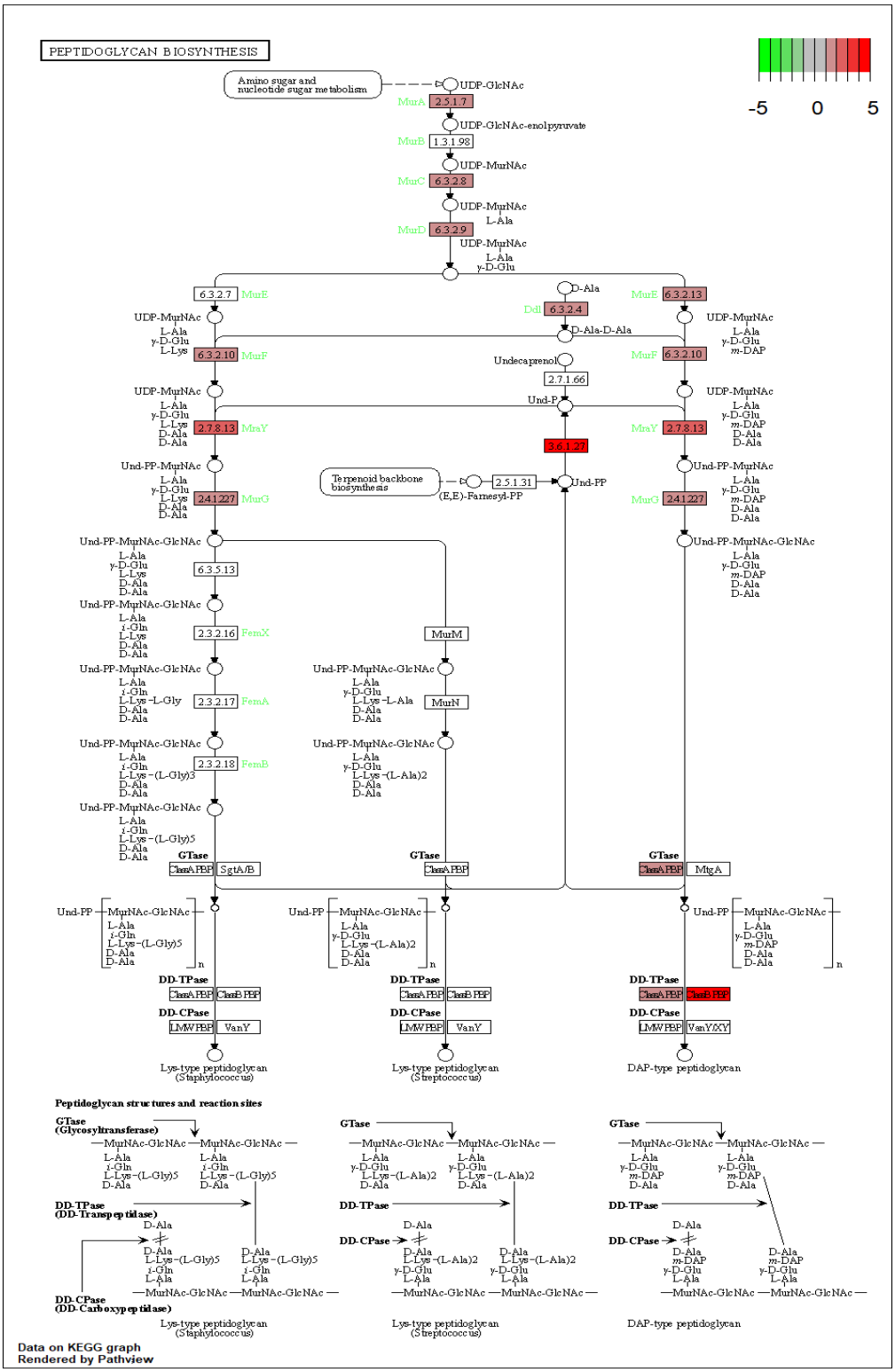

Figure B.2: Pathway view of expression changes of the peptidoglycan biosynthesis pathways in *Δnhab Δnhap Δnhap2 Δmrpa* compared with wildtype during exponential phase growth. Green indicates a negative log2-fold change in expression and red indicates a positive log2-fold change in expression in *Δnhab Δnhap Δnhap2 ΔmrpA* compared with WT. Images are rendered using the Pathview function in Rstudio.

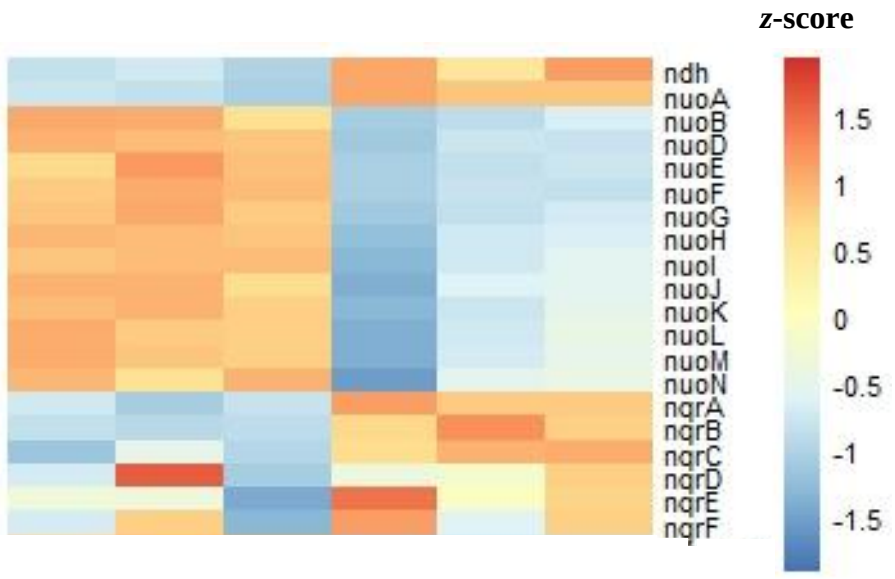

Figure B.3: Expression of the NADH dehydrogenases in Δ*nhab*Δ*nhap*Δ*nhap2*Δ*mrpa* compared with wildtype during exponential phase growth. Heatmap showing levels of transcripts of relevant genes in the quadruple mutant and WT. Total reads for each transcript were normalized and log transformed using the DESeq2 rlog function in Rstudio and are *z*-scored by row. Columns labeled with 'Pa' and 'Quad' represent biological replicate growths.